TECHNICAL REPORT STANDARD TITLE PAGE

1. Report No. FHWATX-77-23-2	2. Government Accession No.	3. Recipient's Catalog No.
4. Title and Subtitle ANALYTICAL AND EXPERIMENTAL INVESTIGATION OF THE THERMAL RESPONSE OF HIGHWAY BRIDGES		5. Report Date February 1977 6. Performing Organization Code
7. Author(s) Kenneth M. Will, C. Philip Johnson, and Hudson Matlock		8. Performing Organization Report No. Research Report 23-2
9. Performing Organization Name and Address Center for Highway Research The University of Texas at Austin Austin, Texas 78712		10. Work Unit No. 11. Contract or Grant No. Research Study 3-5-74-23
12. Sponsoring Agency Name and Address Texas State Department of Highways and Public Transportation; Transportation Planning Division P. O. Box 5051 Austin, Texas 78763		13. Type of Report and Period Covered Interim 14. Sponsoring Agency Code

15. Supplementary Notes

Work done in cooperation with the U. S. Department of Transportation, Federal Highway Administration. Research Study Title: "Temperature Induced Stresses in Highway Bridges by Finite Element Analysis and Field Tests"

16. Abstract

Finite element procedures have been developed for the transient heat conduction and static thermal stress analysis of bridge-type structures. Existing finite element programs were modified and extended for the analyses. Surface temperatures and thermally induced slope change measurements that were obtained during field tests on two prestressed concrete bridges have been included in the study. Also correlations between the field measured slope changes and results that were obtained using the finite element programs have been included.

A finite element program which employs two-dimensional finite elements was used to predict the transient internal temperature distributions for the bridges that were tested. A static analysis program was used to determine the thermally induced movements of bridge-type structures. This program utilizes two-dimensional finite elements in a three-dimensional global assemblage with six degrees-of-freedom at each nodal point. The temperature distributions that were obtained from the heat conduction analysis were used as input data for the static analysis program in order to predict the thermally induced movements and stresses for the bridges that were tested. Several numerical examples were considered to determine the validity of the temperature distribution representation. Additional results were included for one of the bridges that was tested in order to determine the relative magnitudes of the thermally induced stresses and the stresses produced by gravity loading and prestressing.

17. Key Words thermal response, highway bridges, analysis, finite element, temperature distribution, field tests	18. Distribution Statement No restrictions. This document is available to the public through the National Technical Information Service, Springfield, Virginia 22161.

19. Security Classif. (of this report)	20. Security Classif. (of this page)	21. No. of Pages	22. Price
Unclassified	Unclassified	148	

Form DOT F 1700.7 (8-69)

ANALYTICAL AND EXPERIMENTAL INVESTIGATION OF THE THERMAL RESPONSE OF HIGHWAY BRIDGES

by

Kenneth M. Will
C. Philip Johnson
Hudson Matlock

Research Report Number 23-2

Temperature Induced Stresses in Highway Bridges
by Finite Element Analysis and Field Tests

Research Project 3-5-74-23

conducted for

Texas
State Department of Highways and Public Transportation

in cooperation with the
U. S. Department of Transportation
Federal Highway Administration

by the

CENTER FOR HIGHWAY RESEARCH

THE UNIVERSITY OF TEXAS AT AUSTIN

February 1977

PREFACE

Computational procedures for predicting the effect of daily environmental changes on bridge-type structures are presented. Magnitudes of temperature induced movements were established by field tests on two concrete highway bridges. The correlations between the test results and those predicted by the computer simulation of these bridges under field conditions clearly demonstrated the capability and accuracy of the subject procedures.

The internal transient temperature distributions that were predicted by a two-dimensional finite element program were used as input data for a finite element shell program to predict the thermally induced movements and stresses for the bridges that were tested. Several individuals have made contributions in this research. With regard to this project special thanks are due to John Panak, Thaksin Thepchatri, and Atalay Yargicoglu. In addition, thanks are due to Nancy L. Pierce and the members of the staff of the Center for Highway Research for their assistance in producing this report.

ABSTRACT

Finite element procedures have been developed for the transient heat conduction and static thermal stress analysis of bridge-type structures. Existing finite element programs were modified and extended for the analyses. Surface temperature and thermally induced slope change measurements that were obtained during field tests on two prestressed concrete bridges have been included in the study. Also correlations between the field measured slope changes and results that were obtained using the finite element programs have been included.

A finite element program which employs two-dimensional finite elements was used to predict the transient internal temperature distributions for the bridges that were tested. A static analysis program was used to determine the thermally induced movements of bridge-type structures. This program utilizes two-dimensional finite elements in a three-dimensional global assemblage with six degrees-of-freedom at each nodal point. The temperature distributions that were obtained from the heat conduction analysis were used as input data for the static analysis program in order to predict the thermally induced movements and stresses for the bridges that were tested. Several numerical examples were considered to determine the validity of the temperature distribution representation. Additional results were included for one of the bridges that was tested in order to determine the relative magnitudes of the thermally induced stresses and the stresses produced by gravity loading and prestressing.

SUMMARY

This research focused on quantitatively establishing magnitudes of temperature induced movements by field tests on actual bridges and correlating the results with a computer simulation of the structure subjected to the measured field temperatures. The study was separated into three phases: 1) development of a computational procedure to solve for the temperature distribution and temperature induced movements and stresses of bridges, 2) field measurements of bridge temperatures and temperature induced movements, and 3) correlation of measured bridge movements with computer results.

As a result of Phase 1 a finite element procedure was implemented into computer programs for the purpose of predicting temperature distribution and temperature induced stresses of bridges with arbitrary cross sections. A finite element program (39), TSAP, utilizing two-dimensional finite elements was used to predict the temperature distribution. Inputs to this program may be either specified environmental conditions such as solar radiation and air temperature or measured surface temperatures. Having determined the temperature distribution, a finite element static analysis may then be used to determine temperature induced stresses and movements. This program, SHELL8, employs two-dimensional finite elements in a three-dimensional global assemblage. Both membrane and plate bending elements are used. Thermal forces are calculated from a quartic distribution of temperature through the thickness of each element and a linear distribution of temperature over the surface of each element.

In Phase 2 a portable temperature probe was developed to measure surface temperatures at various locations on the bridges to be tested. A mechanical inclinometer was available for determining slope changes induced by temperature. Subsequently field measurements were performed on two bridges: an entrance ramp in Pasadena, Texas, which was skewed and post-tensioned with three continuous spans and a two-span pedestrain overpass in Austin, Texas, with pretensioned beams made continuous for live loads. These

tests were performed during daylight hours on 24 August 1974 and 14 March 1975. Correlations of measured slope changes with results obtained using the finite element procedures were made for each test. Measured surface temperatures were used to predict the internal temperature distribution. The correlations obtained in Phase 3 between the measured slope changes and the results obtained using the subject finite element procedures clearly demonstrate their capability and accuracy in predicting temperature induced stresses and movements under field conditions.

IMPLEMENTATION

The objective of this study which was to quantify magnitudes of temperature induced movements and stresses under field conditions has been accomplished. Correlations with field results using the portable temperature probe developed for measuring the surface temperatures and the mechanical inclinometer for measuring slope changes demonstrated that relatively simple instrumentation with a few selected measurements may be used in the study of the diurnal heating of bridges when coupled with computational tools such as the finite element heat conduction program, TSAP, and static analysis program, SHELL8. The thermally induced stresses predicted in the analysis for both bridges tested are well within design limits. However, it should be emphasized that these stresses are only for the days of the tests which are not believed to be the most severe days for thermal effects. The low magnitude of the stresses in the entrance ramp is also due to the overdesign of the structure since the stiffness of the sidewalks and parapets were neglected in the design process.

The computer programs, TSAP and SHELL8, developed in this project have been recently adapted to the computer facilities of the Texas State Department of Highways and Public Transportation, thus enabling on-going studies as appropriate. User's guides, program listings, and example problems will be contained in the final report of Project No. 3-5-74-23. Although the time required in preparing data and executing these programs is significant, they may be used effectively to determine the effects of skew, transverse behavior, and the stiffness contributions of the parapets and sidewalks, if any. There are other immediate applications of the heat conduction and/or thermal stress analysis programs. They can be readily applied to reinforced concrete pavement to evaluate the effects of temperature. Another area of interest is that of polymer-impregnated concrete in which the surface is dried for several hours at 200-300°F before the bridge deck is impregnated. This drying process could be investigated with the subject procedures, and could help locate potential problems even though the conductivity and tangent stiffness of concrete changes considerably at elevated temperatures.

TABLE OF CONTENTS

LIST OF TABLES

LIST OF FIGURES

CHAPTER 1. INTRODUCTION

1.1 Thermal Stresses and Movements

The exposure of highway bridges to diurnal, daytime, heating produces stresses and movements in these bridges. Uncertainties exist related to the magnitudes of these thermally induced movements and stresses. Current design specifications are of little assistance in providing the bridge designer with magnitudes or suggested methods of analysis related to these stresses and movements. In addition, few methods of analysis have been proposed that are able to yield satisfactory correlation with field measurements. A recent state-of-the-art paper by Reynolds and Emanuel (34)* has attempted to provide engineers with information regarding current design criteria and research. However, the authors indicated the need for further research regarding the prediction of thermal stresses more reliably.

Many bridge designers do not recognize the importance of thermally induced stresses and movements. Consequently, they are often neglected in the design process (34,36). This problem may be due partly to the lack of information and methods of analysis and partly to the fact that no bridge failure has been attributed to thermal stress or movement to the best of the author's knowledge. However, thermal cracking and problems associated with thermally induced movements have been reported. Leonhardt and Lippoth (28) reported crack damage in two-span continuous beams at the bottom surface over the interior support. They attributed this cracking to thermal effects. Hilton (20) discussed the problems of obtaining the proper thickness of bridge decks due to vertical movements in the steel girders caused by thermal

---

* Numbers in parentheses refer to references in the Bibliography.

movements. Vertical movements of 0.4 inch were determined by field measurements for girders with span lengths of 42.5 feet. Researchers in Louisiana (37) have reported problems with swingspan bridges on the highway system from the warpage of structural members due to temperature variations. When the bridges were opened for river traffic, temperature warpage occurred making it sometimes impossible to close the bridges.

Other investigators have noted the significance of thermal movements and strains in concrete slab bridges. In 1973 Willems (43) tested a continuous three-span reinforced concrete slab bridge for the effects of dead load, live load, and temperature. Weldable strain gages were attached to the reinforcing steel to evaluate the effects of the various loadings. The bridge was skewed with the slab thickness varying from 24 inches at the ends to approximately 38 inches over the interior supports. Willems reached the following conclusion for this study: "The effect of temperature was not secondary but in many cases equaled or exceeded the effects of dead loading and overshadowed completely the effect of test live loading." Matlock and co-workers (30) tested a continuous three-span post-tensioned concrete slab bridge in 1970 for the effects of live load. The bridge was skewed with the slab thickness varying from 17 inches at the ends to 34 inches over the interior supports. Slope changes were measured by an inclinometer at 8 locations on the bridge and changes in surface strains were measured using a Berry Strain gage at 9 locations. Temperature effects were found to produce slope changes and surface strains of the same order of magnitude as the live loading.

1.2 Types of Thermal Stress and Movements

Temperature induced stresses and movements in bridges may be divided into three categories: 1) longitudinal and lateral expansion or contraction which may be restrained by abutments or friction at supports, 2) vertical movement and rotations which may be restrained by the indeterminancy of the structure, and 3) the nonlinear distribution of temperature over the depth of the structure. The first type of thermal stress and movement occurs when the structure experiences a rise or fall in the mean bridge temperature (18). As the mean bridge temperature increases or decreases, the structure expands or contracts. If this movement is prevented by abutments, pinned supports, or friction, axial stresses are developed in the structure. Considerable effort has been expended in determining the magnitudes of these longitudinal movements by researchers in Great Britain (10,17).

The second type of thermal stress may be attributed to the low thermal conductivity of concrete (7). Heat entering or leaving the top surface of a concrete slab is not conducted rapidly through the depth of the bridge slab or deck. Thus, temperature differentials are created between the bottom and top surfaces of the bridge. The top surface will expand or contract more than the bottom surface. This produces vertical movement and rotations in the bridge. Indeterminancy of the structure will restrain these rotations and vertical movements. This restraint creates reactions and stresses due to the temperature differential.

The third type is also a function of the low thermal conductivity of concrete and the depth of the section. The nonlinearity of the temperature distribution through the depth of concrete bridges has been observed in field measurements taken by several investigators (18,41,47). The nonlinear expansion due to this nonlinear form of the temperature distribution is restrained within the bridge if plane sections remain plane after deformation. This internal restraint produces a nonlinear stress distribution which is independent of boundary and support conditions. Therefore, even a simply supported beam can exhibit thermal stresses of this type if it has a nonlinear temperature distribution through its depth.

Most bridges exhibit stresses or movements due to all three categories mentioned above. Current specifications in this country provide specific design criteria only for movements of the first type, longitudinal or transverse movements.

1.3 Current Bridge Specifications

The AASHO Standard Specifications for Highway Bridges (1,2,3) governs the design of highway bridges in the United States. Sections of the specifications which are relevant to the study of thermal stress and movement are reproduced here.

1.2.15 - THERMAL FORCES

Provision shall be made for stresses or movements resulting from variations in temperature. The rise and fall in temperature shall be fixed for the locality in which the structure is to be constructed and shall be figured from an assumed temperature at the time of erection. Due consideration shall be given to the lag between air temperature and the interior temperature of massive concrete members or structures.

The range of temperature shall generally be as follows:

Metal Structures

Moderate climate, from 0 to 120 F.
Cold climate, from -30 to 120 F.

Concrete Structures	Temperature rise	Temperature fall
Moderate climate	30 F.	40 F.
Cold climate	35 F.	45 F.

. . . .

1.5.12 - SHRINKAGE AND TEMPERATURE REINFORCEMENT (Concrete)

Reinforcement for shrinkage and temperature stresses shall be provided near exposed surfaces of walls and slabs not otherwise reinforced. The total area of reinforcement provided shall be at least 1/8 square inch per foot and be spaced not farther apart than three times the wall or slab thickness nor 18 in.

. . . .

1.5.23 (B) EXPANSION AND CONTRACTION (Concrete)

(1) In general, provision for temperature changes shall be made in simple spans when the span length exceeds 40 feet.
(2) In continuous bridges, provision shall be made in the design to resist thermal stresses induced or means shall be provided for movement caused by temperature changes.

. . . .

1.5.23 (E) THERMAL AND SHRINKAGE COEFFICIENTS (Concrete)

(1) The thermal coefficient for normal weight concrete may be taken as 0.000006 per deg. F.
(2) The shrinkage coefficient for normal weight concrete may be taken as 0.0002.
(3) Thermal and shrinkage coefficients for lightweight concrete shall be determined for the type of lightweight aggregate used.

. . . .

1.7.16 - EXPANSION AND CONTRACTION (Steel)

In all bridges, provisions shall be made in the design to resist thermal stresses induced, or means shall be provided for movement caused by temperature changes. Provisions shall be made for changes in length of span resulting from live load stresses. In spans more than 300 feet long, allowance shall be made for expansion and contraction in the floor. The expansion end shall be secured against lateral movement.

. . . .

As can be observed from the above code sections, allowable values are given for the longitudinal thermal movement of steel bridges. Designers are also furnished with temperature ranges to be used in computing the longitudinal movement for concrete and metal structures. Minimum reinforcement requirements to prevent thermal cracking in concrete structures are stated. However, it should be noted that in the five sections of the code reprinted above, only thermal movements of the first type are discussed in detail. The only mention of thermal stress is: "Provision shall be made for stresses or movements resulting from variations in temperature." Also mentioned is: "In continuous bridges, provision shall be made in the design to resist thermal stresses induced . . ." Zuk (48) in a review of code provisions for thermal stress found that Germany, Austria, Sweden, and Japan were the only nations with detailed thermal stress provisions. Zuk also noted that the stress provisions in these codes were only for composite bridges.

Current design specifications do not give the designer any information or suggest any analytical tools regarding the conversion of temperatures to stresses or movements. In the United States specifications, temperatures are only stated regarding longitudinal movements. No mention is made of temperatures which produce stresses and movements of the second or third type discussed in Section 1.2.

1.4 Previous Research and Correlations with Field Measurements

Several researchers have developed analytical procedures to predict the temperature distributions in bridges and pavements from environmental conditions. Barber (4) presented a relationship between pavement temperatures, wind, precipitation, air temperature, and solar radiation as a function of the thermal properties of the pavements. Results were compared with field measurements for bituminous and concrete pavements. Satisfactory correlation was obtained for the surface temperatures.

Emerson (17,18) developed methods for calculating the distribution of temperature in concrete, steel, and composite bridges. The calculations were based on the level of solar radiation, wind speed, and air temperatures. Average values for the thermal properties as recommended by Billington (7) were used. The procedure involved an iterative finite difference solution of the partial differential equation for one-dimensional heat flow. In layered systems, experimental data was incorporated to derive methods for calculating the temperatures. Experimental data was applied to layered systems such as asphalt overlays on bridge decks, composite sections, and box girder bridges.

Recently Thepchatri (39) modified a two-dimensional finite element program developed by Wilson and Nickell (45) to include environmental conditions. Thepchatri's work was performed under the same research project as the author's study. Outgoing radiation was also included in the program. The program can, therefore, predict the temperature distribution over a period of days and nights. Two-dimensional heat flow was considered in order to account for the side heating of girders and variable cross sections. The heat conduction program was coupled to a stress analysis program based on beam theory. Studies were undertaken to determine the effects of environmental conditions found in Austin, Texas on three bridge types: 1) a post-tensioned concrete slab bridge, 2) a composite precast pretensioned bridge, and 3) a composite steel bridge. Thepchatri concluded that temperature induced stresses appeared to be significant.

Other researchers have used simplified equations in attempts to provide designers with simple empirical formulas. Zuk (48) presented such a formula for simply supported composite highway bridges. This formula was based on the temperature differential between the top and bottom of the slab and also the total depth of the section. In 1974 Berwanger (6) developed more complex equations which considered other factors affecting thermal stresses in composite bridges. This study accounted for the temperature differential over the depth of the bridge as well as the different coefficients of thermal expansion for concrete and steel. Berwanger concluded: "That the analyses of composite bridges for temperature stresses show significantly large values . . ."

Several attempts have been made to correlate measured thermally induced movements, reactions, or strains with analytical results. Generally these correlations have been unsatisfactory due to one or more of the following factors: 1) malfunctions of the experimental measuring equipment, 2) inaccuracies inherent in the analytical procedure, and 3) erratic structural response due to nonlinear frictional resistance at rollers or slip occurring between the slab and girder of a composite section.

In 1965 Zuk (47) tested composite bridges for thermal effects. Surface and internal temperature measurements were taken using thermocouples while periodic strain readings were taken using a 10 inch Whittemore strain gage. An analytical procedure was developed but correlation was not obtained with field measurements due to axial end restraints and erratic interface slip between the slab and girders.

In 1969 Wah and Kirskey (41) reported tests on a multibeam, simply supported bridge for thermal effects. The bridge was instrumented with 390 thermocouples and 14 concrete embedment gages during construction. A complex set of equations was developed to calculate the thermal stresses and movements. A computer program was developed to solve the equations. The vertical deflection at several locations on the bridge was measured by a transit. Correlation between computer and experimental results was very unsatisfactory. This is illustrated by Fig 1.1 which shows the comparison between analytical and experimental results for one station on August 8, 1967. Other stations and other tests showed similar discrepancies. The authors attributed the discrepancies to inaccuracies in the analytical model and to creep.

In 1971 Krishnamuthy tested a three-span continuous reinforced concrete bridge for thermal effects. Surface temperatures were measured using 32 thermocouples. Reactions were measured by jacking-up the bridge at the supports and installing load cells. Electrical strain gages had previously been affixed to the reinforcing steel. The internal temperature distribution of the bridge was computed using a finite difference equation corresponding to the heat conduction equation. A computer program was developed to solve for the reactions and moments using a slope deflection formulation. Measured changes in reactions were compared with analytical results. Poor correlation was obtained primarily due to malfunctions of the load

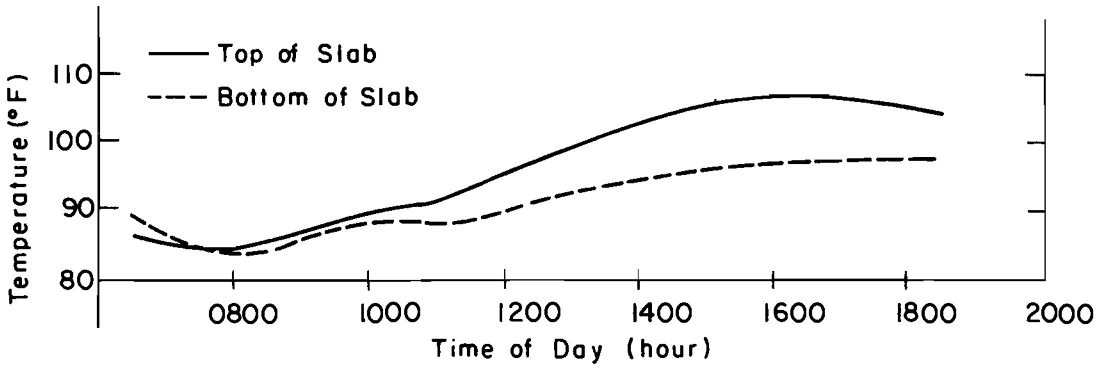

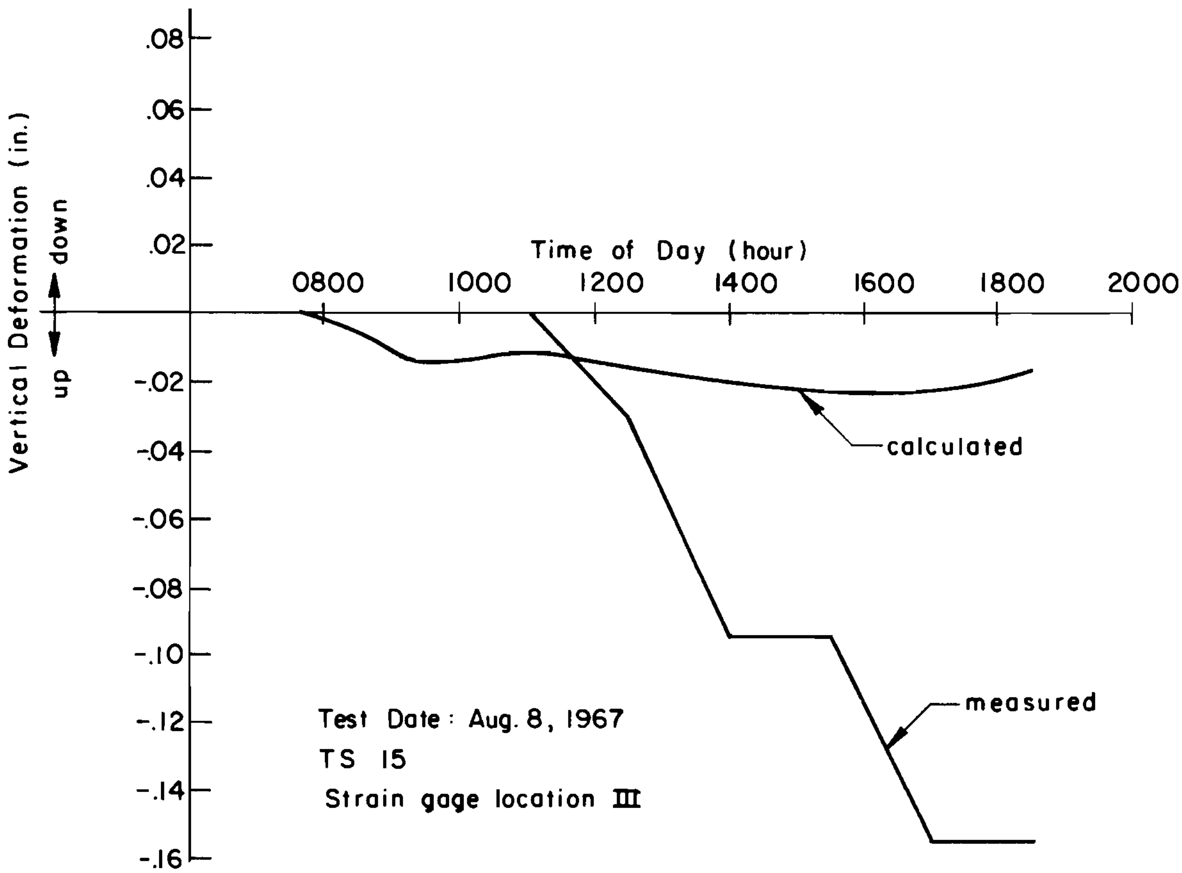

Fig 1.1. Lack of correlation between analytical and experimental results obtained by Wah and Kirksey (Ref 41).

cells. Reaction changes were then computed from the measured strains. Satisfactory correlation was achieved using these measurements but only after modifying the stiffness of the structure to account for a cracked section over the interior supports.

In summary, analytical methods have been developed to determine the temperature distributions in bridges due to environmental conditions. Satisfactory correlation between measured temperatures and computational predictions has been achieved using these methods. However, computational methods developed to predict temperature induced deflections, strains, and stresses of bridges have had limited success in the correlation of computational and experimental results. Most of these methods are applicable to only a limited number of geometric shapes and boundary conditions.

1.5 Objectives and Scope of this Study

Due to the limitations and lack of success in previous studies, this research project (23) was initiated in 1973 to determine temperature induced stresses in highway bridges. This research project was also motivated by the thermal response observed by Matlock and coworkers as discussed in Section 1.1. The basic objective of the research project is to quantitatively establish magnitudes of temperature induced movements by field tests on actual bridges and to correlate these results with a computer simulation of the structure subjected to the measured field temperatures. This study was separated into three phases to accomplish the objective: (1) development of a computational procedure to solve for the temperature distribution and temperature induced movements and stresses of bridges, (2) field measurements of bridge temperatures and temperature induced movements, and (3) correlation of measured bridge movements with computer results.

Finite element procedures are presented to determine the temperature distributions and temperature induced stresses of bridges in order to accomplish the first phase of this study. The heat conduction equation is assumed to be uncoupled from the equilibrium equation in these procedures. The inertia term is neglected in the equilibrium equation and the materials are assumed to behave elastically. In other words, the procedures are based on uncoupled quasi-static linear thermoelasticity. Various boundary conditions and geometries such as for the bridge shown in Fig 1.2 can accurately be represented by these procedures. A finite element program utilizing two-dimensional finite elements is used to solve for the temperature distribution of bridge type structures. This program uses either specified environmental conditions such as solar radiation and air temperatures or measured surface temperatures to solve for the temperature distribution in the bridge idealization. Once the temperature distribution is known, a finite element static analysis program is used to determine the temperature induced stresses and movements. This program employs two-dimensional finite elements in a three-dimensional global assemblage. Membrane and plate bending elements are used. Thermal forces are calculated based on a quartic distribution of temperature through the thickness of each element and a linear distribution of temperature over the surface of each element. The finite element procedure is discussed in detail in Chapter 2.

It should be emphasized that it was not within the intended scope of this study to take extensive field measurements to accomplish the second phase of this study. Rather, selected measurements of temperatures and bridge movements were to be taken to validate the computational procedure. It was felt that neither elaborate instrumentation nor large numbers of field measurements would be necessary in order to provide a meaningful correlation between the field measured movements and computer results. In keeping with this philosophy, a portable temperature probe was developed to measure the surface temperatures at various locations on the bridges to be tested. A mechanical inclinometer was used to determine the slope changes induced by temperature.

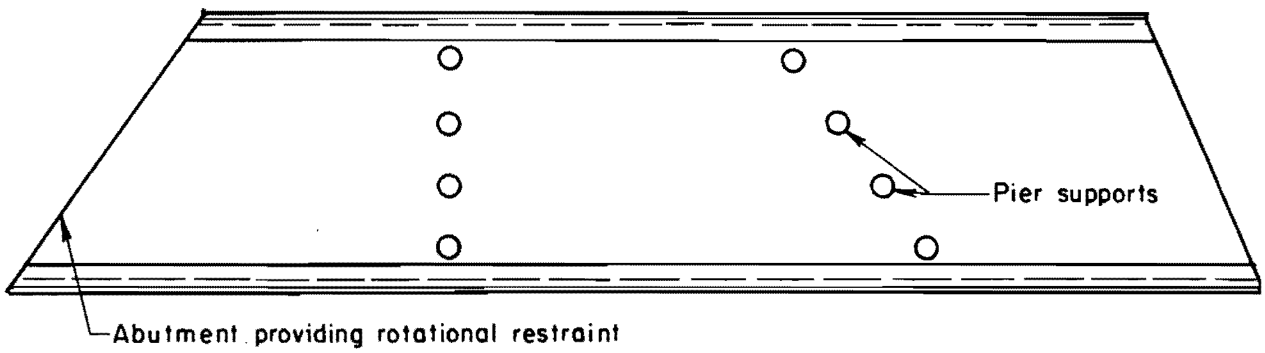

(a) Plan view.

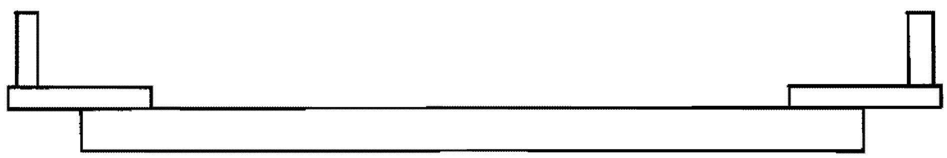

(b) Typical cross section.

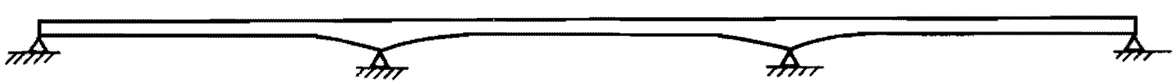

(c) Bridge elevation.

Fig 1.2. Continuous concrete slab structure with variable skew.

Discussion and details of the instrumentation are presented in Chapter 4.

Field measurements were performed on two bridges. The first bridge tested was the same one tested by Matlock and co-workers as discussed in section 1.1. The second bridge tested was a two-span continuous for live load pedestrian overpass. Both tests were performed during daylight hours. Summaries of the field measurements and computer results are presented in Chapter 4. More detailed information regarding these field tests is presented in Appendices A and B. Correlations between field measured movements and computer results are presented in Chapter 5 for the third phase of this study.

CHAPTER 2. FINITE ELEMENT PROCEDURE

2.1 Introduction

Classical solutions are available for the thermal stresses and transient temperature distributions in plates, cylinders, and beams. Solutions for these cases may be found in texts by Timoshenko and Goodier (40), Boley and Weiner (8), and Johns (21) as well as numerous other references. Unfortunately, these classical solutions are restricted to a limited number of boundary conditions and geometrical configurations. Consequently, they have limited applicability to the diurnal heating thermal stress analyses of bridge-type structures.

A general method of analysis is required to determine the transient temperature distributions and temperature induced movements and stresses for bridge-type structures. The finite element method, the subject of texts by Desai and Abel (15) and Zienkiewicz (46), is such a general method. In the finite element method the structure is approximated by an assemblage of a finite number of discrete elements interconnected at nodal points. For the thermal stress analysis, piecewise continuous displacement or temperature fields are assumed in each element. Then, a set of algebraic equations is obtained by the application of variational principles. The unknown displacements or temperatures are obtained by the solution of these equations. In the subject study, previously existing finite element computer programs were modified and extended for the transient heat conduction analysis (45) and the thermal stress analysis (24). A discussion of the finite element procedures for these analyses is presented in this chapter.

2.2 Environmental Variables

Before discussing the finite element heat conduction procedure, it is necessary to briefly discuss the environmental variables which contribute to the diurnal heating of bridge-type structures. Past researchers (18,39) have found that the three main environmental variables are the solar radiation, air temperature, and wind speed.

The solar radiation is the major contributor to the heating of bridges. The intensity of the solar radiation on a horizontal surface is a function of the latitude, elevation, atmospheric contamination, and time of the year and day. Measured solar radiation intensities on a horizontal surface may be obtained from U.S. Weather Bureau records for various meteorological stations. Empirical relationships have been developed to predict the daily variation of the solar radiation intensity on horizontal surfaces. For instance, Gloyne (19) has empirically shown that the daily variation can be approximated by a $(\text{sine})^2$ curve. Also, mathematical models have been developed to predict the radiation intensity on surfaces with arbitrary orientation (14).

The amount of radiation absorbed by a surface is a function of the color and texture of the surface. Values of the absorptivity of concrete have been reported by Billington (7) to lie between 0.5 and 0.8. Emerson (18) and Thepchatri (39) have obtained satisfactory correlation with measured surface temperatures on bridges using a value of 0.5 for the absorptivity.

The wind speed and air temperature contribute to the heat exchange between the surface of a bridge and the air by natural and/or forced convection. The heat gain or loss is greater by forced convection than by natural convection. The heat loss from a surface due to forced convection is given by (8)

$$Q_c = h_c(T_s - T_a) \tag{2.1}$$

where

Q_c = heat gain or loss by convection in $\text{BTU/ft}^2\text{/hr}$,

T_s = surface temperature in °F ,

T_a = air temperature in °F , and

h_c = surface film coefficient in BTU/ft^2/hr/°F .

The surface film coefficient is a function of the wind speed on the surface (4). For a wind speed of 7 mph, Barber (4) stated a value of 4 BTU/ft^2/hr/°F .

2.3 Finite Element Heat Conduction Procedure

The advantages of the finite element method over other numerical solutions of the heat conduction problem are numerous. For example, Emerson's (18) use of experimental data to determine an equivalent thickness of concrete to represent an asphalt overlay for a finite difference solution is not necessary in the finite element method since bodies composed of more than one material can easily be represented. The method has previously been used for the heat conduction analyses of concrete dams (44), and rocket nozzles (9).

A two-dimensional spatial idealization was chosen for the heat conduction analysis. In general, the flow of heat will be negligible in the longitudinal direction of a bridge. The heat will flow primarily through the depth of a section since the top and bottom surfaces are the main locations of heat input due to solar radiation and/or convection. Bridges with north to south orientations may experience significant side heating; thus requiring a two-dimensional idealization. Also, a two-dimensional idealization is required for bridges with girders since heat will flow through the depth and across the width of the girders.

Formulations of the finite element method for heat conduction analyses have been based on a variational approach (5,45). However, Wilson (44) has presented a physical interpretation of the heat conduction process which results in the same set of finite element equations as obtained by the variational approach. Wilson's physical interpretation is based on heat flow equilibrium for each nodal point of the finite element idealization. This equilibrium equation has the following form for each nodal point:

Rate at which heat is stored in elements adjacent to node	+	Rate at which heat flows from elements adjacent to node	=	Rate at which external heat enters node	(2.2)

For the entire structure, Wilson states that the above representation may be written in matrix form as

$$\underset{\approx}{C}\,\dot{\underset{\sim}{T}}(t) + \underset{\approx}{K}\,\underset{\sim}{T}(t) = \underset{\sim}{Q}(t) \tag{2.3}$$

where

$\underset{\approx}{C}$ is defined as the heat capacity matrix and is a function of the specific heat and density of the material in each element,

$\underset{\approx}{K}$ is defined as the conductivity matrix and is a function of the conductivity of the material in each element,

$\underset{\sim}{T}(t)$ is the vector containing the nodal point temperatures which may be a function of time, t ,

$\dot{\underset{\sim}{T}}(t)$ is the vector containing the time rate of change of nodal point temperatures, and

$\underset{\sim}{Q}(t)$ is the nodal point vector containing the external heat rates at each nodal point (e.g., solar radiation).

An existing finite element program based on two-dimensional heat flow (45) was selected for the subject study. The element matrices corresponding to the matrices in Eq 2.3 are derived based on a triangular element with a linear temperature field over the element:

$$T(x,y) = \{1 \;\; x \;\; y\} \begin{Bmatrix} T_i \\ T_j \\ T_k \end{Bmatrix} \tag{2.4}$$

where T_i , T_j , and T_k are the temperatures at the three nodes of the element and x and y are the in-plane coordinate axes. A quadrilateral element composed of four triangles is also incorporated in the program with the equation at the internal node removed by static condensation. The coefficients of $\underset{\approx}{K}$ and $\underset{\approx}{C}$ in Eq 2.3 for the triangular and quadrilateral elements may be found in references 39, 44, 45. After modification of $\underset{\approx}{K}$ and $\underset{\sim}{Q}(t)$ for convective boundary conditions of Eq 2.1, Eq 2.3 becomes

$$\underset{\approx}{C}\,\dot{T}(t) + \underset{\approx}{K}^{*}\,\underset{\sim}{T}(t) = \underset{\sim}{Q}^{*}(t) \tag{2.5}$$

If the temperatures at each nodal point are assumed to vary linearly within the time increment, Δt , then the rate of change of the nodal point temperatures is constant and is given by

$$\dot{T}(t) = \frac{T(t) - T(t-\Delta t)}{\Delta t} \tag{2.6}$$

for time t .

Substituting 2.6 into 2.5 yields

$$\underset{\approx}{\bar{K}}\,\underset{\sim}{T}(t) = \bar{Q}(t) \tag{2.7}$$

where

$$\underset{\approx}{\bar{K}} = \underset{\approx}{K}^{*} + \frac{1}{\Delta t}\underset{\approx}{C} \tag{2.8}$$

and

$$\bar{Q}(t) = Q^{*}(t) + \frac{1}{\Delta t}\underset{\approx}{C}\,T(t-\Delta t) \tag{2.9}$$

Equation 2.7 may then be solved by Gaussian elimination for the temperatures at time t , $\underset{\sim}{T}(t)$. Since there is only one degree-of-freedom at each nodal point, the solution time is relatively small for each time increment. Modifications performed on the computer program were related primarily to improving the finite element input data generation.

2.4 Finite Element Procedure for the Thermal Stress Analysis

A linear elastic thermal stress analysis is performed to determine the thermally induced stresses and deflections after an approximation to the temperature distribution has been determined. A finite element computer program (24), PLS6DOF, which was developed for the static analysis of bridges was extended to perform a thermal stress analysis for bridge-type structures. The finite element representation of the equilibrium equation for the elastic thermal stress analysis is

$$\underset{\approx}{K}'\underset{\sim}{r} = \underset{\sim}{f} \tag{2.10}$$

where

- $\underset{\approx}{K}'$ is the finite element approximation of the stiffness of the structure with boundary constraints included,
- $\underset{\sim}{r}$ is the nodal point displacement vector, and
- $\underset{\sim}{f}$ is the force vector containing the nodal point forces due to temperature and/or other loadings.

The stiffness $\underset{\approx}{K}'$ is formed by assembling all the individual element stiffnesses and modifying for boundary conditions.

The finite elements used are two-dimensional but may be assembled in a three-dimensional assemblage. Each element stiffness contains membrane and plate bending components which are assumed to be uncoupled at the element level. Triangular and quadrilateral elements are incorporated in the program. The nodal point displacement vector, $\underset{\sim}{r}$, contains six degrees-of-freedom (DOF) at each nodal point - three rotational and three displacement components. The force vector, $\underset{\sim}{f}$, is formed by assembling the element force vectors due to temperature, body forces, and pressure loadings. Concentrated nodal forces are also included in this vector.

Since much of the background information and element stiffness derivations related to the program PLS6DOF is contained in references 22 and 24 , only a brief discussion of the finite elements used in the program will be presented. A more detailed discussion will be presented in Sections 2.42 and 2.43 regarding the extensions of the program for the thermal stress analysis.

2.41 Summary of Finite Elements in PLS6DOF

There are three membrane elements and one plate bending element available in the program. The three membrane elements and their nodal point DOF are shown in Fig 2.1. The stiffness of all three elements is derived based on the assumption of plane stress. The element shown in Fig 2.1a is the constant strain triangle (CST). The stiffness of this element is derived from a linear displacement assumption over the surface of the element. As shown in Fig 2.1a each node of the element has two DOF resulting in a total of six for the entire element. The stiffness properties of this element have been shown to be inferior to the other membrane elements in the program (42).

The quadrilateral element shown in Fig 2.1b is composed of four constrained linear strain triangles (CLST). Quadratic expansions are used for the displacements in the interior of the quadrilateral while the displacements along the edges are constrained to be linear (22). Each nodal point has two DOF and the DOF at the internal nodal points are removed by static condensation.

The third membrane element shown in Fig 2.1c is called the QM5(16). The displacement fields in this element are assumed to be linear along the edges but quadratic in the interior of the element. Improved response was obtained in this element by constraining the shear strain to be constant. The DOF at the interior nodal point are removed by static condensation. The stiffness properties of this element do not deteriorate as rapidly as for the other elements when the length to width ratio of the element's sides becomes large. However, the stiffness properties of the QM5 do deteriorate when the element becomes distorted.

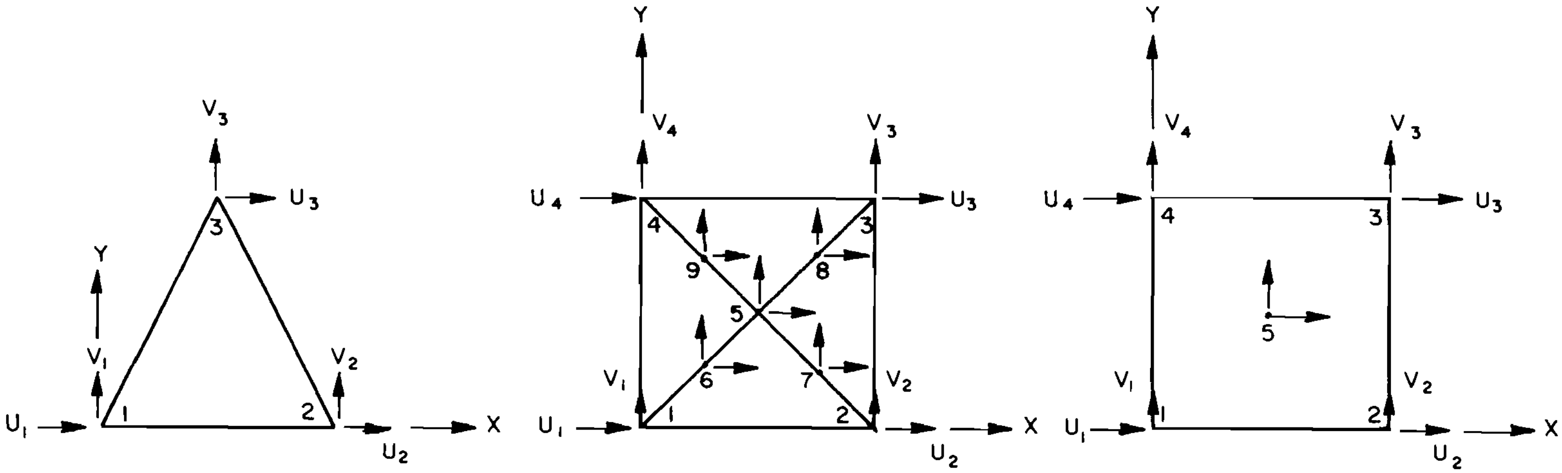

a) CST triangle. b) CLST quadrilateral*. c) QM5 quadrilateral*.

*Interior DOF removed by static condensation

Fig 2.1. Membrane elements available for thermal stress analysis.

In general, the QM5 quadrilateral is preferable to the CLST quadrilateral except when the element geometry is skewed. The CST triangle is recommended only when it is required for the geometric idealization of the structure.

There is basically only one plate bending element in the program, PLS6DOF. This element is a triangular element called the HCT(11). The stiffness of this element is derived based on Kirchhoff's plate bending assumptions and the assumption that the element is in a state of plane stress. Quadrilateral elements are composed of four HCT triangles. The triangle and quadrilateral elements are shown in Fig 2.2 with their appropriate DOF. The internal DOF are removed by static condensation for the quadrilateral element. Complete displacement and slope compatability is achieved in the HCT element by subdividing the element into three subtriangles as shown in Fig 2.2a. Separate cubic shape functions for the w displacement are expressed for each subtriangle Using the shape functions suggested by Felippa, Johnson (22) illustrated that compatability at the interior point, point 0 in Fig 2.2a, is automatically achieved.

The CST and the HCT triangles are combined when the structural idealization dictates the use of a triangular element. The resulting element has 5 DOF at each nodal point and thus a total of 15 DOF for the element. The combination of the CLST or QM5 quadrilaterals with the plate bending quadrilateral composed of four HCT's results in an element with 20 DOF - 5 DOF at each corner nodal point.

The sixth DOF for each element was included using an approach suggested by Zienkiewicz (46). Zienkiewicz's approach used a fictitious rotational stiffness for the rotational DOF normal to the element. The rotational stiffness coefficients were constructed such that equilibrium was preserved at the element level. However, Zienkiewicz pointed out that the fictitious stiffness will affect the response of the structure if all the elements are not co-planar. In general, this fictitious stiffness will stiffen the structure if all the elements are not co-planar.

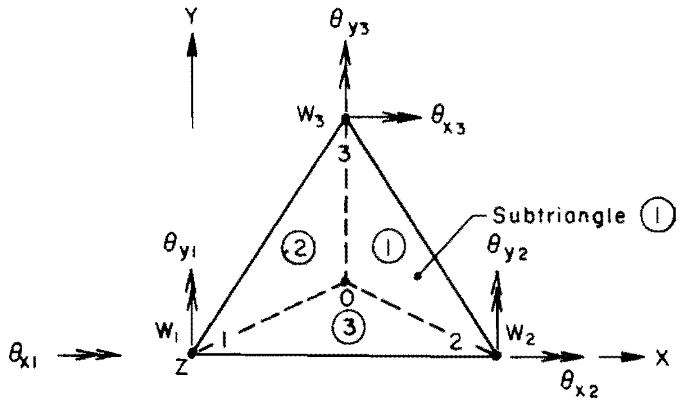

a) HCT triangle.

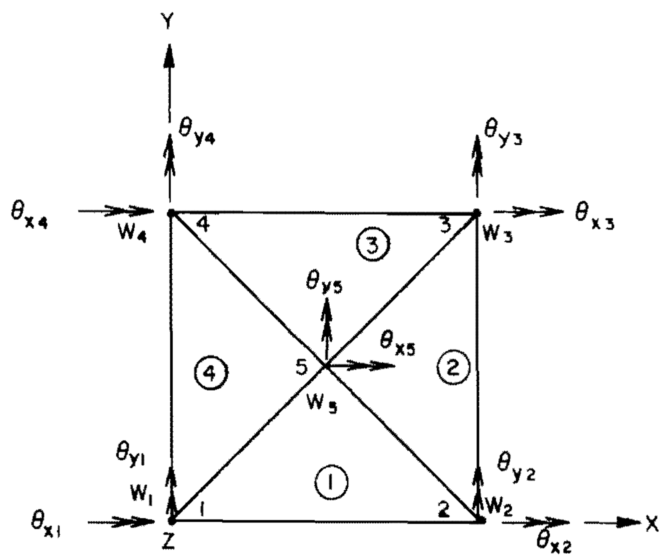

b) Quadrilateral composed of 4 HCT triangles.
(Interior DOF removed by static condensation)

Fig 2.2. Plate bending element available for thermal stress analysis.

The fictitious rotational stiffness coefficients recommended by Zienkiewicz (46) have the following form in the equilibrium equation for the triangular element:

$$\begin{Bmatrix} M_{z1} \\ M_{z2} \\ M_{z3} \end{Bmatrix} = E\,\bar{\alpha}\,t\,A \begin{bmatrix} 1 & -0.5 & -0.5 \\ & 1 & -0.5 \\ \text{Sym.} & & 1 \end{bmatrix} \begin{Bmatrix} \theta_{z1} \\ \theta_{z2} \\ \theta_{z3} \end{Bmatrix} \tag{2.11}$$

where E is the modulus of elasticity of the element,
$\bar{\alpha}$ is a constant to be discussed below,
t is the average thickness of the corner nodes of the element, and
A is the area of the element.

The stiffness components above are about the normal to each element, the z-direction in Fig 2.2a. For a rectangular element, the fictitious rotational stiffness presented by Thepchatri (39) is

$$\begin{Bmatrix} M_{z1} \\ M_{z2} \\ M_{z3} \\ M_{z4} \end{Bmatrix} = E\,\bar{\alpha}\,t\,A \begin{bmatrix} 1.5 & -0.5 & -0.5 & -0.5 \\ & 1.5 & -0.5 & -0.5 \\ & & 1.5 & -0.5 \\ \text{Sym.} & & & 1.5 \end{bmatrix} \begin{Bmatrix} \theta_{z1} \\ \theta_{z2} \\ \theta_{z3} \\ \theta_{z4} \end{Bmatrix} \tag{2.12}$$

These components are about the normal to the quadrilateral element in Fig 2.2b. Zienkiewicz recommends a value for $\bar{\alpha}$ in Eqs 2.11 and 2.12 of 0.03 or less. A constant of 0.02 was used in PLS6DOF (24).

2.42 Thermal Forces

The major modifications made to the program PLS6DOF were related to the calculation of equivalent nodal point thermal forces. These forces are the forces required to prevent the initial thermal strains due to temperature in the structure. The internal work done on an element by the temperature change in the element is given by (46)

$$W_I = -\int_V \sigma^T \underset{\sim}{\varepsilon}_o \, dV \tag{2.13}$$

where for plane stress

$$\underset{\sim}{\sigma}^T = \{\sigma_x \ \sigma_y \ \sigma_{xy}\} \tag{2.14}$$

and for free thermal expansion in an isotropic material

$$\underset{\sim}{\varepsilon}_o = \begin{Bmatrix} \epsilon_{x_o} \\ \epsilon_{y_o} \\ 2\epsilon_{xy_o} \end{Bmatrix} = \begin{Bmatrix} \alpha \ \Delta T(x,y,z) \\ \alpha \ \Delta T(x,y,z) \\ 0 \end{Bmatrix} \tag{2.15}$$

where α is the coefficient of thermal expansion and $\Delta T(x,y,z)$ is the polynomial expression for the change in temperature over the volume, V, of the element from a reference temperature.

The internal work (and consequently the equivalent nodal forces) may also be uncoupled into membrane and bending components:

$$W_I = -\int_V \underset{\sim}{\sigma}_M^T \underset{\sim}{\varepsilon}_o \, dV - \int_V \underset{\sim}{\sigma}_B^T \underset{\sim}{\varepsilon}_o \, dV \tag{2.16}$$

where $\underset{\sim}{\sigma}_M$ and $\underset{\sim}{\sigma}_B$ are the membrane and bending stresses respectively and are given by

$$\underset{\sim}{\sigma}_M = \underset{\approx}{D} \, \underset{\sim}{\varepsilon}_M \tag{2.17}$$

$$\underset{\sim}{\sigma}_B = \underset{\approx}{D} \, \underset{\sim}{\varepsilon}_B \tag{2.18}$$

In Eqs 2.17 and 2.18 $\underset{\approx}{D}$ is the material stress strain relationship. For a linear elastic isotropic material in a state of plane stress, $\underset{\approx}{D}$

is given by

$$\underset{\approx}{D} = \left[\frac{E}{1-\nu^2} \begin{matrix} 1 & \nu & 0 \\ \nu & 1 & 0 \\ 0 & 0 & \frac{1-\nu}{2} \end{matrix} \right] \tag{2.19}$$

where E is the modulus of elasticity and ν is Poisson's ratio. The strains $\underset{\sim}{\epsilon}_M$ and $\underset{\sim}{\epsilon}_B$ in Eqs 2.17 and 2.18 are the membrane and bending strains respectively and are given by

$$\underset{\sim}{\epsilon}_M = \begin{Bmatrix} u,_x \\ v,_y \\ u,_y + v,_x \end{Bmatrix} \tag{2.20}$$

and

$$\underset{\sim}{\epsilon}_B = \begin{Bmatrix} -\,zw,_{xx} \\ -\,zw,_{yy} \\ -\,2zw,_{xy} \end{Bmatrix} \tag{2.21}$$

where u and v are the membrane displacements in the x- and y-directions and w is the displacement normal to the element in the z-direction. In Eqs 2.20 and 2.21 the $,_x$ denotes the $\frac{\partial}{\partial x}$ and $,_{xx}$ denotes the $\frac{\partial}{\partial x^2}$, etc.

Now, we introduce shape functions for the u , v , and w displacements:

$$u(x,y) = \underset{\sim}{\phi}_u^T \underset{\sim}{u}_e \tag{2.22}$$

$$v(x,y) = \underset{\sim}{\phi}_v^T \underset{\sim}{v}_e \tag{2.23}$$

and

$$w(x,y) = \underset{\sim}{\phi}_w^T \underset{\sim}{w}_e \tag{2.24}$$

The total displacement vector for the element, $\underset{\sim}{r}_e$, is given by

$$\underset{\sim}{r}_e^T = \{\underset{\sim}{u}_e, \underset{\sim}{v}_e, \underset{\sim}{w}_e\} \tag{2.25}$$

For a triangular element with three nodal points and 5 DOF at each nodal point, $\underset{\sim}{r}_e$ is

$$\underset{\sim}{r}_e^T = \{u_1, u_2, u_3, v_1, v_2, v_3, w_1, \theta_{x1}, \theta_{y1}, w_2, \theta_{x2}, \theta_{y2}, w_3, \theta_{x3}, \theta_{y3}\} \tag{2.26}$$

where

$$\theta_{xi} = (w,_y)_i \qquad i = 1,2,3$$

and

$$\theta_{yi} = -(w,_x)_i \qquad i = 1,2,3$$

The locations of the displacement and rotation components of Eq 2.26 have been shown in 2.1 and 2.2.

Substituting the shape functions in Eqs 2.22, 2.23, and 2.24 into Eqs 2.20 and 2.21 yields

$$\underset{\sim}{\varepsilon}_M = \left\{ \begin{array}{l} \underset{\sim}{\phi}_{u,x}^T \; \underset{\sim}{u}_e \\ \underset{\sim}{\phi}_{v,y}^T \; \underset{\sim}{v}_e \\ \underset{\sim}{\phi}_{u,y}^T \; \underset{\sim}{u}_e + \underset{\sim}{\phi}_{v,x}^T \; \underset{\sim}{v}_e \end{array} \right\} \tag{2.27}$$

and

$$\underset{\sim}{\varepsilon}_B = -z \left\{ \begin{array}{l} \underset{\sim}{\phi}_{w,xx}^T \\ \underset{\sim}{\phi}_{w,yy}^T \\ 2\underset{\sim}{\phi}_{w,xy}^T \end{array} \right\} \underset{\sim}{w}_e \tag{2.28}$$

Now expressing

$$\underset{\sim}{\epsilon}_M = \left\{ \underset{\approx}{B}_M \bar{\underset{\sim}{u}}_e \right\} \tag{2.29}$$

where

$$\bar{\underset{\sim}{u}}_e^T = \{ \underset{\sim}{u}_e \ \underset{\sim}{v}_e \} \tag{2.30}$$

and

$$\underset{\sim}{\epsilon}_B = \left\{ \underset{\approx}{B}_B \ \underset{\sim}{w}_e \right\} \tag{2.31}$$

and substituting 2.29 and 2.31 into 2.16 yields

$$W_I = - \int_V \bar{\underset{\sim}{u}}_e^T \ \underset{\approx}{B}_M^T \ \underset{\approx}{D} \ \underset{\sim}{\epsilon}_o \, d\,V - \int_V \underset{\sim}{w}_e \ \underset{\approx}{B}_B^T \ \underset{\approx}{D} \ \underset{\sim}{\epsilon}_o \, d\,V \tag{2.32}$$

By equating the external work done by the nodal point loads to the internal work in Eq 2.32 the equivalent nodal point forces are derived. The membrane forces are given by

$$\underset{\sim}{f}_{e_M} = - \int_V \underset{\approx}{B}_M^T \ \underset{\approx}{D} \ \underset{\sim}{\epsilon}_o \, d\,V \tag{2.33}$$

and the bending forces are given by

$$\underset{\sim}{f}_{e_B} = - \int_V \underset{\approx}{B}_B^T \ \underset{\approx}{D} \ \underset{\sim}{\epsilon}_o \, d\,V \tag{2.34}$$

The membrane and plate bending equivalent nodal point forces may be evaluated using Eqs 2.33 and 2.34. The shape functions of the constant strain triangle (CST) were chosen for the evaluation of the membrane thermal forces. Thermal forces for quadrilateral elements were evaluated using two triangles. The shape functions for the CST are

$$\underset{\sim}{\phi}_u^T = \{ L_1 \ L_2 \ L_3 \} \tag{2.35}$$

and

$$\underset{\approx}{\phi}_v^T = \{L_1\ L_2\ L_3\} \tag{2.36}$$

where L_1, L_2, and L_3 are triangular coordinates as shown in Fig 2.3a. Constants used to describe the geometry of the triangle are also shown in Fig 2.3b. The matrix $\underset{\approx}{B}_M$ is (15,22)

$$\underset{\approx}{B}_M = \frac{1}{2A} \begin{bmatrix} b_1 & b_2 & b_3 & 0 & 0 & 0 \\ 0 & 0 & 0 & a_1 & a_2 & a_3 \\ a_1 & a_2 & a_3 & b_1 & b_2 & b_3 \end{bmatrix} \tag{2.37}$$

where A is the area of the triangle and is given by

$$A = a_3 b_2 - a_2 b_3 \tag{2.38}$$

and the a_i and b_i (i=1,2,3) in 2.37 and 2.38 are shown in Fig 2.3b.

The next step in the calculation of the thermal forces is to determine a representation of the temperature distribution, $\Delta T(x,y,z)$ for use in Eq 2.15. An analysis of temperature distributions obtained using the heat conduction program for the diurnal heating of concrete bridge slabs revealed that a quartic polynomial through the thickness provided a satisfactory approximation. An example is presented in Chapter 3 to illustrate the fit of the quartic polynomial to predicted temperature distributions determined by the heat conduction analysis. The temperature, $\Delta T(x,y,z)$ was allowed to vary linearly over the surface of the element. The expression for $\Delta T(x,y,z)$ is

$$\Delta T(x,y,z) = \{L_1\ L_2\ L_3\} \begin{Bmatrix} \Delta T_1(z) \\ \Delta T_2(z) \\ \Delta T_3(z) \end{Bmatrix} \tag{2.39}$$

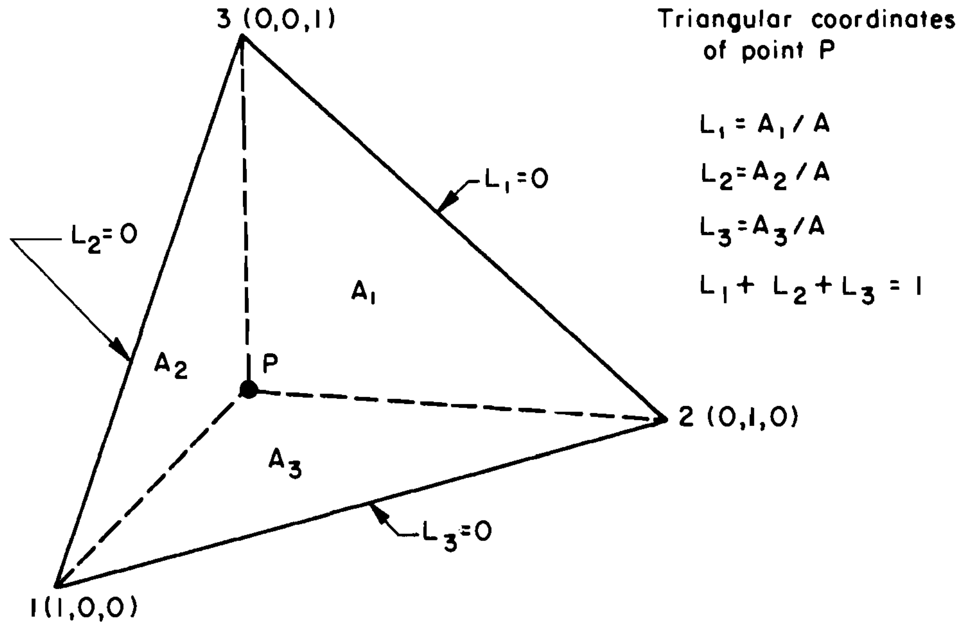

a) Triangular coordinates.

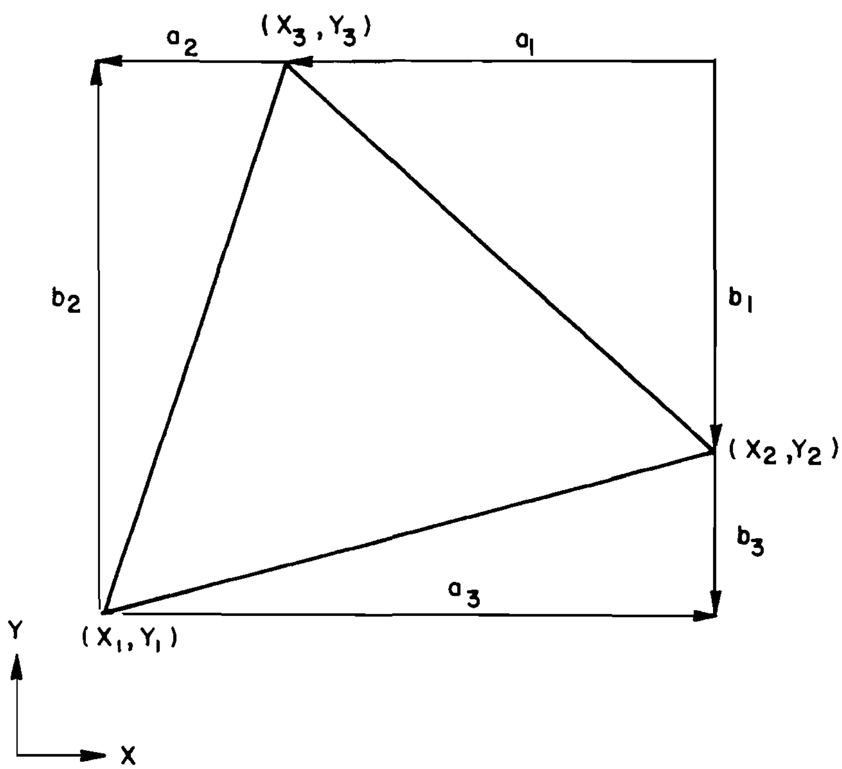

b) Geometry of triangle.

Fig 2.3. Triangular Coordinates and Geometry.

where the $\Delta T_i(z)$ (i=1,2,3) describe the temperature variation through the thickness at nodal point i of the triangle. For a quartic temperature distribution, the assumed ΔT_i may be represented as

$$\Delta T_i(z) = A_i z^4 + B_i z^3 + C_i z^2 + D_i z + E_i \tag{2.40}$$

The constants A_i , B_i , C_i , D_i , and E_i are determined from five temperatures through the thickness of the element at each nodal point. The five temperatures used in this study and their locations through the thickness are shown in Fig 2.4. Also shown in Fig 2.4 are the constants A_i through E_i expressed in terms of the five temperatures through the thickness.

Substituting 2.39 into 2.33 yields

$$\underset{\sim}{f}_{e_M} = -\int_V \alpha \, \underset{\approx}{B}_M^T \, \underset{\approx}{D} \begin{Bmatrix} 1 \\ 1 \\ 0 \end{Bmatrix} \{L_1 \; L_2 \; L_3\} \begin{Bmatrix} \Delta T_1(z) \\ \Delta T_2(z) \\ \Delta T_3(z) \end{Bmatrix} dV \tag{2.41}$$

Substituting Eq 2.37 into 2.42 and performing the integration yields

$$\underset{\sim}{f}_{e_M} = \begin{Bmatrix} f_{x1} \\ f_{x2} \\ f_{x3} \\ f_{y1} \\ f_{y2} \\ f_{y3} \end{Bmatrix} = -\frac{E\alpha T'}{6(1-\nu)} \begin{Bmatrix} b_1 \\ b_2 \\ b_3 \\ a_1 \\ a_2 \\ a_3 \end{Bmatrix} \tag{2.42}$$

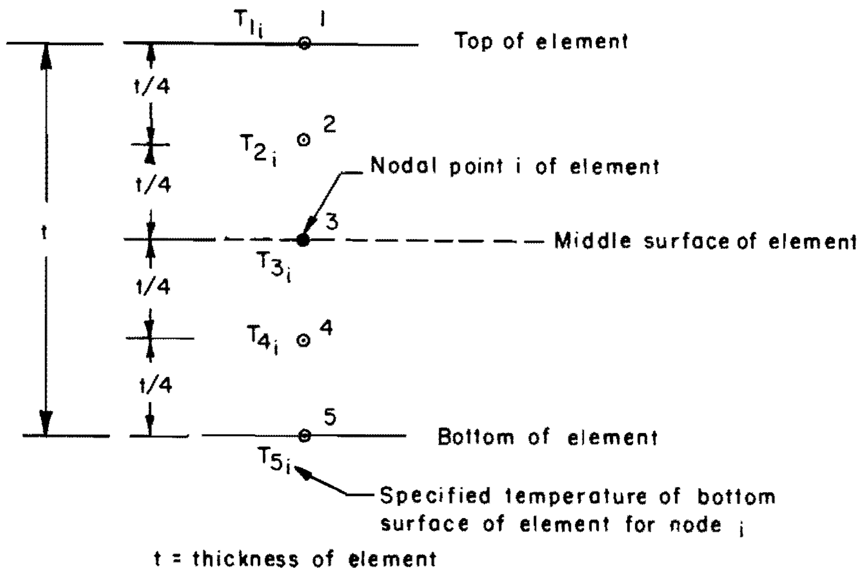

a) Specified nodal point temperatures.

$$A_i = \frac{128}{3t^4}\left(\frac{T1_i + T5_i + 6T3_i}{4} - T2_i - T4_i\right)$$

$$B_i = \frac{16}{3t^3}\left(T1_i - T5_i - 2T2_i + 2T4_i\right)$$

$$C_i = \frac{32}{3t^2}\left(T2_i + T4_i - \left(\frac{T1_i + T5_i}{16}\right) - \frac{15}{8}T3_i\right)$$

$$D_i = \frac{8}{3t}\left(T2_i - T4_i - \left(\frac{T1_i - T5_i}{8}\right)\right)$$

$$E_i = T3_i$$

b) Constants in Eq 2.40.

Fig 2.4. Specified temperatures at each nodal point of element.

where

$$T' = (A_1 + A_2 + A_3)\, t^5/80 + (C_1 + C_2 + C_3)\, t^3/12 + (E_1 + E_2 + E_3)\, t \qquad (2.43)$$

and t is the thickness of the element. As expected, only the symmetric terms $(z^4, z^2, 1)$ in Eq 2.40 contribute to the membrane thermal forces.

The shape functions of the HCT triangle were chosen for the evaluation of the plate bending thermal forces. The thermal forces are calculated for each subtriangle and the contributions to each of the element's corner nodal points are summed to determine the total thermal force for the triangle.

The thermal plate bending forces from Eq 2.34 are

$$\underset{\sim}{f}_{e_B} = -\int_V \underset{\approx}{B}_B\, \underset{\approx}{D}\, \underset{\sim}{\varepsilon}_o\, dV$$

For each subtriangle of the HCT, the $\underset{\approx}{B}_B$ matrix is expressed as a linear combination of the curvatures at each corner of the subtriangle (22):

$$\underset{\approx}{B}_B = -z\, \underset{\approx}{L}\, \underset{\approx}{\varepsilon}'_{(i)} \qquad (2.44)$$

where

$$\underset{\approx}{L} = \begin{bmatrix} L_1 & L_2 & L_3 & 0 & 0 & 0 & 0 & 0 & 0 \\ 0 & 0 & 0 & L_1 & L_2 & L_3 & 0 & 0 & 0 \\ 0 & 0 & 0 & 0 & 0 & 0 & L_1 & L_2 & L_3 \end{bmatrix} \qquad (2.45)$$

and

$$\underset{\approx}{\varepsilon}'^{T}_{(i)} = \{\underset{\sim}{\varepsilon}_{x1}\; \underset{\sim}{\varepsilon}_{x2}\; \underset{\sim}{\varepsilon}_{x0}\; \underset{\sim}{\varepsilon}_{y1}\; \underset{\sim}{\varepsilon}_{y2}\; \underset{\sim}{\varepsilon}_{y0}\; \underset{\sim}{\varepsilon}_{xy1}\; \underset{\sim}{\varepsilon}_{xy2}\; \underset{\sim}{\varepsilon}_{xy0}\} \qquad (2.46)$$

The $\underset{\sim}{\varepsilon}_{x1}$, $\underset{\sim}{\varepsilon}_{x2}$ --- $\underset{\sim}{\varepsilon}_{xy0}$ are obtained from differentiating the shape function for the particular subtriangle and evaluating the result at the corners of the subtriangle. It should also be noted that the triangular coordinates in Eq 2.45 are those of the particular subtriangle being considered.

Substituting Eq 2.44 into 2.34 yields

$$\underset{\sim}{f}_{e_B} = \epsilon'^{T}_{(i)} \int_V z \, \underset{\approx}{L}^T \underset{\approx}{D} \, \underset{\sim}{\epsilon}_o \, dV \tag{2.47}$$

The temperature variation $\Delta T(x,y,z)$ is now expressed as

$$\Delta T(x,y,z) = \{L_1 \ L_2 \ L_3\} \begin{Bmatrix} \Delta T_1(z) \\ \Delta T_2(z) \\ \Delta T_0(z) \end{Bmatrix} \tag{2.48}$$

where $\Delta T_0(z)$ is the temperature distribution through the thickness at point 0 of the triangle. Again, the triangular coordinates in 2.48 are for the particular subtriangle being considered. Substituting 2.48 into $\underset{\sim}{\epsilon}_o$ and then expanding Eq 2.47 yields

$$\underset{\sim}{f}_{e_B} = \underset{\approx}{\epsilon}'^{T}_{(i)} \int_V z \, \underset{\approx}{L}^T \underset{\approx}{D} \begin{Bmatrix} 1 \\ 1 \\ 0 \end{Bmatrix} \{L_1 \ L_2 \ L_3\} \begin{Bmatrix} \Delta T_1(z) \\ \Delta T_2(z) \\ \Delta T_0(z) \end{Bmatrix} dV \tag{2.49}$$

Performing the multiplications and integrating over the volume of the subtriangle gives

$$\underset{\sim}{f}_{e_B} = \left(\frac{E\alpha A}{1-\nu}\right) \underset{\approx}{\epsilon}'^{T}_{(i)} \ \underset{\approx}{\bar{B}} \, \underset{\sim}{T}'' \tag{2.50}$$

where

$$\bar{\underset{\approx}{B}}^T = \begin{bmatrix} \frac{1}{6} & \frac{1}{12} & \frac{1}{12} & \frac{1}{6} & \frac{1}{12} & \frac{1}{12} & 0 & 0 & 0 \\ \frac{1}{12} & \frac{1}{6} & \frac{1}{12} & \frac{1}{12} & \frac{1}{6} & \frac{1}{12} & 0 & 0 & 0 \\ \frac{1}{12} & \frac{1}{12} & \frac{1}{6} & \frac{1}{12} & \frac{1}{12} & \frac{1}{6} & 0 & 0 & 0 \end{bmatrix} \tag{2.51}$$

and

$$\underset{\sim}{T}'' = \begin{Bmatrix} B_1 t^5/80 + D_1 t^3/12 \\ B_2 t^5/80 + D_2 t^3/12 \\ B_0 t^5/80 + D_0 t^3/12 \end{Bmatrix} \tag{2.52}$$

B_1 , B_2 and B_0 and D_1 , D_2 , and D_0 are determined at points of the subtriangle. The area of the subtriangle is A in 2.50 while t is the thickness of the subtriangle in Eq 2.52.

2.43 Calculation of Thermal Stresses

The membrane and plate bending thermal forces are calculated for each element and assembled into the force vector $\underset{\sim}{f}$ in Eq 2.10. The nodal point displacements, $\underset{\sim}{r}$, are then obtained by a direct solution of Eq 2.10. Once the displacements are determined, then the strains and stresses in each element may be obtained. The stresses are calculated at each nodal point of an element for the top, middle, and bottom surfaces. The stresses are evaluated using

$$\underset{\sim}{\sigma} = \underset{\approx}{D}(\underset{\sim}{\varepsilon} - \underset{\sim}{\varepsilon}_o) \tag{2.53}$$

where $\underset{\sim}{\varepsilon}$ are the strains calculated from the nodal point displacements, $\underset{\approx}{D}$ is given by Eq 2.19 and $\underset{\sim}{\varepsilon}_o$ is given by Eq 2.15.

2.5 Additional Aspects of the Procedures

In the uncoupled thermoelasticity procedure presented, different finite element idealizations are used for the heat conduction and thermal stress analyses. This imposes hardships on the user of the two programs since two different finite element meshes must be coded. In addition, where the thermal stress finite element idealization is not planar, judgement must be exercised in order to determine the appropriate temperatures to be used for the thermal stress analysis. At the present time, the heat conduction and thermal stress analysis programs are separated. By merging the two programs, the transfer of predicted temperatures from the heat conduction program to the thermal stress analysis program could easily be performed by the computer.

CHAPTER 3. NUMERICAL EXAMPLES

The accuracy of the static analysis program (22,24) and the heat conduction program (45) has been discussed in previous studies. In this chapter, examples will be presented regarding the thermal force representation in the static analysis program. The modifications performed on the heat conduction program were related only to improving the input data generation.

3.1 Temperature Representation

The decision to use a quartic representation of the temperature distribution through the thickness of an element (Eq 2.40) in deriving the equivalent thermal forces in Section 2.42 was based on analyses performed using the heat conduction program. The analyses were performed using the finite element idealization shown in Fig 3.1. The mesh shown in Fig 3.1 idealizes a section of unit width through a concrete slab bridge. Heat flow was assumed to be only through the depth of the section.

The material constants used in the analyses are also shown in Fig 3.1. These constants correspond to values with which Emerson (18) had success in predicting internal temperature distributions for concrete slab bridges in Great Britain. The film coefficients shown in Fig 3.1 also correspond to values suggested by Emerson. The top surface film coefficient is higher since Emerson used it to also approximate the reradiation of the top surface.

Air temperature and solar radiation intensities were specified in the analyses which corresponded to values that might be encountered on a hot summer day in Austin, Texas (38). They are depicted in Fig 3.2. The initial temperature distribution was assumed to be uniform through

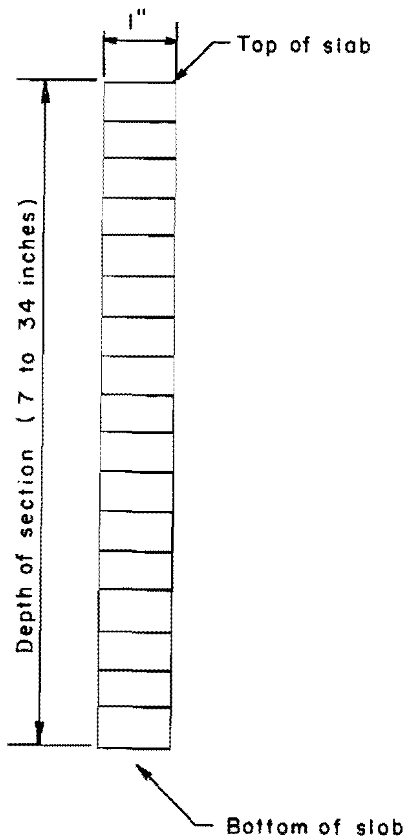

Conductivity = 0.0675 BTU/in/hr/°F

Specific heat = 0.23 BTU/lb/°F

Density = 0.0868 lb/in^3

Absorptivity of top surface = 0.5

Film coefficient for top surface = 0.028 $BTU/in^2/hr/°F$

Film coefficient for bottom surface = 0.0071 $BTU/in^2/hr/°F$

Fig 3.1. Material properties and finite element idealization for heat conduction analysis.

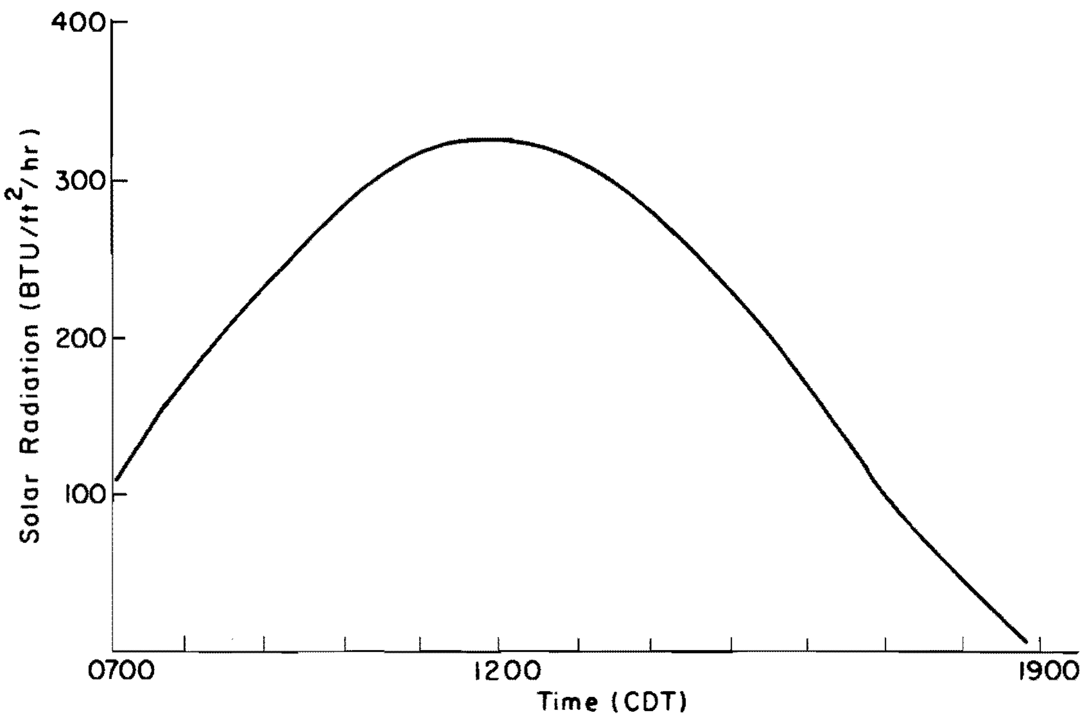

a) Solar radiation variation.

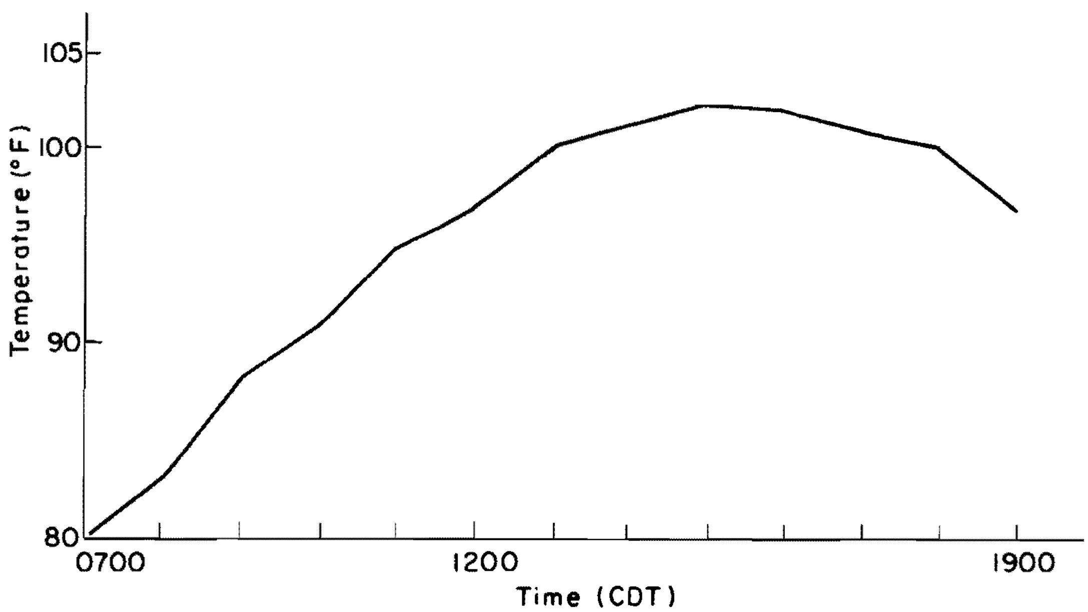

b) Air temperature variation.

Fig 3.2. Solar radiation and air temperature variation for heat conduction analyses.

the depth of the section at 0700 hours (CDT). This is a simplifying assumption with which Emerson (18) had success in predicting the temperature distributions.

Analyses were performed on sections of various depths from 7 inches to 34 inches. The quartic polynomial presented in Eq 2.40 was constructed using the predicted temperatures at the locations illustrated in Fig 2.4. A quadratic polynomial was also constructed using the predicted temperatures at the top, middle, and bottom of the section. The quartic polynomial proved to be a consistently more accurate approximation to the predicted temperature distributions than the quadratic polynomial. However, for sections less than approximately 20 inches deep and in the middle of the afternoon, the quadratic polynomial also accurately approximated the predicted temperature distributions. The fit of the two polynomials to the predicted temperature distributions is shown in Fig 3.3 for a section 16 inches deep at 1200 and 1400 hours. For sections of depth greater than 20 inches and/or in the early morning hours, the quadratic polynomial did not provide a satisfactory approximation. Thepchatri (39) has presented results illustrating the poor fit of the quadratic polynomial to predicted temperature distributions for deep sections. The quartic polynomial was found to be a more satisfactory representation although it required five temperatures to be specified through the depth in order to define the constants in Eq 2.39 while the quadratic required only three to define its constants.

The time increment, Δt in Eq 2.6, used in the analyses was one hour. Additional analyses were performed using a time increment of 15 minutes. The differences in temperatures obtained with the smaller increment were negligible.

3.2 Simply Supported Rectangular Plate with Linear Temperature Gradient through Thickness

In this example, a rectangular plate was analyzed in order to determine the accuracy of the plate bending thermal force representation. The plate was simply supported on all sides with a linear temperature gradient through the thickness. The solution obtained

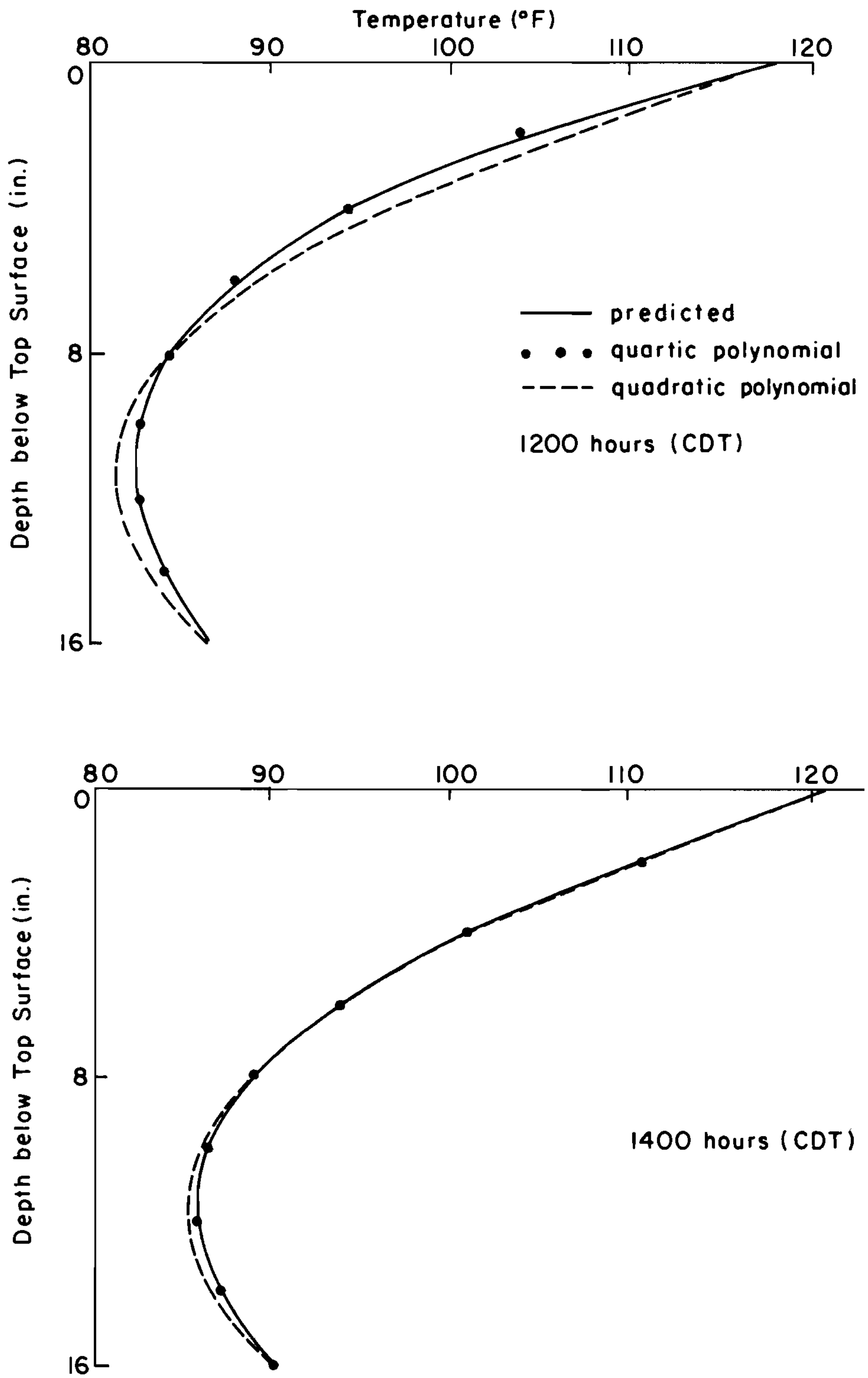

Fig 3.3. Polynomial fits to predict temperature distribution.

from the static analysis program was compared with a classical solution in order to verify the accuracy of the static analysis solution.

A plan view of the plate is shown in Fig 3.4a. Also shown in 3.4a are the material properties and the finite element mesh. By using symmetry only a quadrant of the plate was analyzed. A linear temperature gradient of 100°F was specified through the thickness as depicted in Fig 3.4a.

The vertical deflection and stresses obtained at the center of the plate, point p in Fig 3.4a, are presented in Fig 3.4b. Also shown in 3.4b are the corresponding results obtained from a classical series solution (21) using eight terms. The results obtained by the static analysis program were within 5 percent of the classical solution. Thus, the plate bending thermal force representation yielded satisfactory results.

The same plate was also analyzed with the edges of the plate fully fixed. The static analysis predicted zero vertical deflection at all nodal points and the stress components in the x- and y-directions were the same and equal to $-E\alpha T(z)/(1-\nu)$ everywhere. These results exactly corresponded to classical solutions (8,21).

3.3 Simply Supported Beam with Parabolic Temperature Gradient

The final example presented is a simply supported beam with a parabolic temperature distribution over its depth. This example was chosen to illustrate the accuracy of the membrane thermal force representation. The geometry of the beam, material properties, and temperature gradient are shown in Fig 3.5a along with the finite element mesh used in the analysis. Poisson's ratio was set equal to zero in order to compare the results with classical solutions. Otherwise, the material would correspond to steel.

A classical solution presented by Timoshenko and Goodier (40) was used to verify the accuracy of the analysis. It was determined from the classical solution that the longitudinal stress distribution would be parabolic. Also, at a sufficient distance from the ends of the beam, the top and bottom stresses would be 6000 psi in tension and

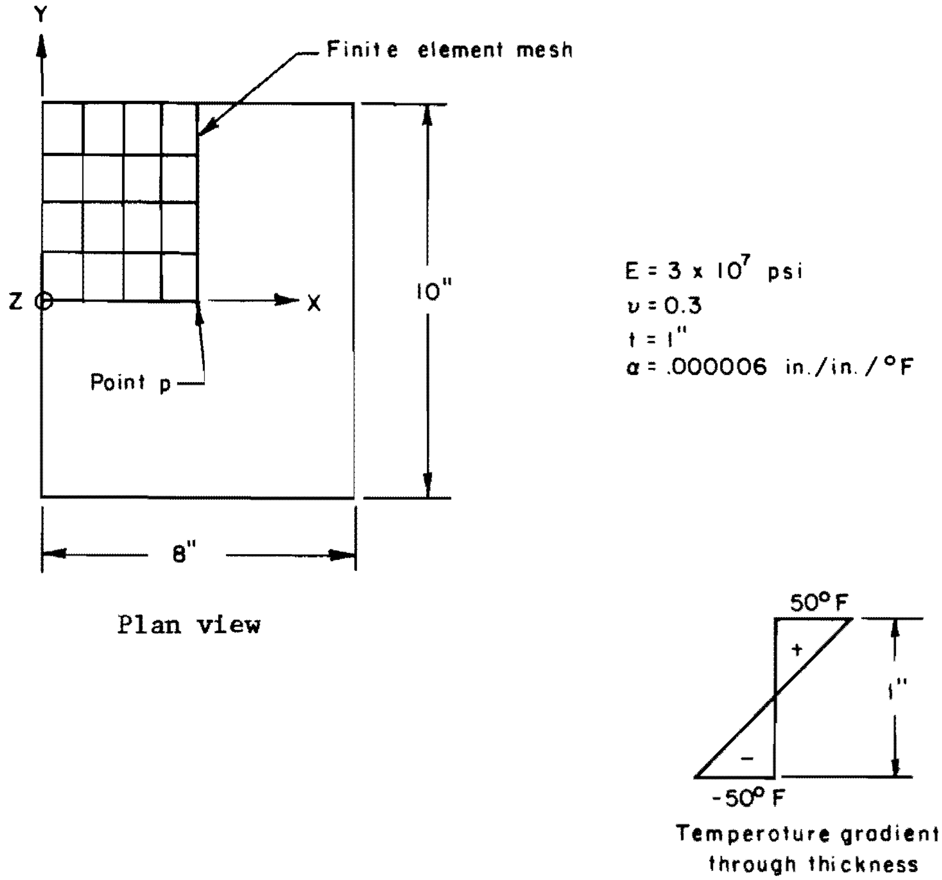

a) Problem description.

	Classical (21)	Finite Element
Vertical deflection at p (in)	4.47×10^{-3}	4.42×10^{-3}
σ_x in bottom surface at p (psi)	3.13×10^{3}	3.26×10^{3}
σ_y in bottom surface at p (psi)	5.87×10^{3}	5.91×10^{3}

b) Results.

Fig 3.4. Simply supported rectangular plate with linear temperature gradient.

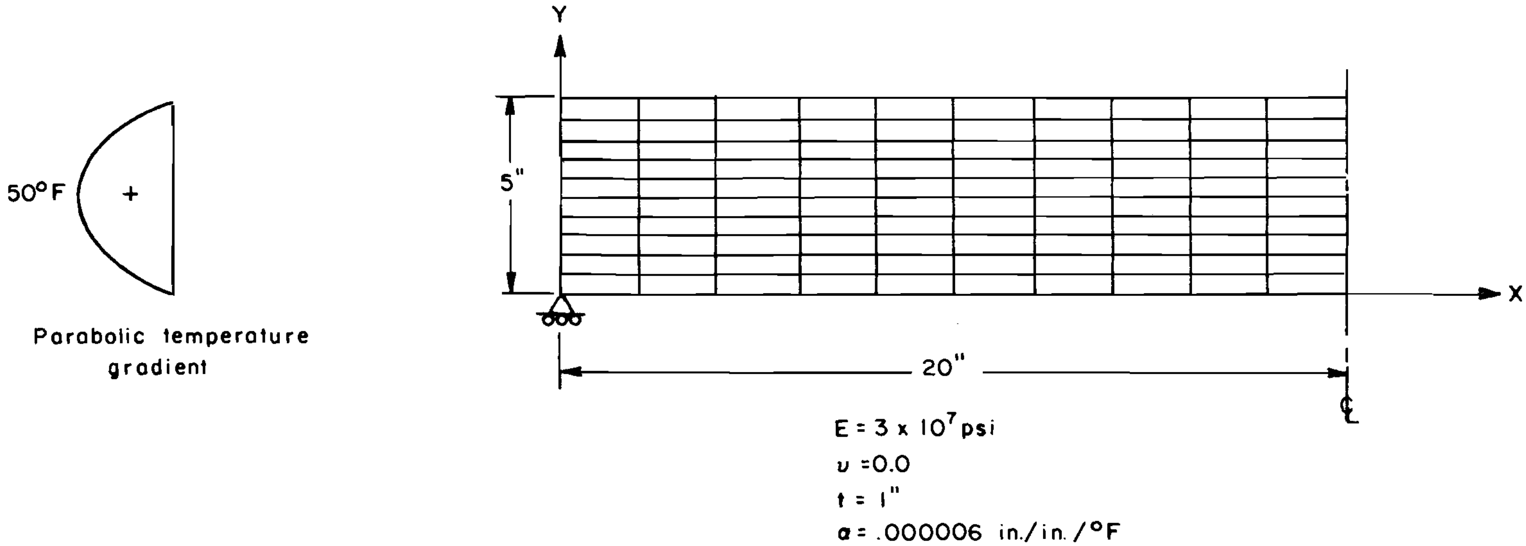

a) Description of problem.

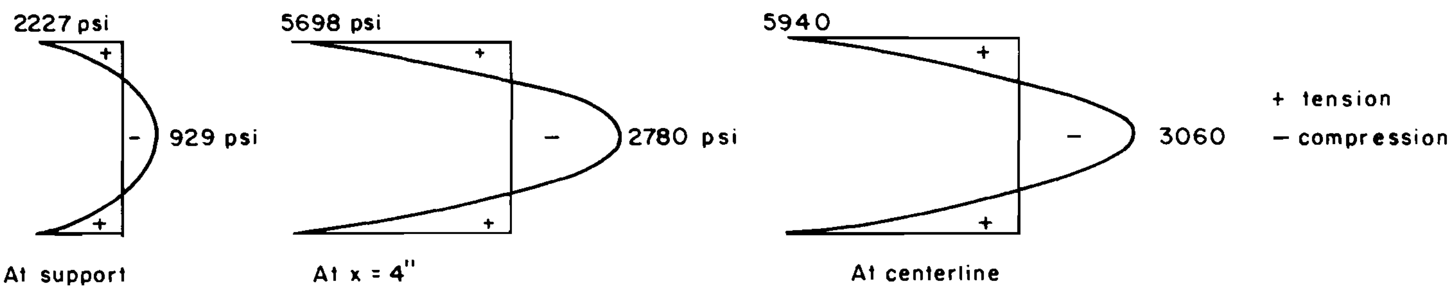

b) Longitudinal stresses.

Fig 3.5. Simply supported beam with parabolic temperature gradient.

the stress at mid-depth would be equal to 3000 psi in compression. The longitudinal stress distributions obtained from the finite element static analysis are shown in Fig 3.5b for three locations along the length of the beam. There should not be any stress at the end of the beam since it is a free boundary. However, the finite element solution does predict stresses at the end as shown in Fig 3.5b. The errors in the stresses at the free end should decrease as the number of elements over the depth of the beam increases. This is due to the fact that the membrane elements are restricted to a linear temperature gradient over the surface while the specified temperature gradient is parabolic. The more elements used in the idealization; the better the representation of the parabolic temperature gradient with linear segments. At $x = 4$ inches, the stresses are within 10 percent of the classical solution. The stresses at the centerline are within 2 percent of the classical solution. Thus, discrepancies that occur at the boundary due to the inaccurate representation of the nonlinear temperature gradient do not appear to adversely affect the stresses a short distance from the boundary.

CHAPTER 4. INSTRUMENTATION AND MEASUREMENTS

As stated in Chapter 1, it was not within the intended scope of this study to perform extensive field tests nor to use elaborate instrumentation. Only selected measurements were to be taken to validate the computational procedure. These measurements are divided into two categories: (1) those measurements necessary to determine the temperature distribution and (2) those measurements necessary to determine the thermally induced movement of the structure at various locations. The primary purpose of this chapter is to discuss the instrumentation used in both of these categories. Also presented are summaries of field tests performed on two bridges located in Texas. More detailed information regarding these tests is presented in Appendices A and B.

4.1 Instrumentation to Determine Bridge Temperature Distribution

Two approaches have been employed by researchers in the past to determine the temperature distribution in bridge-type structures. The first approach consists of the internal instrumentation of the bridge using thermocouples. This approach provides a direct determination of the transient temperature distribution. For constant thickness concrete slab bridges only a limited number of thermocouples are required since the temperature distribution would be approximately constant in the longitudinal and transverse directions. However, for bridges with variable depths, parapets, sidewalks, or numerous girders, a large number of gages is required to determine the temperature distribution. For example, Wah and Kirksey (41) instrumented a multibeam, simply supported bridge with 390 thermocouples during construction in order to determine the temperature distribution. Due to the time and cost required for instrumentation of this nature, this approach was not adopted in the subject study.

The second approach to determine the temperature distribution was developed by Emerson (17,18) in Great Britain. This approach consists of specifying environmental conditions as inputs for a finite difference computer program based on one-dimensional heat flow. The program then computes an approximate solution for the transient heat conduction problem. Environmental conditions such as solar radiation and air temperature are specified together with simplifying assumptions regarding the initial temperature distribution in Emerson's procedure. Emerson was able to achieve satisfactory correlation with measured temperature distributions using this procedure. Thus, it is only necessary to measure the transient air temperature and the solar radiation intensity in Emerson's approximate procedure.

An extended version of Emerson's procedure was adopted for this study. The finite element heat conduction program discussed in Chapter 2 is more general since it is based on two-dimensional heat flow and can represent more than one material. Air temperature and solar radiation may also be specified in the finite element program. However, they are not necessary if the surface temperature distribution is known with respect to time. The finite element program can predict the transient internal temperature distribution by only specifying the surface temperature variation with time and an initial temperature distribution. In the field tests air temperatures and solar radiation intensities were measured but were used for qualitative purposes to be discussed later.

4.11 Surface Temperature Measurements

In an effort to avoid elaborate instrumentation and reduce installation time and cost, it was decided that a portable temperature measuring device would be used that could be moved from one location to another on the bridge surface. By observing temperatures at each location at least once an hour, it was believed that a satisfactory record of the temperature variation could be obtained. Two types of temperature measurement devices were taken into consideration:

1) mechanical surface thermometers, and
2) temperature sensor gages.

Six mechanical surface thermometers manufactured by Pacific Transducer Corporation were acquired for evaluation purposes. These thermometers had a temperature range from 0°F to 270°F with a stated accuracy of plus or minus 2% of the scale range. The accuracy of the thermometers was found to be insufficient for this study. The temperatures registered by the thermometers were affected by air flowing past the exposed sensing element on the bottom of the thermometers. In addition, the thermometers were not practical for measuring the surface temperatures under the bridges since most bridges are a considerable distance above the ground and reading the thermometers from these distances would be extremely difficult. A more practical method of determining the temperature on the bottom surfaces would have the sensing device in contact with the surface but provide for the readout of the temperature to be observed on the ground or at some other more convenient location.

With this in mind a portable temperature probe was developed utilizing a temperature sensor gage. This gage is commercially available and is configured much like an electrical strain gage since the sensing grid is fabricated from nickel foil. The resistance of the sensing grid varies as a function of the temperature of the grid. Thus, when the gage is provided with the appropriate circuitry, the temperature of the surface in contact with the gage grid may be read from a strain indicator in the same way strain is read for an electrical strain gage. The probe consisted of a segmental aluminum pole fitted with a contact head containing the temperature sensor gage. The strain gage indicator was connected to the contact head by wires running along the length of the pole. Plan and elevation views of the probe are shown in Fig 4.1. As can be seen from this figure, the head consists of a Plexiglas cylinder

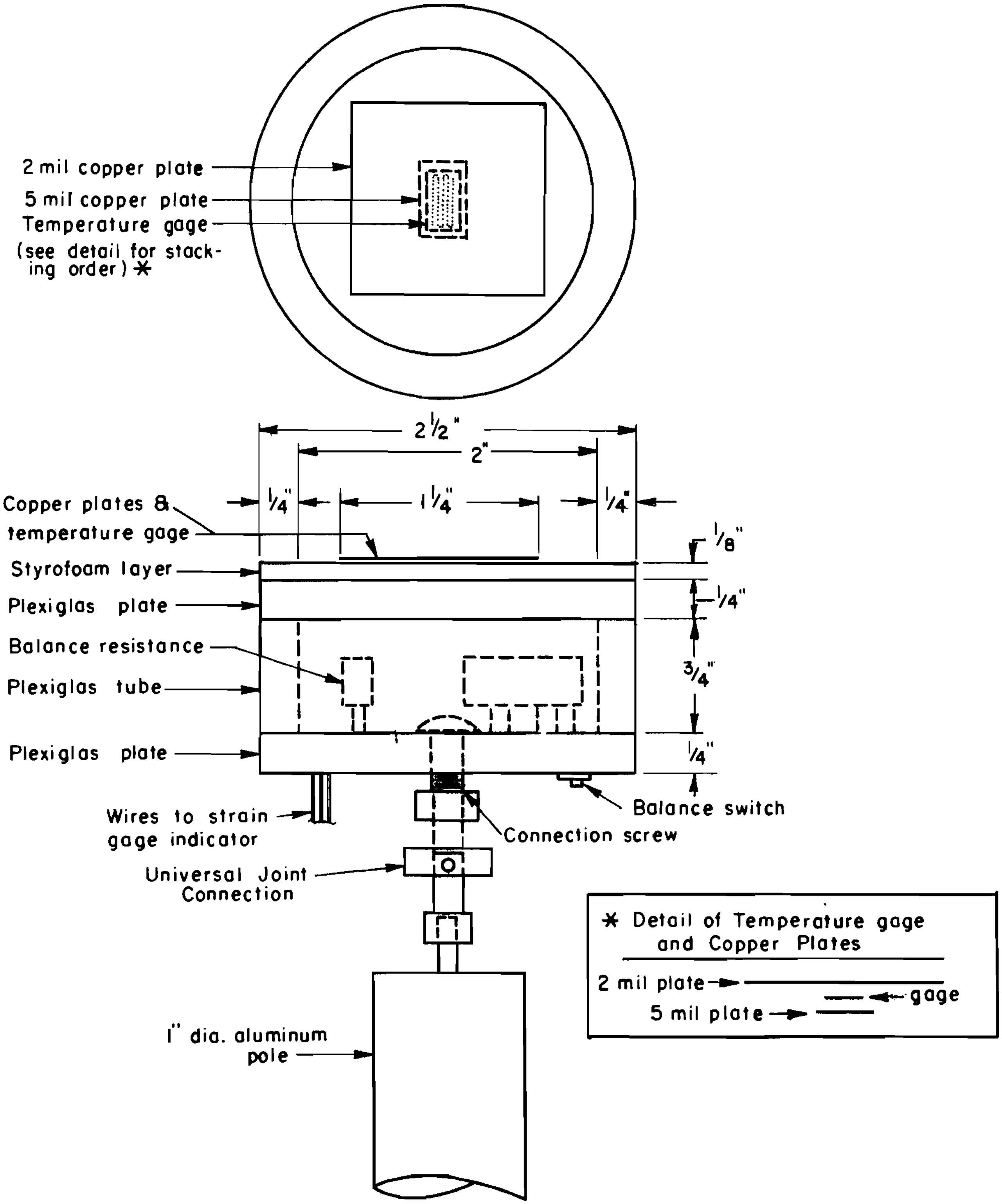

Fig 4.1. Temperature probe used to measure surface temperature.

with the temperature sensor gage and copper plates on the outer surface and the necessary circuitry contained within the Plexiglas cylinder. The outer copper plate provides protection for the gage from rough surfaces and also provides more contact area. This enables an accurate and rapid determination of the temperature on rough surfaces such as concrete bridge decks. The copper plate under the gage provides support for the gage and prevents punch through by particles on the bridge surface. The copper plates were made as thin as possible in order not to increase the thermal capacitance of the contact head. The layer of Styrofoam reduces the heat flow between the copper plates and the Plexiglas.

A schematic diagram of the circuitry and the electrical components of the probe are shown in Fig 4.2. The balancing resistance and switch shown in this figure are used to balance the strain indicator at 75°F. This permits a quick balancing of the strain indicator in the field. The balancing resistance was matched to the temperature sensor resistance at 75°F by a laboratory calibration procedure. The matching network unit shown in Figs 4.1 and 4.2 is a small passive network encapsulated in a molded plastic case. This unit performs the following functions: 1) linearize the gage resistance as a function of the gage temperature, 2) increase the response of the gage to 100 microstrain per degree F, and 3) present a balanced 120-ohm half-bridge circuit to the strain indicator at the reference temperature of 75°F.

The use of the probe is simple and required little time to perform the measurement at each station. The head is placed in contact with the surface with only light pressure required to ensure contact. The measured temperature is observed directly from the strain indicator after the temperature sensor has reached equilibrium with the surface. On warm days approximately 30 seconds is required for the first reading with less time required for readings at other stations. On very cold days approximately two minutes is required for the first reading. The influence of the gage itself can be minimized by placing the head of

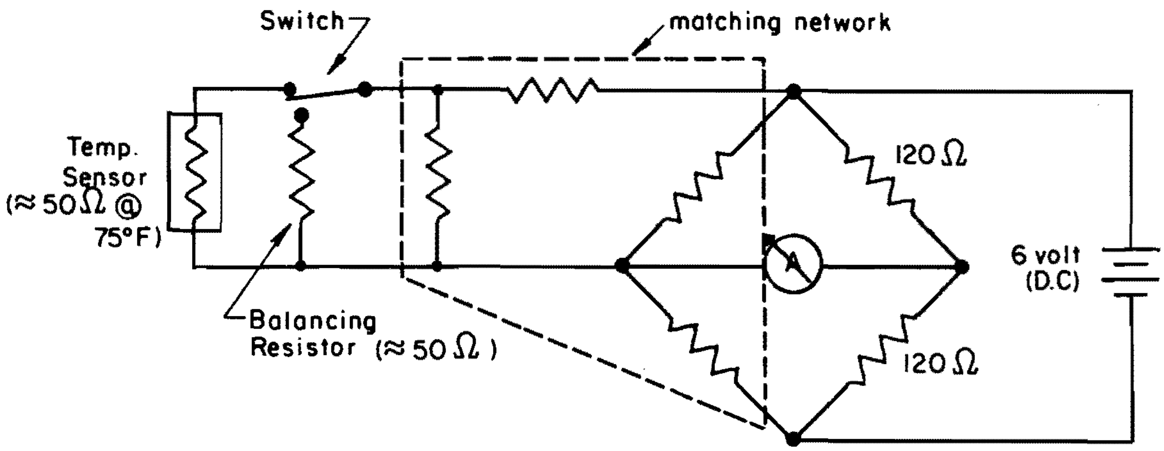

(a) Circuit schematic.

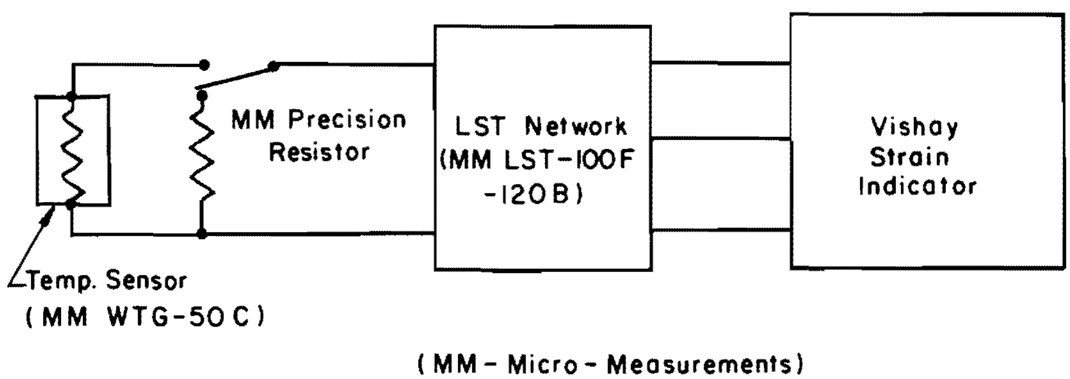

(b) Circuit components.

Fig 4.2. Circuitry schematic and electrical components for temperature probe.

the probe in contact with the surface at a location near the desired location, allowing the gage to reach equilibrium with the surface, and then quickly moving the probe to the desired location. At each location the time and the reading are recorded.

4.12 Solar Radiation Measurements

As mentioned previously, solar radiation measurements were used only for qualitative purposes in this study. Since surface temperatures were observed approximately once an hour at each station, the solar radiation variation during the time between readings could be used to interpolate and explain the surface temperature variation. However, solar radiation measurements observed during one of the field tests were used by Thepchatri (39) to predict the surface temperatures and to compare them with measured quantities. Thepchatri obtained favorable comparisons using this approach.

Two different pyranometers were used to measure the solar radiation. Both of these instruments measured the global radiation on a horizontal plane, i.e. the total of the direct, diffuse, and reflected radiation. One instrument, a 50 junction Eppley pyranometer, used electrical output from thermocouples to measure the solar radiation. A voltmeter is required to use this instrument. The other instrument used was a Casella pyranometer. The Casella measures the solar radiation mechanically by utilizing the thermal bending of metal components. The radiation intensity is recorded by a pen on a mechanically driven rotating drum. The response time is extremely fast for the Eppley but requires approximately 4 - 7 minutes for the Casella (35). More detailed information regarding both of these instruments can be found in a text edited by Robinson (35).

4.13 Air Temperature and Wind Speed Measurements

The air temperature was measured during both field tests while the wind speed was measured only during the first test. Again, these measurements were only used for qualitative purposes in this study but Thepchatri (39) used them in predicting the slab temperatures. The air temperature was simply measured by suspending a shaded mercury thermometer above the surface of the bridge. In the first field test the wind speed was measured by an anemometer. The wind speed was measured by raising the rotating cups of the anemometer above the bridge surface and reading a battery operated recorder at selected time intervals.

4.2 Instrumentation to Measure Bridge Movement

A primary part of the objective was to measure the temperature induced movements in the field tests. Past research has concentrated on measuring the thermally induced longitudinal or vertical movements. For instance, Capps (10) used a linear potentiometer as a movement transducer to measure the longitudinal movement on a bridge in Great Britain. Wah and Kirksey (41) used a transit to measure the vertical movement of a bridge in San Antonio, Texas. For the present study it was decided to measure the temperature induced slope changes on the bridge surface since an instrument had previously been developed to measure slope changes (30). Besides the availability of the instrument, it was selected also for its simplicity, reliability, and accuracy.

A mechanical inclinometer had been developed by Matlock and coworkers (30) to measure slope changes on a bridge tested for live load effects in Pasadena, Texas. Basically, the inclinometer measures the change in elevation between pairs of ball bearing test points that are cemented to the bridge deck at 24-inch spacings. The slope between the two points is then computed by dividing the difference in elevation between the two points by the length of the inclinometer, 24 inches. Slope changes are computed by subtracting a reference slope from any other reading.

The inclinometer which was used and a typical ball point are shown in Fig 4.3. The inclinometer has two steel feet in line with the level bubble, one with a V-grooved foot and the other the flat end of a micrometer screw. The lateral support six inches to the side of the

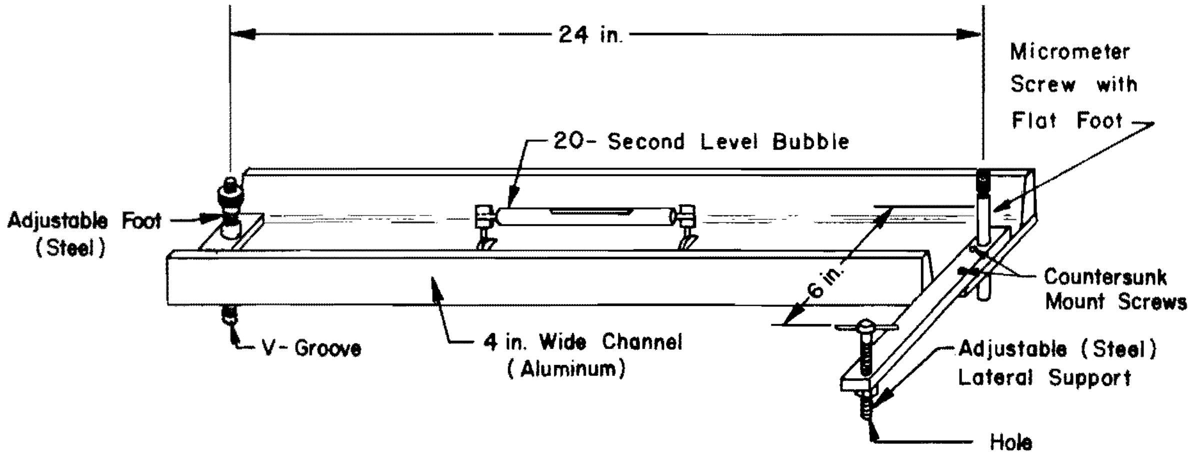

(a) Inclinometer.

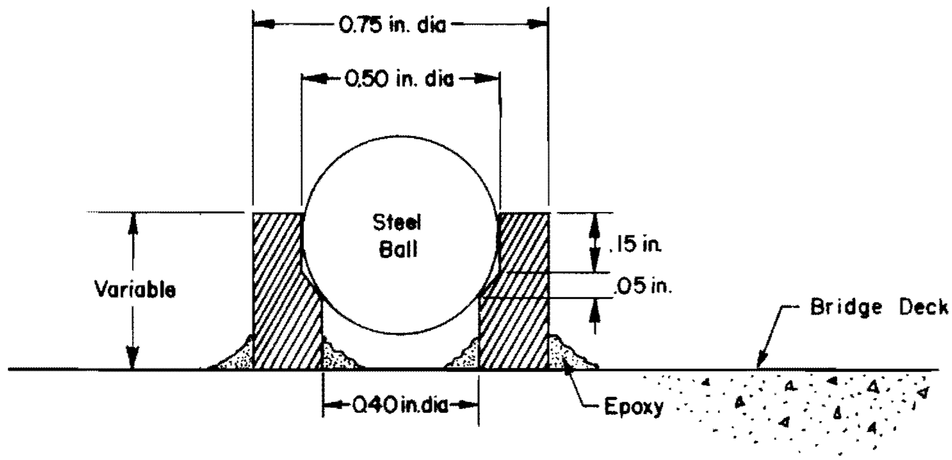

(b) Ball point.

Fig 4.3. Slope measuring instrument and test point (Ref 30).

longitudinal axis has a circular hole in the bottom of the foot to seat on auxiliary points. This provides for precise repositioning of the inclinometer during later readings. The ball points are cemented to the bridge deck using a quick setting epoxy cement. An aluminum template is used to accurately position the four ball points required at each station while they are being cemented.

Each slope reading was taken using two observations of the micrometer with the inclinometer reversed end-for-end between the two readings. This provides a self-checking system for the readings and also cancels instrument errors. Using this system only instrument errors that occurred between the two readings would not be canceled.

An example for recording the inclinometer readings is shown below. The sum of the direct and reverse readings should remain approximately constant for the instrument regardless of the measurement station or time. Significant variations of the sum indicated a need for the re-check of the readings. The time of the reading was recorded between the direct and reverse reading to provide an average time of reading for subsequent analyses.

Station	3
Time	0645 (CDT)
Direct reading (in.)	0.5749
Reverse reading (in.)	0.5463
Sum (in.)	1.1212
-2 × reverse (in.)	-1.0926
= 2 × differential elevation of points (in.)	0.0286
/ 48 (in.) = slope (radians)	5.95×10^{-4}

4.3 Summary of Field Measurements on Pasadena Bridge

The Right Entrance Ramp Structure at Richey and Margrave Streets on State Highway 225 in Pasadena, Texas was selected for the first field test. The bridge was a skewed, post-tensioned, three-span continuous slab structure. A previous test for live load effects on this structure had found that thermal response was of the same order of magnitude as the live load response. A partial plan view and cross section of the bridge are shown in Fig 4.4.

The bridge was tested on 24 August 1974 between 0615 and 1800 hours (CDT). Instrument locations and measurement stations were established the previous night. Inclinometer measurements were taken at nine locations on the slab: three locations at the northern abutment, three over the northernmost interior supports, and three locations in the center of the structure. All inclinometer stations were located so as to measure the change in slope along the longitudinal axis. Surface temperatures were measured at 40 stations: 12 stations on the top of the slab, 12 on the bottom of the slab, and 16 stations on the parapet and sidewalk. Solar radiation readings were observed using both the Casella and Eppley pyranometers located on the top surface of the bridge. Wind speed and air temperature readings were also observed. Positions of all the inclinometer and surface temperature measurement stations are described in Appendix A.

Weather conditions for the day of test were generally poor for purposes of the test. Considerable cloudiness was present almost the entire day and a heavy rain fell between 1615 and 1745 hours (CDT). Only a few spot inclinometer and surface temperature measurements were taken after the rain stopped. After these measurements the test was terminated. The cloudiness is illustrated by the rapid changes in the Eppley solar radiation measurements shown in Fig 4.5a. Shown in Fig 4.5b are the average top and bottom slab temperatures and the air temperature measured during the test. The maximum slab temperature observed was 107.1°F. Normally for that time of the year, and clear weather, one would expect slab temperatures as high as 120-130°F (39). Plots of all the temperature measurements are also presented in Appendix A for completeness.

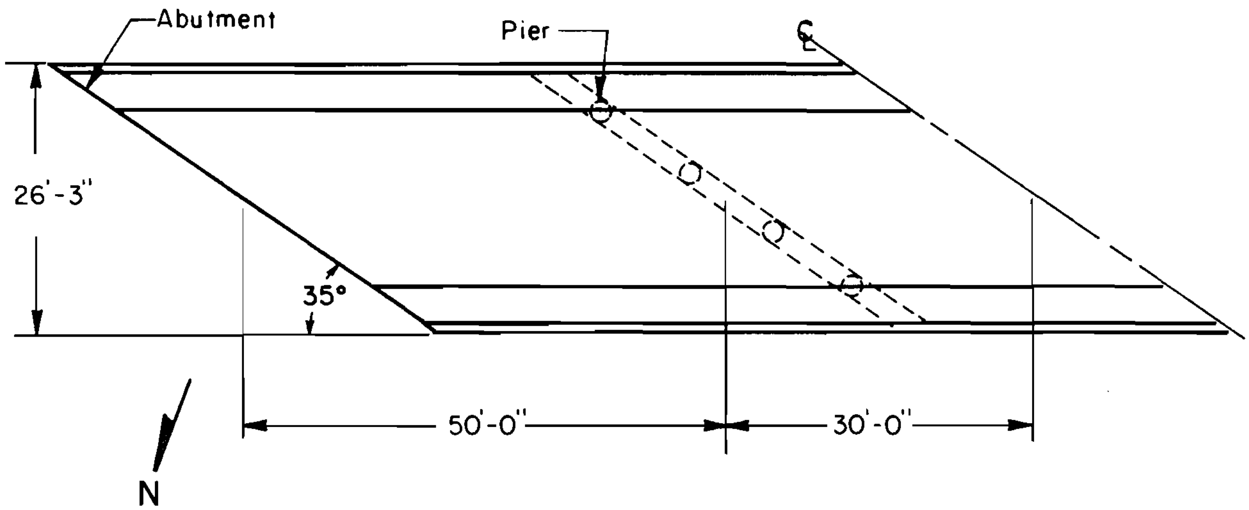

(a) Plan view.

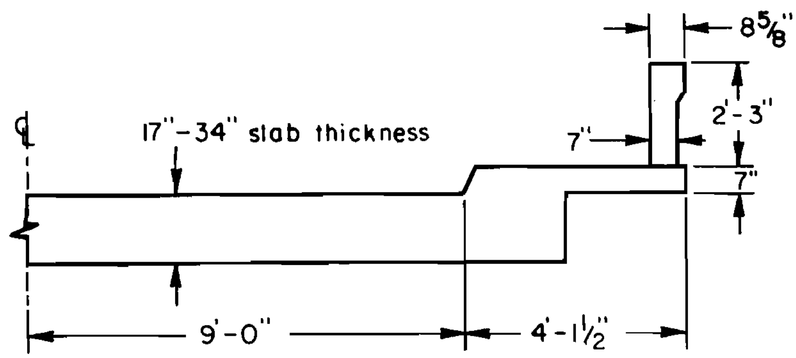

(b) Cross section.

Fig 4.4. Pasadena bridge.

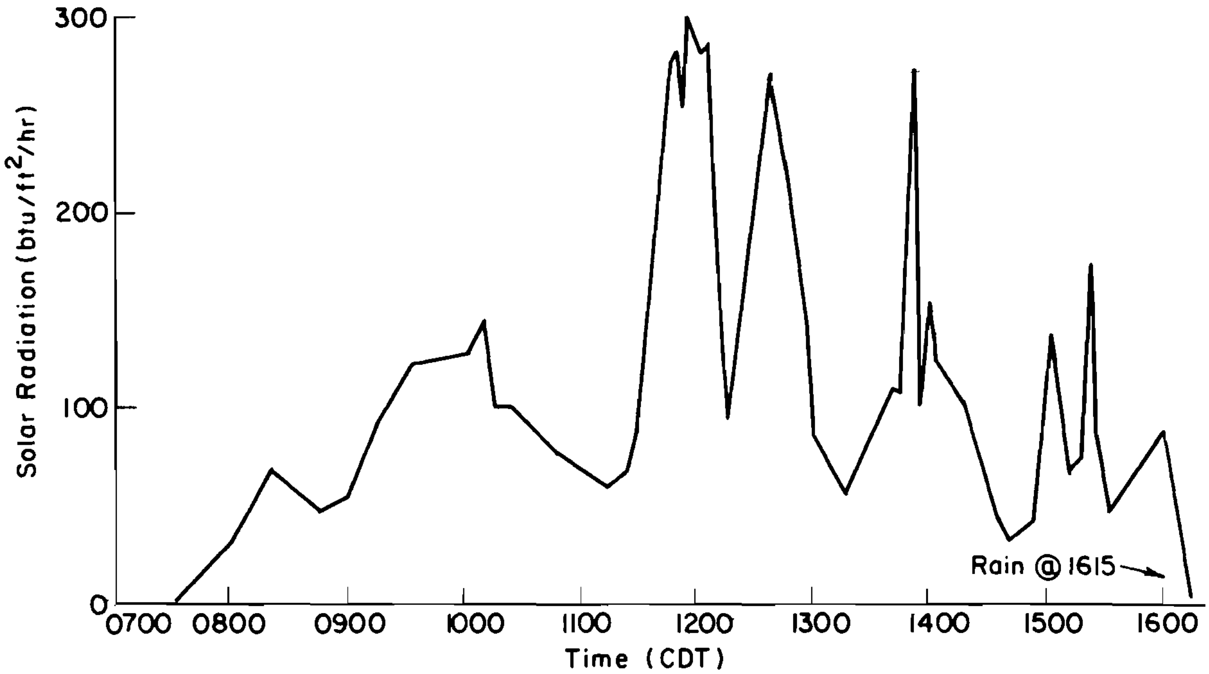

(a) Eppley solar radiation observed during Pasadena test.

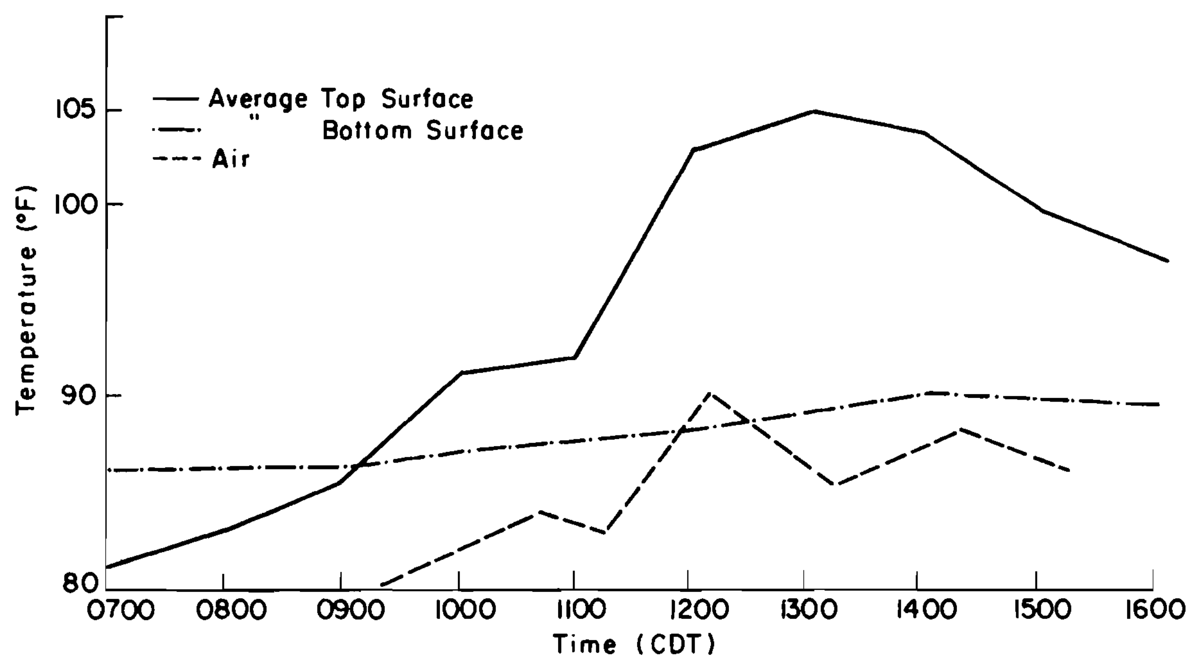

(b) Temperatures observed during Pasadena test.

Fig 4.5. Measured solar radiation and temperatures for Pasadena test.

The maximum slope changes recorded were from inclinometer stations located at the northern abutment. Despite the undesirable testing conditions, a maximum slope change of 5.73×10^{-4} was measured. This compares with a maximum slope change of 5.63×10^{-4} measured in a previous field test (30) due to live load. Plots of all inclinometer measurements are also in Appendix A. Correlation and discussion of slope change measurements and the finite element procedure results are presented in Chapter 5.

4.4 Summary of Field Measurements on Pedestrian Overpass

The second bridge tested was a pedestrian overpass located on U.S. Highway 183 near T. A. Brown Elementary School in Austin, Texas. The bridge was a composite two-span structure using precast pretensioned beams made continuous for live load by placing reinforcing steel in the cast-in-place concrete slab over the interior support. Plan and cross section views of the bridge are shown in Fig 4.6. As can be observed from this figure, the slab thickness, the length and depth of the girder, and spacing of the girders are typical of construction used for highway bridges. This fact, the convenience of the structure and freedom from vehicle traffic, justified the testing of the pedestrian overpass for thermal effects.

A preliminary test was performed on 21 December 1974. The purpose of this preliminary test was to determine the number of temperature measurement locations necessary to accurately define the surface temperature distribution and also determine whether the overpass exhibited sufficient thermal response to justify a more complete test. Eleven locations were used for surface temperature measurements and three locations for inclinometer measurements. Results obtained indicated that a greater number of surface temperature stations were required to define the surface temperature distribution. This was due to side heating of the girders and partial shading of the top slab by the parapets. The maximum slope change observed during this test, 7.0×10^{-5}, was small in comparison with the slope change measured on

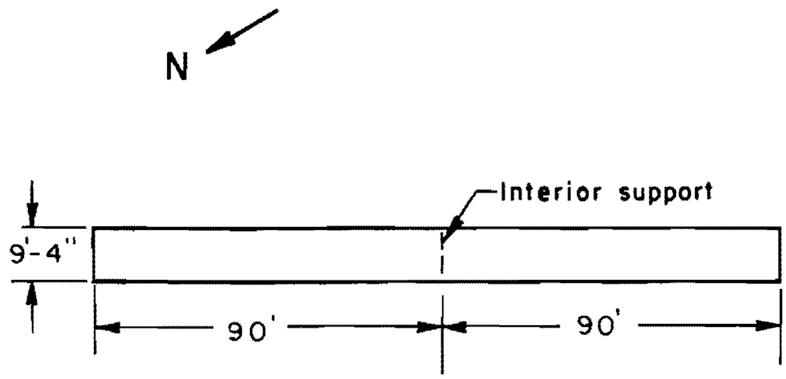

(a) Plan view.

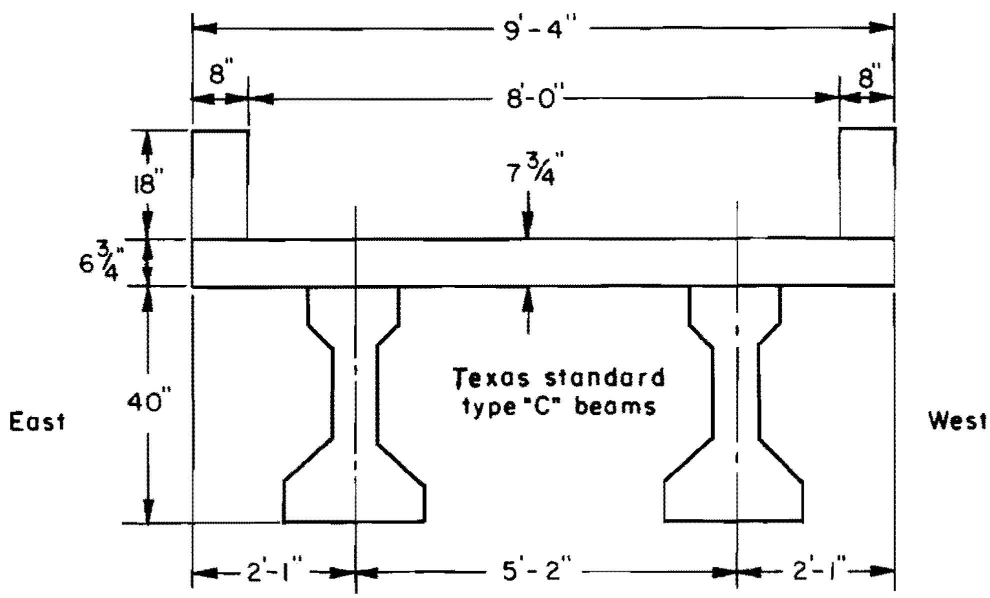

(b) Cross section.

Fig 4.6. Plan and cross section views of pedestrian overpass.

the bridge in Pasadena. This was attributed to the fact that the solar radiation intensity is at its lowest level of the year on the 21st of December. Only a 7°F temperature differential was measured between the top and bottom of the slab during this test.

Another field test was performed on the overpass on 14 March 1975 between 0730 and 1900 hours (CDT). Weather conditions for this test were good with an air temperature range of 28°F and clear skies. For this test, surface temperatures were measured at 53 locations. The air temperature variation and the surface temperature variation for points located at the center of the slab, top and bottom, are shown in Fig 4.7. Locations of all the surface temperature measurements and measured temperature variations for all locations are presented in Appendix B.

Inclinometer measurements were recorded at three locations along the longitudinal axis of the bridge. The inclinometer discussed in section 4.2 was used at the north end of the bridge aligned along the longitudinal axis at the center of the slab. The maximum slope change measured at this location was 3.67×10^{-4} radians. Another inclinometer was used at the other two locations. This inclinometer was in the shape of an equilateral triangle and designed to measure the slope change in any direction as well as the principal slope changes. Problems due to the micrometer slipping arose with this inclinometer during the test so results obtained at the two locations were discarded. Correlation of the measured slope changes and the finite element procedure results for the one station are presented in Chapter 5.

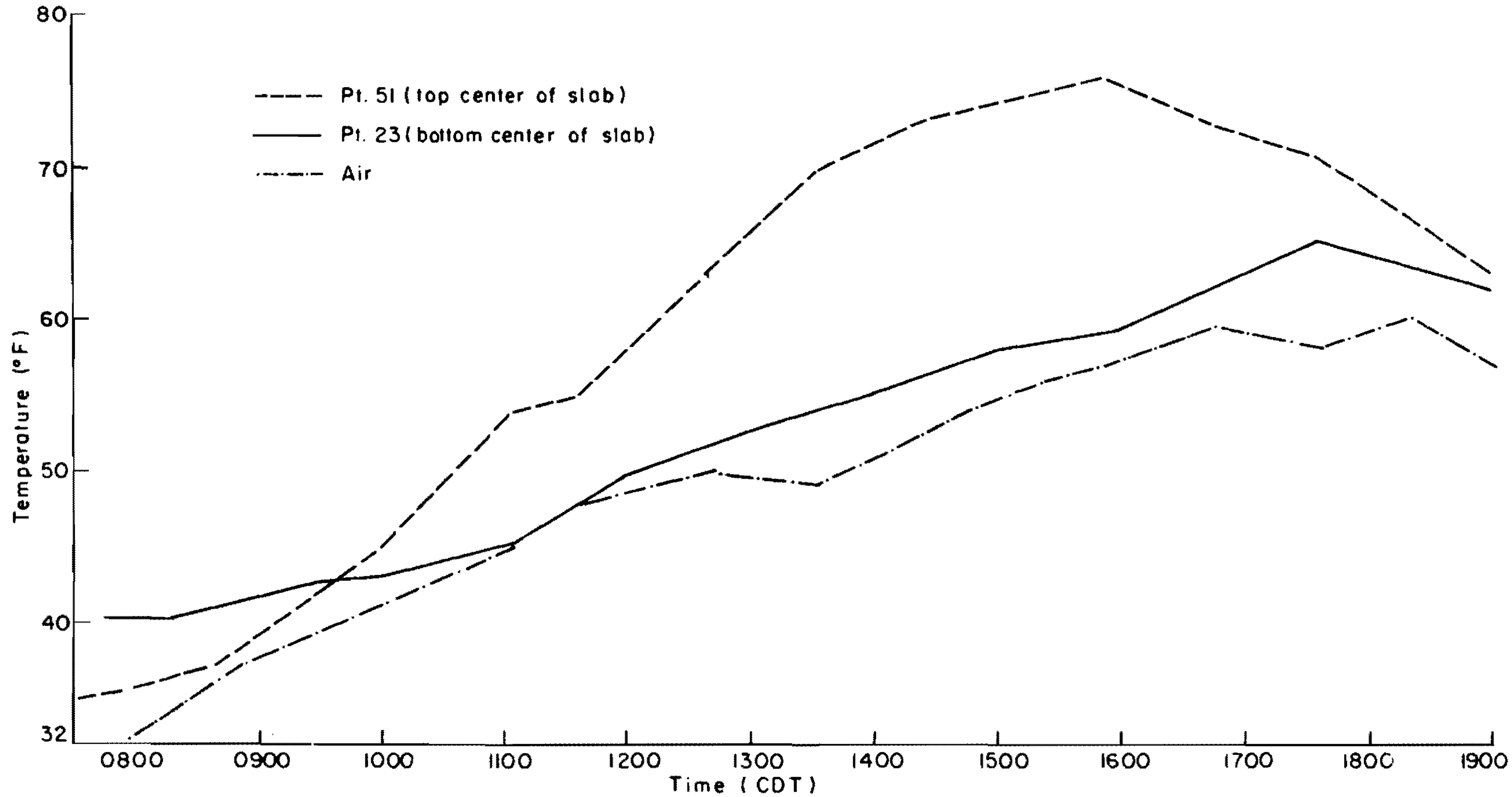

Fig 4.7. Measured slab and air temperatures for March test on pedestrian overpass.

CHAPTER 5. CORRELATION OF FIELD MEASURED SLOPE CHANGES AND COMPUTER RESULTS

The final phase of the study began after each field test had been completed and the results had been compiled. This phase consisted of the correlation of the measured slope changes from each field test with predicted slope changes using the finite element procedure presented in Chapter 2. Results of the correlations are presented in this chapter for the field tests on the entrance ramp structure in Pasadena, Texas and on the pedestrian overpass in Austin, Texas. A parameter study on the Pasadena bridge is also presented as well as a comparison of the temperature stresses with the dead load plus prestress stresses.

5.1 Correlation of Field Measured Slope Changes and Computer Results for the Pasadena Bridge (24 August 1974)

The first step in the analysis of the Pasadena bridge was to determine the transient internal temperature distribution using the measured surface temperatures presented in Appendix A. The following sections were analyzed to determine an approximation to the bridge's temperature distribution considering only one-dimensional heat flow but using the two-dimensional heat conduction program:

1) slab sections that were 17, 18.5, 24.55, and 34 inches thick,
2) the top and the bottom of both parapets, and
3) the inside and the outside of both sidewalks.

These particular sections were analyzed since they approximately corresponded to locations chosen for nodal points for the static analysis. One-dimensional heat flow was used since it was believed that there would be negligible heat flow in the longitudinal and transverse directions of the bridge. This belief was based on the low thermal conductivity of concrete and also due to the fact that there was little variation, a maximum of 4°F, in the measured slab surface temperatures in the longitudinal or transverse directions of the slab. Heat flow in the longitudinal direction was confirmed to be negligible by a later analysis of the haunch region of the slab using two-dimensional heat flow.

The assumed initial uniform temperature distribution and starting time were determined from the plots of the measured surface temperature distributions presented in Appendix A. A previously presented figure of the average top and bottom slab temperatures, Fig 4.5, illustrated that the average top and bottom slab temperatures were the same at approximately 0900 hours (CDT) at a temperature of 86°F. Therefore, the slab sections were assumed to be at a uniform temperature of 86°F at 0900 hours. At 0900 hours the temperatures in the sidewalks and parapets were lower than the slab. This is attributed to the fact that the sidewalks and parapets were thinner sections and also that the parapets were more exposed to wind and reradiation effects. An initial uniform temperature distribution of 82°F was assumed for the sidewalks and parapets based on the plots in Appendix A.

The one-dimensional heat conduction analyses were performed using half-hour time intervals from 0900 to 1600. Surfaces temperatures were interpolated for the sidewalk and parapet analyses using the figures in Appendix A. Figure 4.5 was used to determine the average top and bottom slab surface temperatures at the required times. The following concrete material properties were used for the heat conduction analyses: a thermal conductivity of 0.81 BTU/ft/hr/°F, a specific heat of 0.23 BTU/lb/°F, and a density of 150 lb/ft^3. The thermal conductivity and specific heat are average properties obtained from Billington (7). An example of the temperature distributions predicted by the analysis for the 17-inch slab section is shown in Fig 5.1. As can be seen from this figure, heat entering the top and bottom of the slab

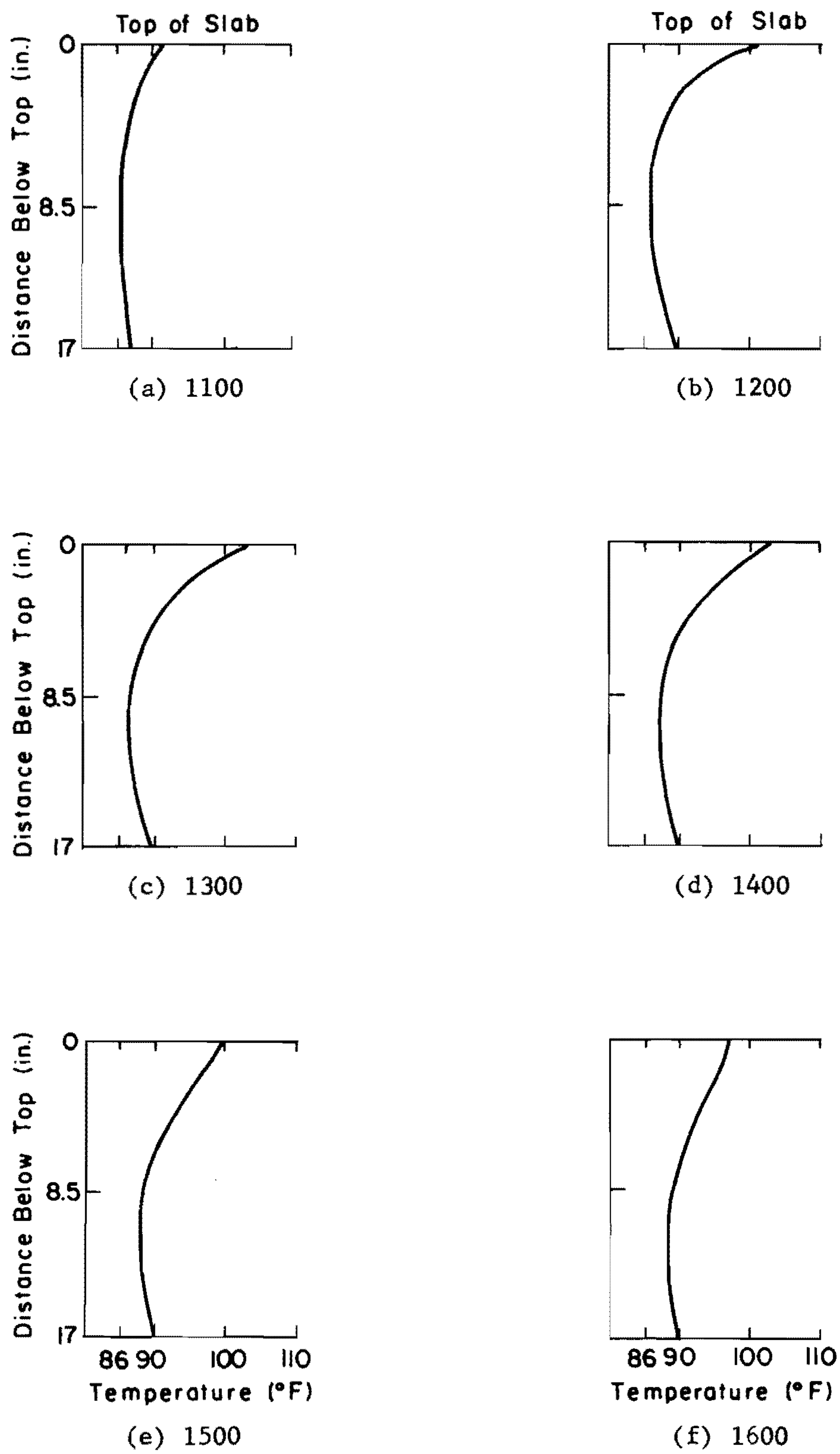

Fig 5.1. Predicted temperature distributions at several times for 17 inch thick section on Pasadena bridge.

required considerable time to penetrate to the interior of the slab. By 1400 hours the predicted temperature at the mid-depth of the section had increased only 1.2°F.

Once the transient temperature distributions had been predicted for all the sections, static analyses were performed using the predicted temperature changes from the 0900 initial temperatures at one hour intervals from 0900 to 1600. A plan view and cross section of the finite element mesh used for these analyses are shown in Fig 5.2. Boundary conditions used in the static analyses are as follows:

1) vertical movement restrained at all pier supports and nodal points along both end abutments and
2) rotation about the surface coordinate ξ_2 shown in Fig 5.2a restrained at all nodal points along both abutments.

The surface coordinate system was used only at the abutments in order to provide rotational restraint about ξ_2 since the bottom surface of the slab rested on the abutments continuously along the skew. The expansion joints shown in Fig 5.2 were only in the parapets and sidewalks at the indicated locations. These joints were idealized in the finite element representation by providing nodal points on both sides of the expansion joints. These nodal points were not connected to each other. Therefore, movement of a nodal point on one side of the expansion joint did not directly induce movement in the nodal point on the other side. The following material properties were used for the static analyses:

1) a modulus of elasticity of 4,690,000 psi for the slab based on a compressive strength of 6000 psi,
2) a modulus of elasticity of 3,320,000 psi for the sidewalk and parapets based on a compressive strength of 3000 psi,
3) Poisson's ratio of 0.15, and
4) a coefficient of thermal expansion of .000006 in/in/°F.

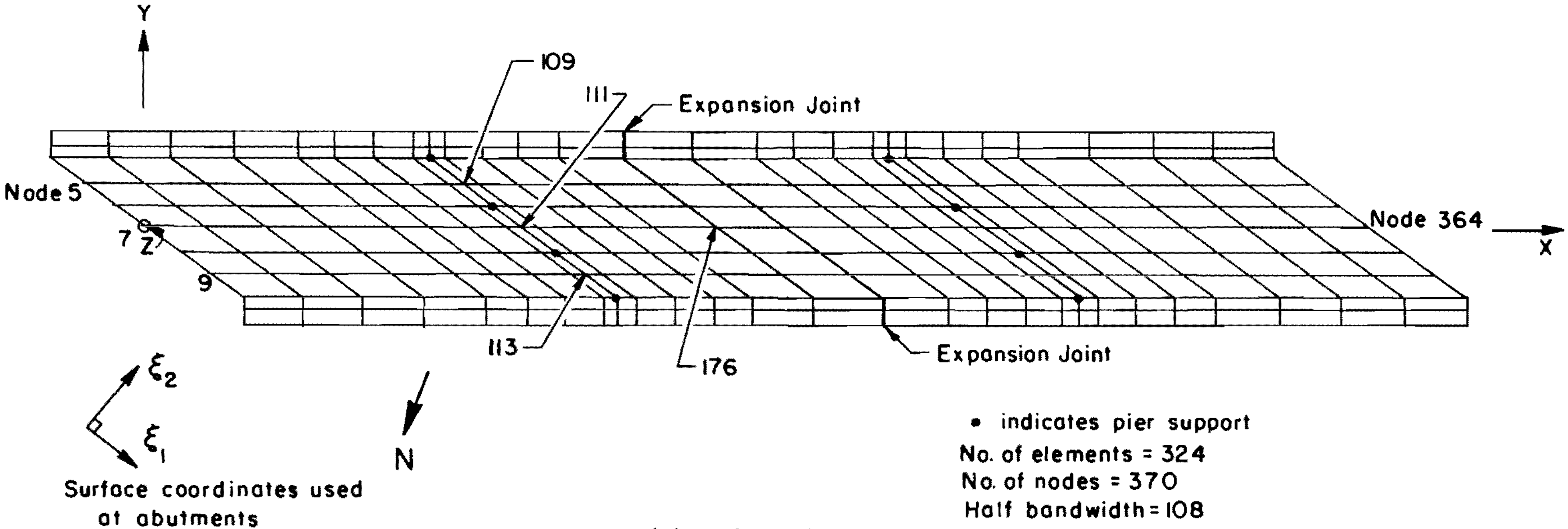

(a) Plan view.

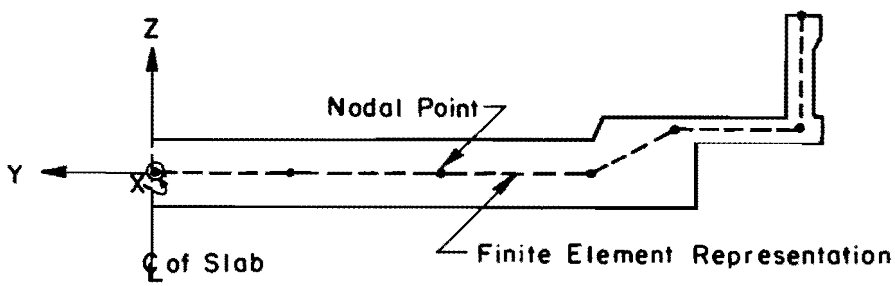

(b) Cross section.

Fig 5.2. Static analysis finite element mesh for Pasadena bridge.

Correlations of the measured and computer predicted slope changes for locations along the northeast abutment are presented in Fig 5.3. As shown in Appendix A, three inclinometer points, numbers 1, 2, and 3, were measured along this abutment. These locations corresponded to nodal points 5, 7, and 9 respectively in the finite element mesh. Since measured slope changes were about the Y-axis in Fig 5.2 and the computer results were about ξ_1 , the computer results were transformed so that they too were about the Y-axis. The inclinometer measurements shown in Fig 5.3 were obtained by subtracting the 0900 slope changes interpolated from the measurements presented in Appendix A. This was necessary since the static analyses slope changes were from the 0900 starting time. The following observations may be made from Fig 5.3:

1) the computer results follow the same trend as the field measurements with the exception of the computer results at 1100 hours,
2) the computer results are generally less than the field measurements, and
3) the difference between the maximum slope change measured at inclinometer point 3 and the corresponding computer result at nodal point 9 is approximately 15 percent.

The comparison in 3) above was selected since inclinometer point 3 exhibited the maximum slope change in the field measurements.

Correlations of the measured and computer predicted slope changes for locations along the line of the northeast pier supports are presented in Fig 5.4. Three inclinometer locations, points 4, 5, and 6, were measured along this line of pier supports. These locations corresponded to nodal points 109, 111, and 113 respectively of the finite element mesh. The slope changes obtained from the inclinometer measurements and the computer results were about the Y-axis in Fig 5.2. The following observations may be made from Fig 5.4:

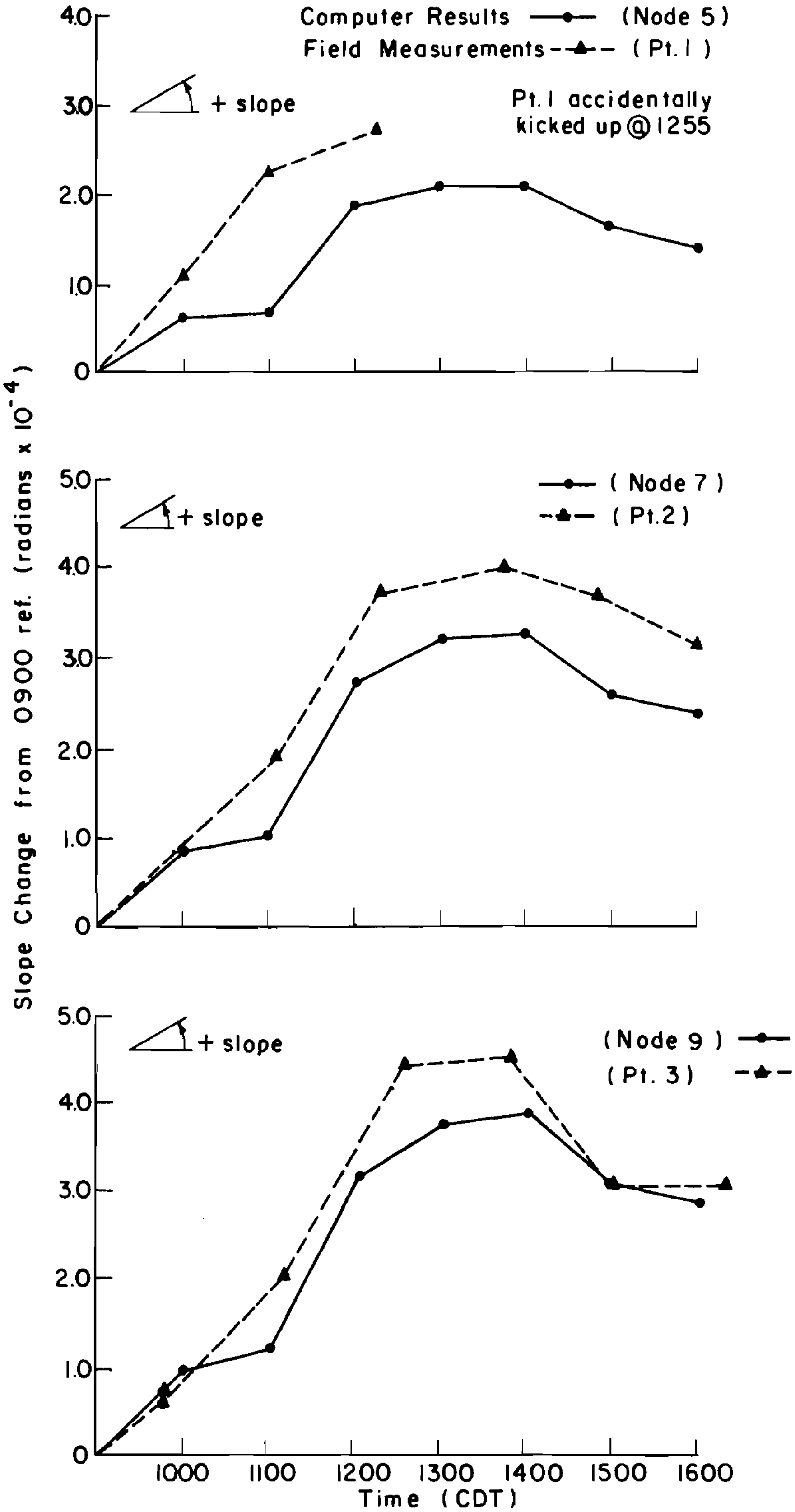

Fig 5.3. Correlation of measured and computer slope changes for locations along abutment.

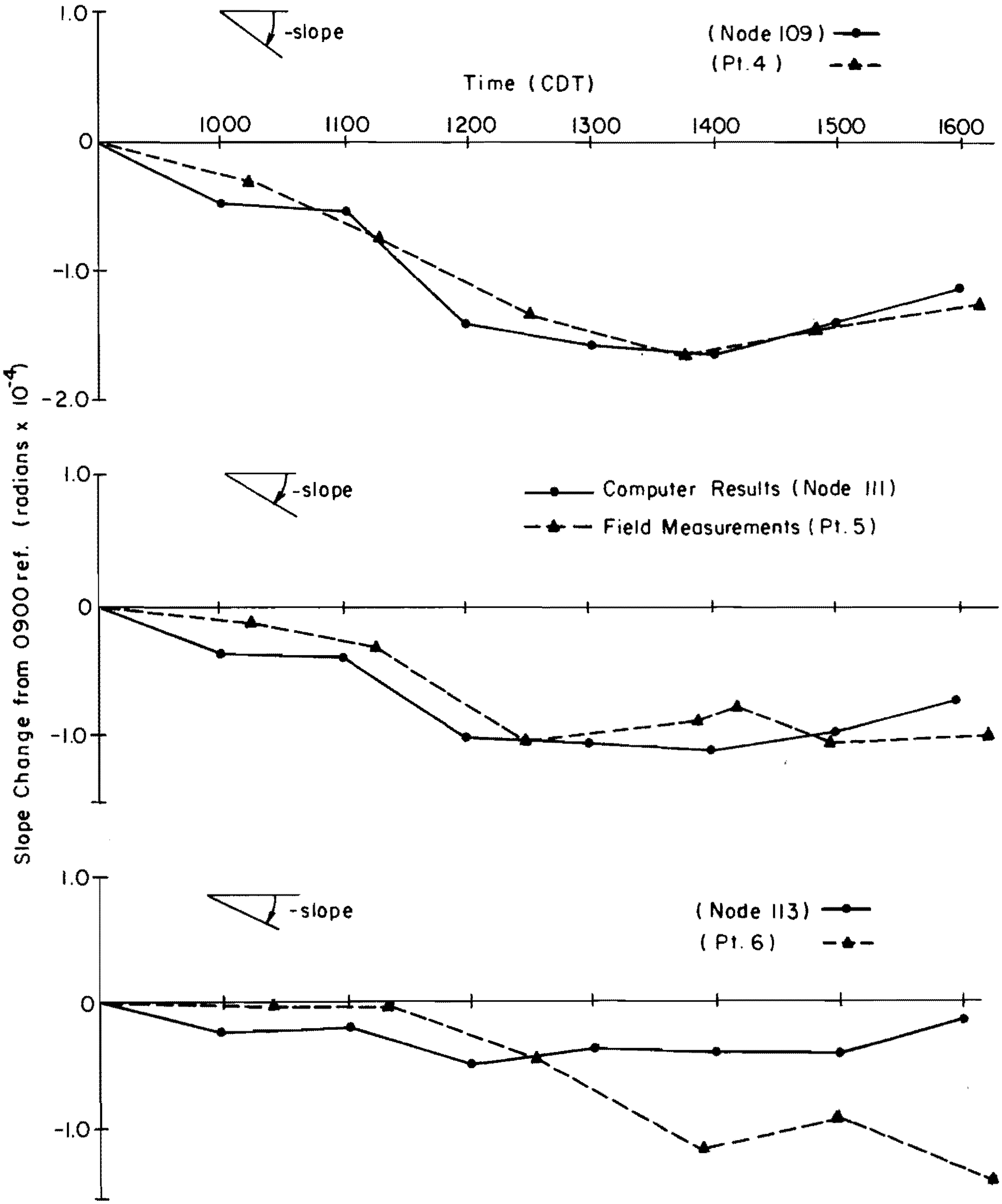

Fig 5.4. Correlation of measured and computer slope changes for locations along line of pier supports.

1) the computer results generally follow the same trend as the field measurements with the exception of the results at node 113 and inclinometer point 6,
2) the computer results are of the same order of magnitude as the field measurements, and
3) the slope changes measured and computed along the line of the pier supports are approximately one-third or less of the slope changes measured or computed at the abutment.

No explanation is available for the discrepancies between the measured results obtained at inclinometer point 6 and the computer results obtained at node 113. A parameter study to explore possible sources of discrepancies in the computational procedure will be presented in Section 5.11. However, the correlations as presented both along the abutment and the line of pier supports are considered favorable.

The temperature induced stresses obtained from the static analyses showed that the top of the slab was in compression at all nodal points at all times that the stresses were evaluated. Stresses predicted at mid-depth of the slab were tensile while stresses predicted for the bottom of the slab varied from small magnitudes of tension to small magnitudes of compression. An example of the temperature induced stresses for node 176 of the finite element mesh is illustrated in Fig 5.5. This figure shows the variation in the longitudinal stress with time for the top, bottom, and middle surfaces of the slab. The maximum tensile stress predicted at this node was 147 psi while the maximum compressive stress predicted was 455 psi. Both of these stresses occurred at 1300 hours. The rapid increase in the stresses shown in Fig 5.5 between 1100 and 1200 is attributed to the rapid increase in the surface temperatures due to the cloud cover clearing between these hours. This rapid temperature increase has previously been illustrated in Fig 4.5, Fig 5.1 and the measured surface temperature variations of Appendix A. The temperature induced stresses shown in Fig 5.5 are the changes in stress from the assumed 0900 reference time. The low magnitudes of

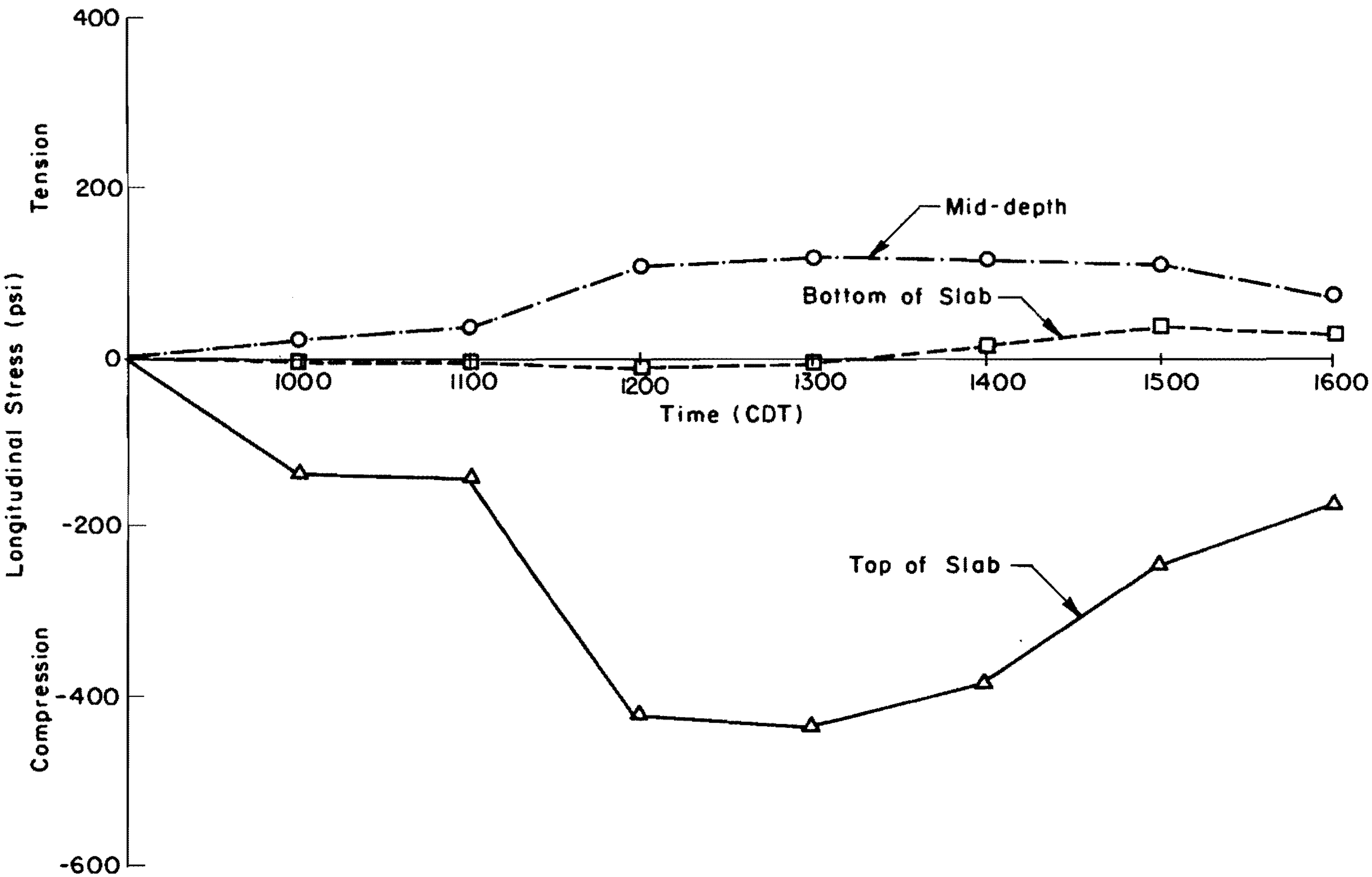

Fig 5.5. Variation of the longitudinal temperature stresses at node 176 with time.

these stresses are due to the poor testing conditions for temperature effects on the day of the test. Based on studies performed by Thepchatri (39), one would expect the maximum temperature induced stresses to be approximately twice those shown in Fig 5.5 under environmental conditions such as clear skies and little wind.

5.11 Parameter Study on Pasadena Bridge

A parameter study was undertaken to determine the effects of various quantities on the response of the Pasadena bridge using temperature data from the field test. Heat conduction and/or static analyses were performed to determine the effects of the following parameters:

1) a small variation, 1°F, of the initial uniform temperature distribution assumed for the slab in Section 5.1,
2) the temperature distributions present in one or more of the following components of the structure: a) the sidewalks, b) the parapets, and c) the element joining the sidewalk and and slab as shown in Fig 5.2, and
3) the magnitude of the fictitious rotational stiffness constant, $\overline{\alpha}$, from Eq 2.12.

The above parameters were varied and the results compared with the field measurement and computer slope change results from Section 5.1. The slope changes were compared for the various parameters at only one time, 1300 hours, since the maximum slope changes observed during the field test occurred between 1300 and 1400 hours.

The first parameter considered was the magnitude of the initial temperature distribution in the slab only. The magnitude was decreased from 86°F to 85°F. Heat conduction analyses were performed to determine the new internal temperature distribution for the various slab thicknesses. The temperature changes at 1300 hours from the 0900 initial temperatures were then used for a static analysis to determine the slope changes. Results obtained from the static analysis indicated that the small variation in the starting temperature distribution had a negligible effect on the slope changes. This is illustrated in Table 5.1 for several locations. Other parameter results are also presented in Table 5.1.

The next set of parameters studied was the temperature distributions in the parapet, sidewalk, and the element that joined the slab to the sidewalk as shown in the finite element mesh cross section in Fig 5.1b. These temperatures were studied in the hope that they had a negligible effect on the slope changes and that they could be neglected in future analyses since they greatly complicated the heat conduction analysis. Static analyses were performed ignoring the temperature distributions in first the parapet, then the sidewalk, and finally the temperatures in the element joining the slab and sidewalk. Results of the analyses indicated that the temperature distribution in the parapets had a significant effect on the slope changes. The temperature distributions in the sidewalk and element joining the slab and sidewalk had a much smaller effect on the slope changes. The effects of this set of parameters is also shown in Table 5.1.

The final parameter studied was the magnitude of the rotational stiffness constant, $\overline{\alpha}$, in Eq 2.12. This constant was reduced from 0.02 to 0.002. Results obtained indicated that the slope changes at the abutments increased approximately 7 percent while the slope changes at points with smaller magnitudes increased considerably more on a percentage basis. This indicated that some of the discrepancies shown in Fig 5.3 and Fig 5.4 were due to the rotational stiffness constant. It should be noted that while the slope changes at some locations varied considerably, the stresses in the slab changed very little. This is due to the fact that most of the predicted stresses in the slab were from the nonlinearity of the temperature gradient and not the indeterminancy of the structure.

TABLE 5.1. Parameter Study on Pasadena Bridge at 1300 Hours

	Slope Changes (radians $\times 10^{-4}$)			
Field measurement location	Pt. 2	Pt. 3	Pt. 4	Pt. 6
Finite element mesh location	Node 7	Node 9	Node 109	Node 113
Field measurements (interpolated from Figs 5.3 and 5.4)	3.89	4.47	-1.50	-0.70
All of the following are results obtained from the finite element static analysis program.				
Results presented in section 5.1	3.26	3.76	-1.60	-0.39
Initial uniform temperature in slab changed from 86°F to 85°F	3.22	3.73	-1.58	-0.36
Temperatures in				
a) parapet neglected,	2.55	3.16	-0.94	-0.47
b) sidewalk neglected, and	3.24	3.74	-1.54	-0.30
c) element from sidewalk to the slab neglected	3.18	3.65	-1.58	-0.33
Rotational stiffness constant, $\bar{\alpha}$, from Eq 2.12 reduced from 0.02 to 0.002	3.43	3.99	-1.67	-0.48

In summary, the temperature distribution in the parapets has a significant effect on the slope changes of this structure. The absolute magnitude of all slope changes are decreased by neglecting the temperatures in the parapets. The magnitude of the fictitious rotational stiffness constant has an effect on the slope changes. The rotational stiffness artificially stiffens the structure as was expected.

5.12 Temperature, Dead Load, and Prestress Stresses on Pasadena Bridge

The final study performed on the Pasadena bridge was the superposition of the temperature effects with those of the dead load and prestress. The temperatures used were those from the day of the field test at 1300 hours. The time, 1300, was selected since the temperature induced stresses had been found to be a maximum then. The equivalent loading method suggested by Lin (29) and Khachaturian (26) was used to determine the prestress effects on the structure. The dead load effects were determined by simply specifying the unit weight of the concrete in the static analysis program.

The equivalent prestress loading for a unit width of the structure was computed using the prestress conduit layout and the geometric shape of a longitudinal section of the slab. The longitudinal section and conduit layout are shown in Fig 5.6. The equivalent loading that was computed is depicted in Fig 5.7. This loading is for a unit width of the slab and a unit force of one kip of prestress force. The final loading was computed by multiplying the unit loading from Fig 5.7 by the total prestressing force after losses and then distributing the load over the width of the slab. Eleven prestressing tendons were distributed over the width of the slab with a final prestressing force of 368 kips in each tendon at release. These forces were reduced to account for losses due to friction, shrinkage, elastic shortening, creep, etc. An average force was computed and assumed to be constant over the length of the bridge to simplify the calculations. A loss of 33000 psi in each tendon was used to account for losses other than

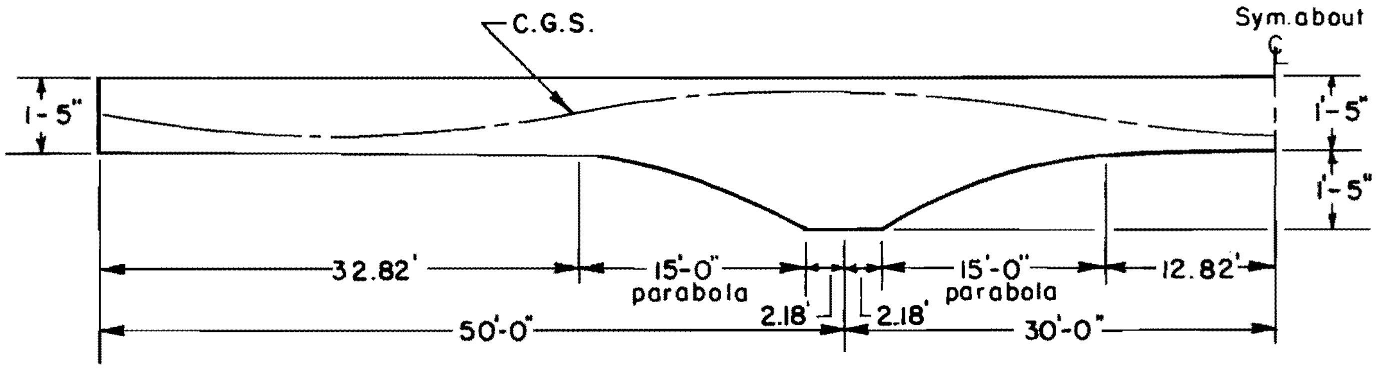

(a) Typical longitudinal section of slab.

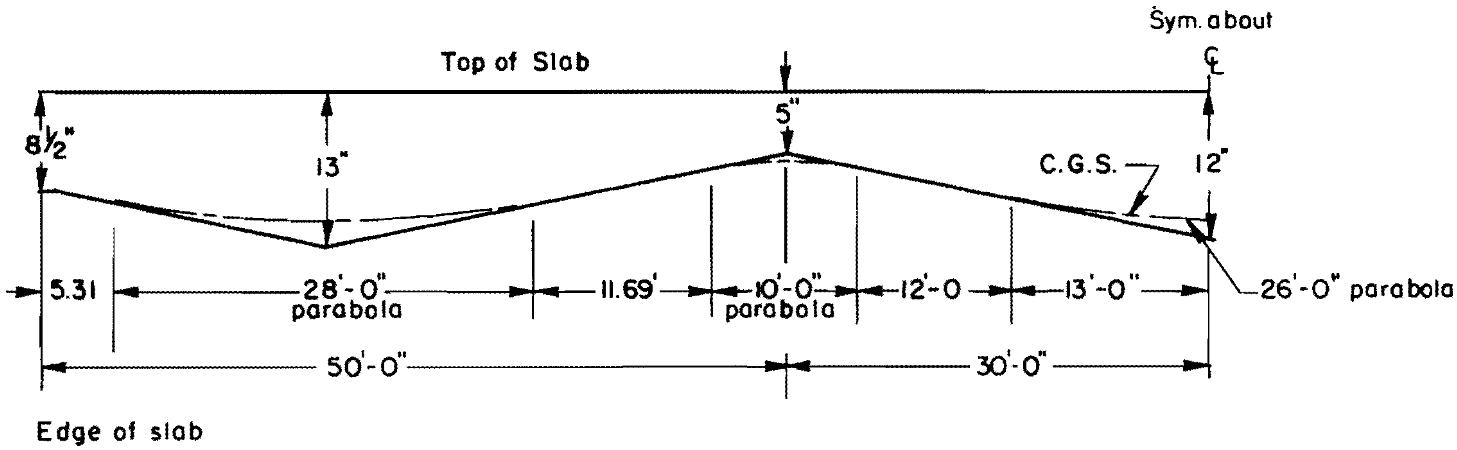

(b) Prestressing conduit layout using the top of the slab as a level datum.

Fig 5.6. Typical longitudinal section and prestressing conduit layout for Pasadena bridge.

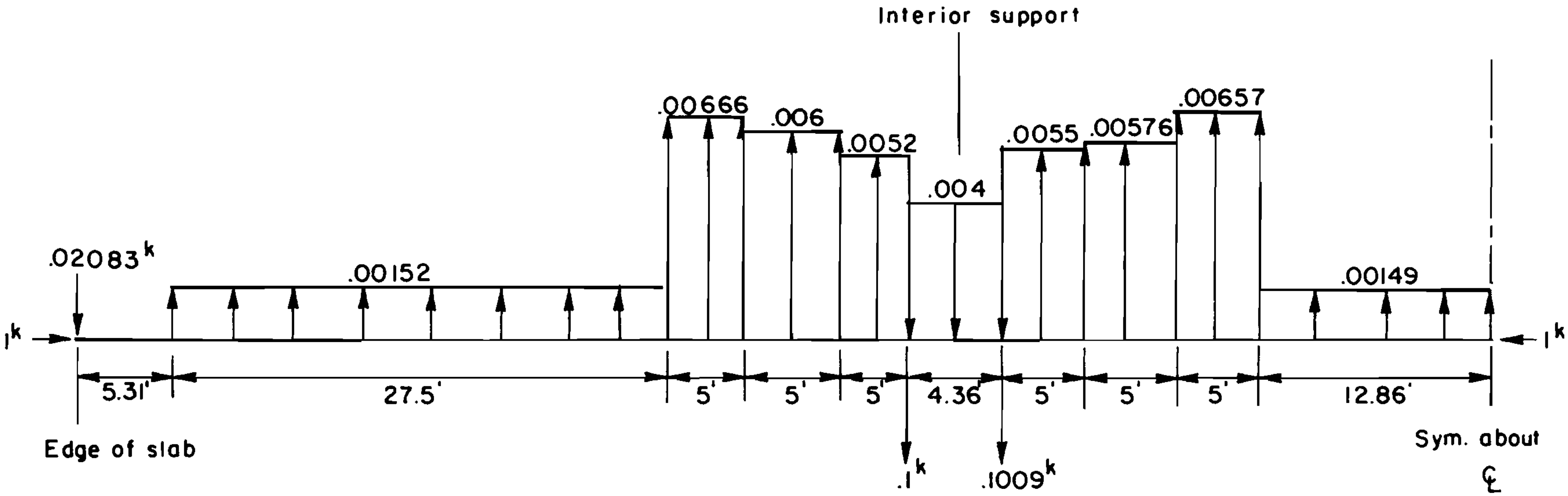

Note: All uniform loads in units of kips/ft of length
Equivalent loads shown are for 1^k of prestress force

Fig 5.7. Equivalent prestress loading for unit width of Pasadena bridge.

friction. This figure was obtained from the 1975 AASHTO Interim Specifications for Bridges (3). The loss of 33000 psi is recommended for concrete with a compressive strength of 5000 psi while the slab strength was 6000 psi. Friction losses were calculated at each point of angle change in the conduit using the formula suggested in the 1973 AASHO Bridge Specifications (1). The friction losses were calculated assuming the tendons were jacked at both ends of the bridge. These friction losses were then averaged and assumed to be constant over the length of the bridge. The average friction loss computed was 22500 psi. The total loss in prestress reduced the force in each tendon to 262 kips, or 29 percent total losses.

Stresses due to the dead loading and prestressing forces were computed first and then the stresses due to the temperature changes were included. The results obtained from the analyses are illustrated in Fig 5.8 for a longitudinal section of the slab at the center of the roadway. Stresses are presented in Fig 5.8 for the top, middle and bottom surfaces of the slab. In general, the temperature induced stresses would not be symmetrical due to the different distributions in the parapets and sidewalks on opposite sides of the bridge. However, at the time used in the analysis, 1300 hours, the difference in temperatures of the parapets and sidewalks on opposite sides was small; thus, the difference in stresses on each side of the axis of symmetry were negligible. The following observations can be made from Fig 5.8:

1) the temperature stresses increases the top surface compressive stresses due to the dead loading and prestressing by at least 400 psi at all locations along the length of the section,
2) the temperature stresses had little or no effect on the stresses at the bottom and middle surfaces of the slab,
3) the superposition of the dead loading, prestressing, and temperature did not produce tensile stresses at any location, and

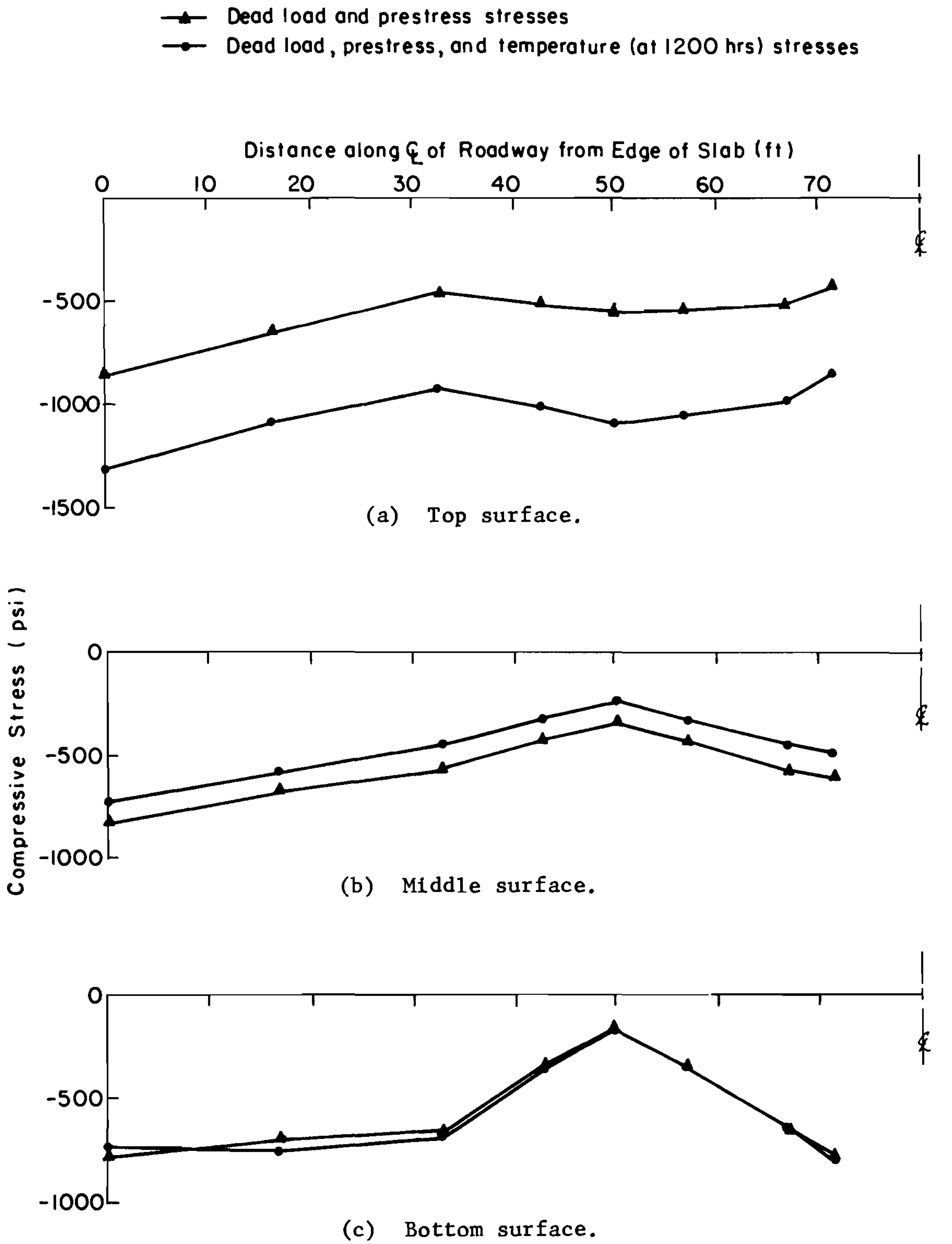

Fig 5.8. Dead load, prestress, and temperature (1300 hours) stresses along length of slab.

4) all stresses were within allowable design limits (compressive allowable = 0.4 f'_c (1)).

The low magnitudes of the stresses are attributed to the over-design of the bridge since the inertia and area of the parapets and sidewalks are neglected in the design process. Even though the parapet and sidewalks are lower strength concrete and are assumed to have a lower modulus of elasticity, they contribute considerable to the stiffness of the structure. Also, the temperatures measured on the day of the field test were much less than would normally be encountered on a clear day.

5.2 Correlation of Field Measured Slope Changes and Computer Results for Pedestrian Overpass (14 March 1975)

The large variation in the measured temperatures about the cross section of this bridge required a two-dimensional heat conduction analysis to determine the transient internal temperature distribution. The finite element mesh used for the heat conduction analysis is depicted in Fig 5.9a. The temperature distribution was assumed to be constant along the longitudinal axis of the bridge. Average concrete thermal properties as used for the analysis of the Pasadena bridge were used for the analysis of the pedestrian overpass also. Surface temperatures obtained from measurements at the 53 locations about the cross section were specified as boundary conditions. As mentioned previously in Section 4.2, the locations and the measured temperature variation with time are presented in Appendix B. Linear interpolation between measurement locations was used to approximate the surface temperatures at nodal points in the finite element mesh where measurements were not taken. The most difficult problem faced in the analysis, other than the large amount of input data required, was the determination of the initial uniform temperature distribution and starting time approximations. This was due to the side heating of the east side of the bridge in the early morning while the rest of the bridge remained relatively cool. An analysis of the measured surface temperatures

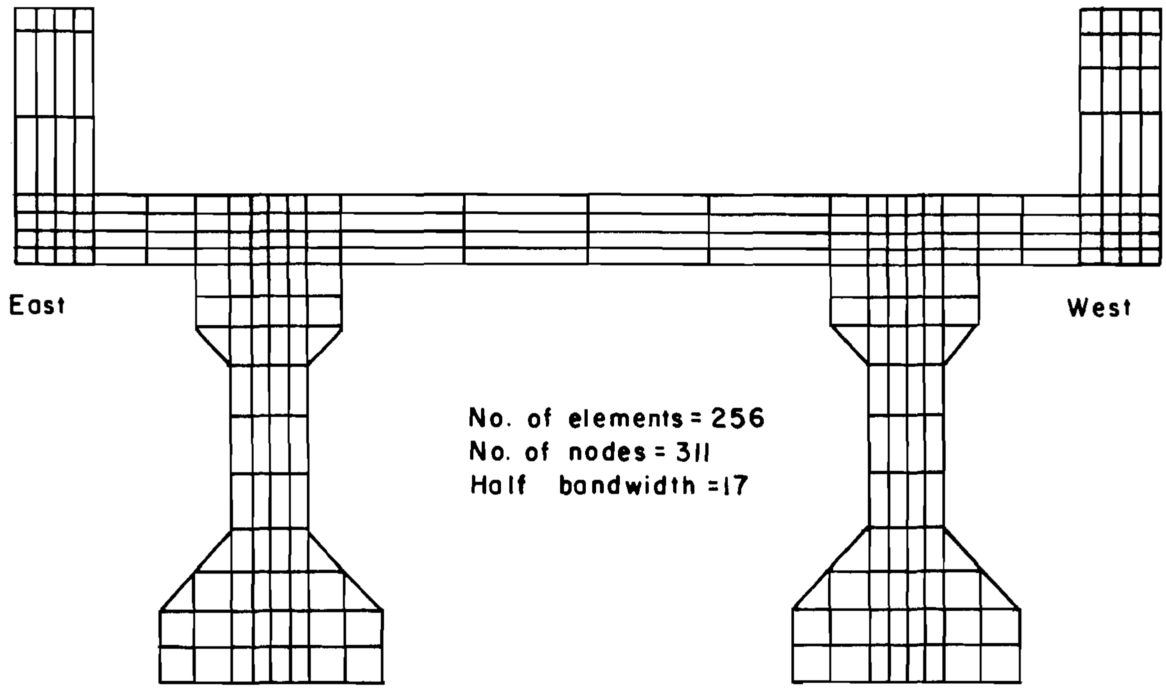

(a) Heat conduction mesh.

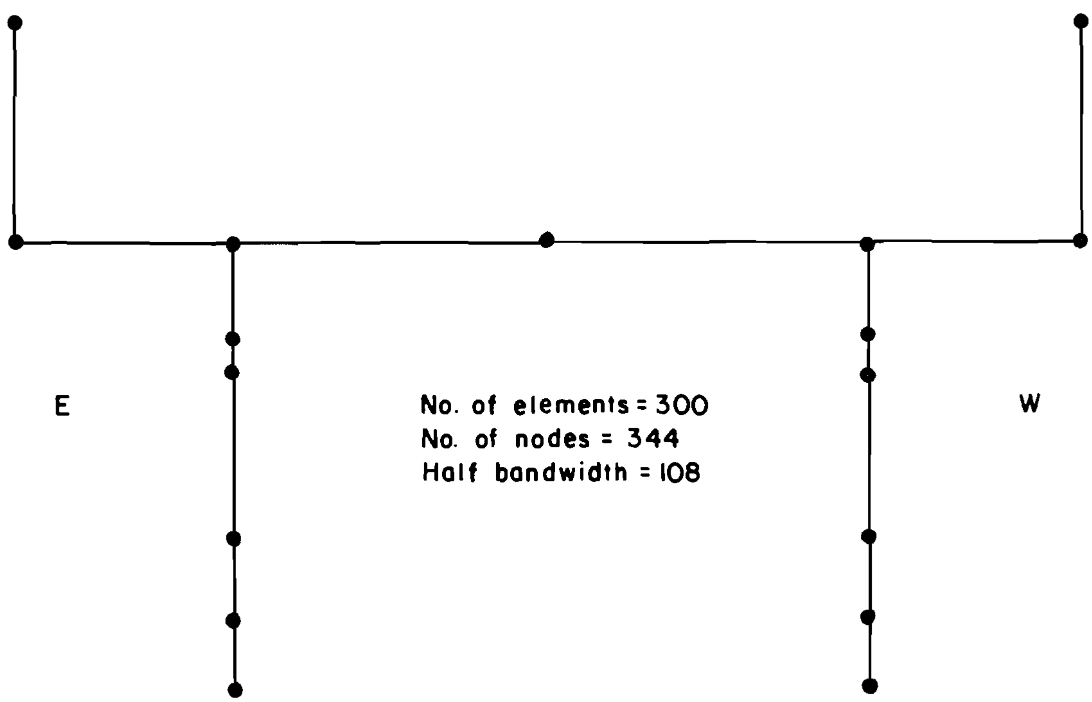

(b) Cross section of static analysis mesh.

Fig 5.9. Finite element meshes used for pedestrian overpass analysis.

revealed that a 41°F initial uniform temperature distribution at 0830 (CDT) would provide the smallest variation in temperature around the cross section.

The heat conduction analysis was performed every hour between 0830 and 1830 hours (CDT). Temperatures were also calculated at 1000 hours since a static analysis had to be performed at this time to obtain a reference slope for comparison with the inclinometer slope changes. An example of the internal temperature approximations and the specified surface temperatures at 1530 is shown in Fig 5.10 for both girders. The time, 1530, was selected for comparison since the maximum measured slope change occurred at that time. The temperature distributions along the centerline of the girders were nonlinear as can be observed in Fig 5.10. The nonlinearity occurred primarily in the flanges of both girders and in the slab. Temperatures in the east girder were slightly higher at this time as a result of side heating in the morning. The temperatures in the top of the slab were slightly higher over the west girder due to the shading of the east side of the slab by the parapet in the morning.

Temperature changes from the 41°F initial temperate distribution were then used for the static analyses. A cross section of the mesh used for the static analyses is shown in Fig 5.9b. Longitudinal divisions were specified every five feet in this mesh. The bridge response was assumed to be symmetric about the interior support; therefore, only the north span of the bridge was idealized for the static analyses. Expansion joints in the parapets were neglected in the finite element idealization. The following material properties were used in the analyses:

1) a modulus of elasticity of 4,690,000 psi for the girders based on a compressive strength of 6000 psi,
2) a modulus of elasticity of 3,320,000 psi for the slab and parapets based on a compressive strength of 3000 psi,

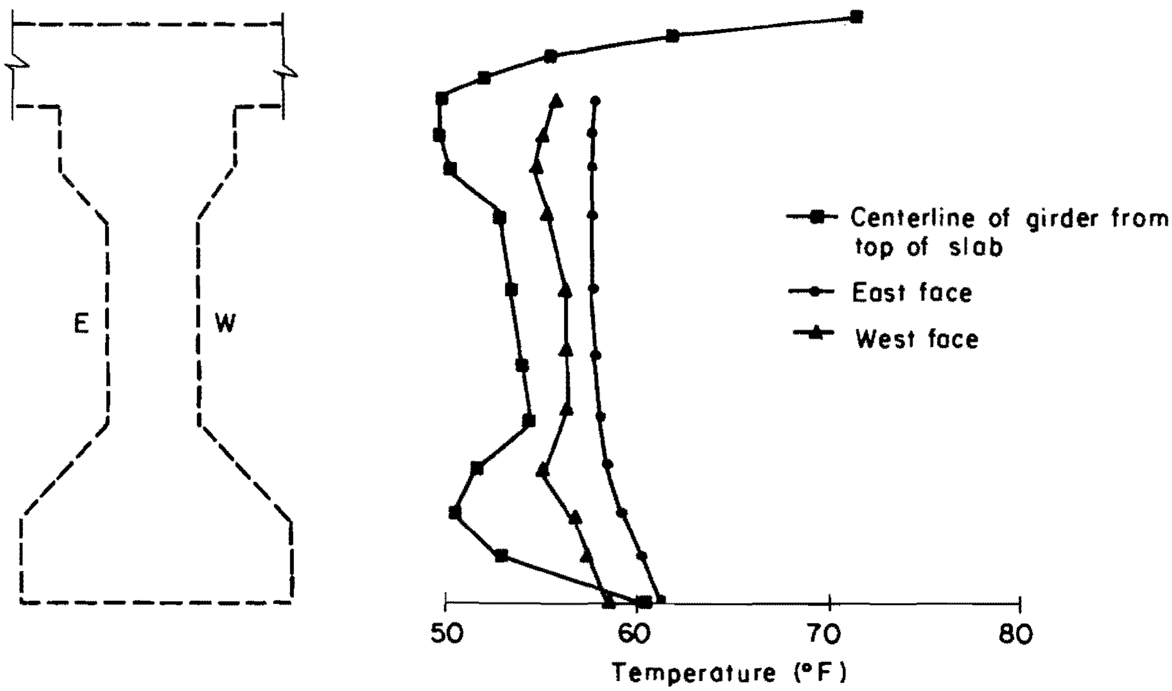

(a) Temperature distribution in East girder at 1530 hours.

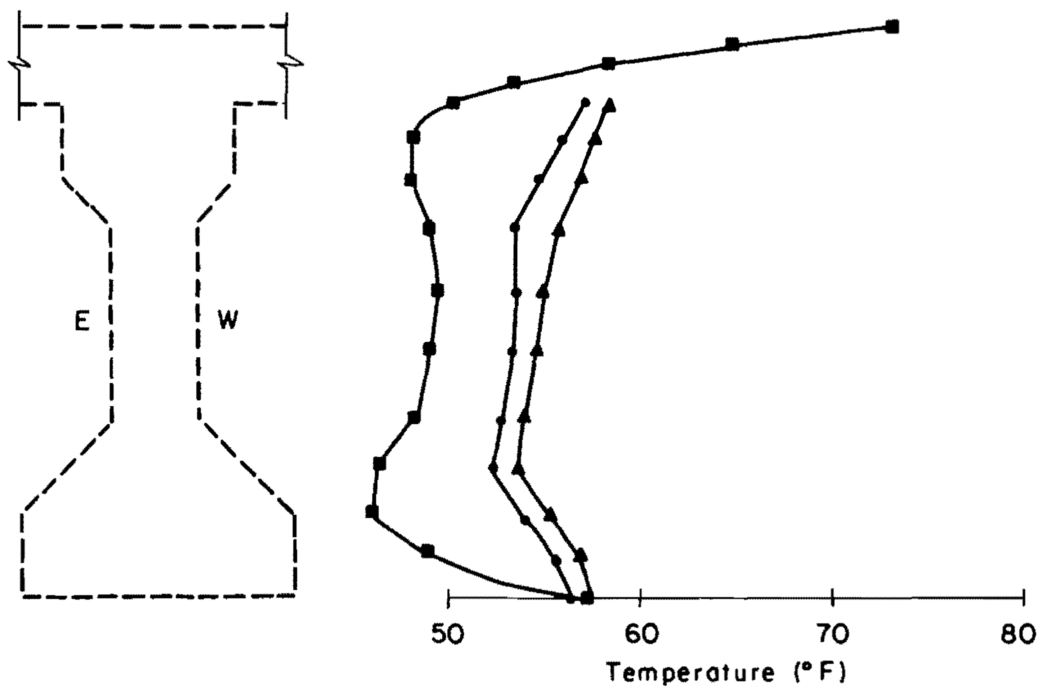

(b) Temperature distribution in West girder at 1530 hours.

Fig 5.10. Predicted girder temperature distributions at 1530 hours.

3) Poisson's ratio of 0.15, and

4) a coefficient of thermal expansion of .000006 in/in/°F.

The concrete was assumed to be uncracked for the analyses.

Analyses were performed at 1000 and then from 1030 until 1830 in one hour time intervals. The 1000 analysis was performed to provide a reference slope for comparison with the inclinometer results. The slope obtained at this time was subtracted from slopes at other times at the nodal point corresponding to the inclinometer location. This was necessary to obtain the slope change from 1000 since inclinometer measurements were not observed until 1010 on the day of the test. The ten minute difference in reference times was assumed to be negligible. Correlation of the measured slope changes and static analyses results is shown in Fig 5.11. The correlation was excellent as can be observed from Fig 5.11. The finite element analysis was able to accurately track the slope change as it increased and decreased. As mentioned in Section 4.2, slope changes were obtained at only one location during the field test due to a malfunction of a new inclinometer. The slope change about the transverse axis of the bridge was found to be a maximum at the location of the inclinometer from the finite element analyses.

An example of the longitudinal stress distributions at 1530 in the girders at the exterior support is presented in Fig 5.12. The time and location were selected for illustration since the maximum tensile stress obtained in the analyses, 415 psi, was predicted at 7 inches from the bottom of the west girder at the interior support. Stresses in the slab were compressive at all locations and times analyzed. The stresses at the middle of the slab width at the interior support at 1530 were as follows: top of the slab, 384 psi compression, mid-depth of the slab, 90 psi compression, and the bottom of the slab, 47 psi compression. Vertical movements predicted by the analyses were small with a maximum movement of 0.05 inches predicted at 1530 hours.

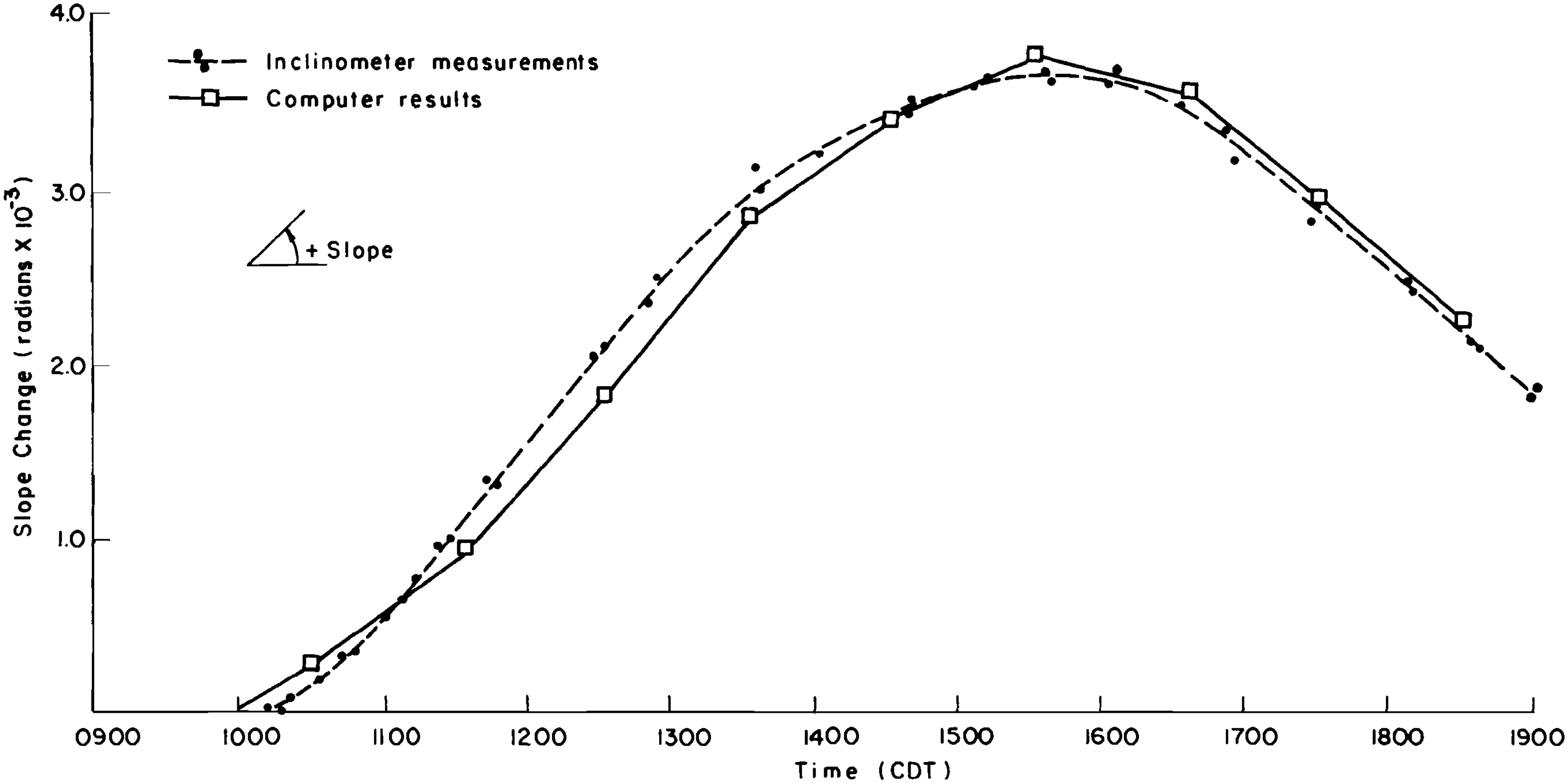

Fig 5.11. Correlation of measured slope changes and computer results for pedestrian overpass (14 March 1975).

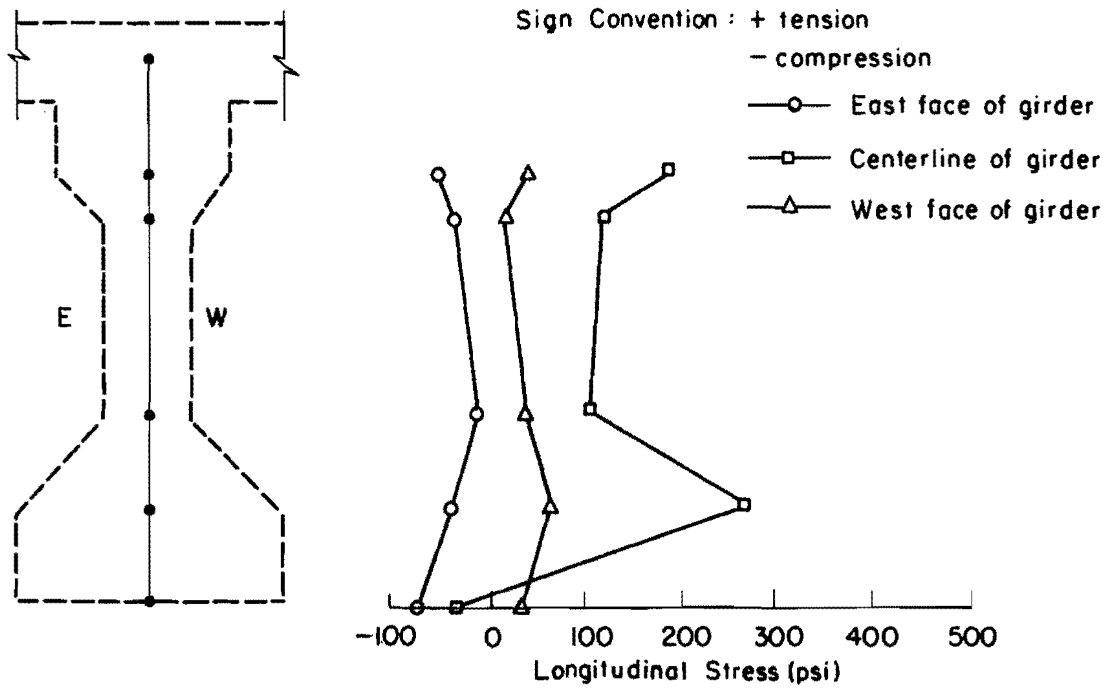

(a) Stress variation thru depth of East girder @ 1530.

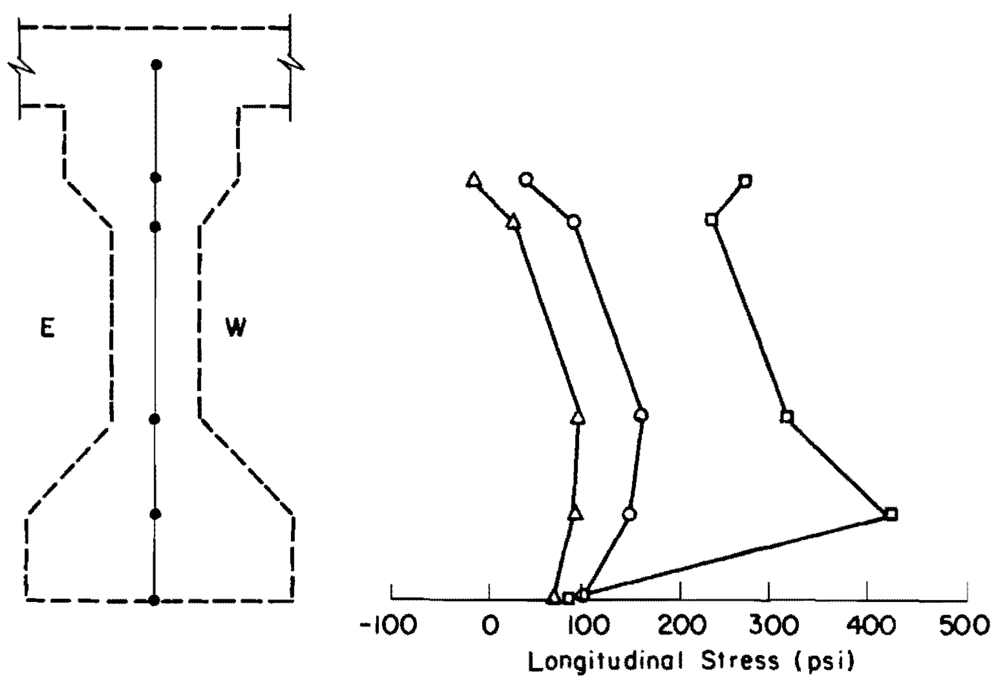

(b) Stress variation thru depth of West girder @ 1530.

Fig 5.12. Predicted girder temperature stresses over interior support at 1530 hours.

5.3 Application of the Present Analyses to Other Bridge-Types

The subject heat conduction and thermal stress analyses may be applied to other bridge-types. The first step in the analysis is related to determining the transient temperature distributions of the bridge. There are three methods to determine the temperature distributions:

1) the direct measurement of the temperatures by the internal instrumentation of the bridge using thermocouples,
2) the measurement or approximation of the solar radiation intensity and the air temperature variation coupled with the heat conduction analysis as exemplified in Section 3.1 and Thepchatri's study (39), and
3) the measurement of surface temperatures coupled with the heat conduction analysis as illustrated by the Pasadena and pedestrian overpass analyses discussed in Sections 5.1 and 5.2 respectively.

The solar radiation used in 2) above may be measured using pyranometers as discussed in Section 4.12. The solar radiation intensity may also be obtained from selected U.S. Weather Bureau stations or from handbooks such as Strock's (38). The air temperature variation may be obtained from the same sources or newspapers. However, data may not be available for the exact geographical location of the bridge being analyzed. Therefore, approximate climatic data from the nearest available location must be used.

One of the most difficult aspects in applying 2) and 3) above is the determination of an initial temperature distribution for the heat conduction analysis. The following methods have been used in this study and previous research:

1) the establishment of a time when the bridge temperature is approximately the same as the air temperature as discussed in Section 3.1, Emerson's work (18), or Thepchatri's (39), and

2) the use of measured surface temperatures and assuming that an initial uniform temperatures distribution exists when the top and bottom surfaces have the same temperatures (Section 5.1) or when the deviation of the measured temperatures is the smallest from the average measured temperatures (Section 5.2).

Once the transient internal temperature distribution of the bridge has been determined, then the thermal stress analysis is performed. At each nodal point in the thermal stress idealization, five temperatures are input as illustrated in Fig 2.4. These temperatures are obtained either from direct measurement or from the heat conduction analysis. The thermal stress analysis may be performed repeatedly for as many times as there are temperature distributions.

CHAPTER 6. SUMMARY, CONCLUSIONS, AND RECOMMENDATIONS

Finite element procedures were presented for the transient heat conduction analysis and static thermal stress analysis of bridge-type structures. These procedures were shown to be able to solve for the thermal response of a wide variety of bridge types including bridges with skew, various boundary conditions, multiple girders, parapets, and sidewalks. Classical solutions have limited applicability to the thermal stress analysis of bridges. Previous numerical solutions have only been able to accurately solve for the thermal response of beam-type structures.

In addition to the development and modification of the finite element procedures, field tests were conducted on two bridges to determine temperature induced movements and surface temperatures. Favorable correlations were presented between the field measured movements and results that were obtained using the finite element procedures.

6.1 Summary of Finite Element Procedures

A finite element program (45) employing two-dimensional quadrilateral or triangular elements was used to predict the transient temperature distributions in the bridges studied. Solar radiation heat input and convective boundary conditions may be specified in the program. The program was mainly used in the subject study to determine the internal temperature distributions by specifying measured surface temperatures. Modifications performed on this program were minor and related only to improving the input data generation schemes.

A finite element static analysis program (23) was extended to determine the thermally induced stresses and movements of bridge-type structures. This program utilized two-dimensional triangular and quadrilateral elements in a three-dimensional global assemblage with six degrees-of-freedom at each nodal point. Uncoupled in-plane and plate bending stiffnesses are incorporated in each element stiffness providing the element with five degrees-of-freedom at each nodal point. The sixth degree-of-freedom was incorporated by using a fictitious rotational stiffness recommended by Zienkiewicz (46). Primary modifications made to the static analysis program were related to the calculation of thermal forces and stresses. Expressions for the thermal forces of each element are presented based on the quartic approximation of the temperature distribution through the thickness of each element and a linear approximation to the temperature distribution over the surface of each element.

The thermal forces calculated at each node are "average" quantities for a nonlinear temperature distribution. These average forces produce errors in the computed stresses for nonlinear temperature distributions at boundaries and points of rapid change in the geometry of temperature distribution. However, the example in Chapter 3 shows that the errors disappear within a short distance of their incidence. Another example presented compared the thermal deflection and stresses of a plate obtained by a classical analysis with those obtained by the finite element analysis. The comparison was excellent.

6.2 Summary of Instrumentation and Field Tests

Field measurements were performed on two bridges located in the state of Texas to determine thermally induced slope changes and surface temperatures. Simple instruments were used to measure both the surface temperatures and slope changes. A portable temperature probe was developed to measure the surface temperatures at selected locations on the bridge's surface. Temperature induced slope changes were measured on the bridge's top surfaces with a mechanical inclinometer.

The first bridge tested was an entrance ramp structure in Pasadena, Texas. This bridge was a skewed, post-tensioned, three-span continuous slab structure. The test was conducted on 24 August 1974. Despite undesirable testing conditions for thermal effects, the slope changes measured due to thermal effects were of the same magnitude as the live load response observed in a previous test (30).

The second bridge tested was a pedestrian overpass located in Austin, Texas. This bridge was a two-span structure using precast pretensioned beams made continuous for live load. The test was performed on 14 March 1975. The surface temperature distribution of this structure was complex due to the side heating of the two girders and the partial shading of the top of the slab by the parapets. Due to the complexity of the surface temperature distribution, surface temperatures were measured at 53 stations. Inclinometer results were obtained at only one location due to the fact that one of the inclinometers malfunctioned.

6.3 Summary of Correlations of Field Measurements and Finite Element Results

Correlations of measured slope changes and results obtained using the finite element procedures were presented for both field tests. The measured surface temperatures were used to predict the internal temperature distributions. The static analysis program was then used to compute the thermally induced movements and stresses in the bridges. Correlations of the measured slope changes and finite element results were satisfactory for both structures.

Additional results were presented for the entrance ramp structure to determine the relative magnitudes of the temperature induced stresses with those of the gravity loading and prestressing. Results indicated that the temperature stresses increased the top surface longitudinal stresses by approximately 50 percent but had little effect on the stresses at the middle or bottom surfaces of the slab.

6.4 Conclusions

The objective of this study which was to quantitatively establish magnitudes of temperature induced movements by field tests on actual bridges and to correlate these results with a computer simulation of the structure subjected to the measured field temperatures has been accomplished. The correlations obtained between the measured slope changes and the results obtained using the subject finite element procedures demonstrate the capability and accuracy of the procedures.

The probe developed for measuring the surface temperatures demonstrated that relatively simple instrumentation may be used in the study of the diurnal heating of bridges when coupled with computational tools such as the finite element heat conduction program. The pedestrian overpass was a severe test of the predictive capabilities of the heat conduction program due to the side heating of the girders and shading of the slab by the parapet.

On cloudy days such as the one encountered for the field test on the entrance ramp, surface temperature measurements should be performed more frequently to define their variation with time. Surface temperatures were only measured hourly during the field test and the variation at each station was assumed to be linear between measured values.

The thermally induced stresses predicted in the analyses for both bridges are well within design limits. However, it should be emphasized that these stresses are only for the days of the tests which are not believed to be the most severe days for thermal effects. It was not within the scope of this study to predict the maximum temperature induced stresses or to determine the most severe weather conditions for these bridges. The low magnitude of the stresses in the entrance ramp structure is also due to the overdesign of the structure since the stiffness of the sidewalks and parapets are neglected in the design process.

6.5 Recommendations

The author's procedure in conjunction with Thepchatri's (39) now provide a means for investigating a wide range of variables in an attempt to isolate types and geographical locations of bridges that may be severely affected by thermal effects. Thepchatri's procedure which utilized a two-dimensional heat conduction program coupled with a stress analysis based on beam theory provides an economical tool to isolate possible severe thermal stress cases. Since two different finite element idealizations are used in this author's analyses, different input data must be prepared for the heat conduction and static analyses. The time involved in preparing the data for the two programs is significant and the computer time required for the static analysis program is also significant. The solution time for the analysis of three temperature load cases for the entrance ramp structure was approximately 416 TM seconds on the CDC 6600 at The University of Texas. Due to this significant amount of time required for preparation of input data and the solution of the problem, it is recommended that Thepchatri's program be used to determine possible severe thermal stress cases. Once these cases are isolated, then the author's stress analysis program can be used to determine the effects of skew, transverse behavior, and the stiffness contributions of the parapets and sidewalks, if any.

There are other immediate applications of the heat conduction and/or thermal stress analysis programs. The heat conduction program can readily be applied to the study of reinforced concrete pavement to evaluate the effects of temperature. Recent research in this area (31) has used a simplified temperature prediction model based on only the air temperature. Another area of interest is that of polymer-impregnated concrete. This is a relatively new area and is currently being investigated (25) as a solution of the bridge deck deterioration problem. Before the bridge deck is impregnated with monomer plastic, the surface is dried for several hours at 200 - 300°F to remove any moisture in the top of the surface (32). It is the drying process that could be investigated with the heat conduction and static analysis programs to determine the thermal effects of drying the surface at these temperatures. These programs might help locate any problems even though the conductivity (7) and tangent stiffness (13) of concrete change considerably at elevated temperatures.

APPENDIX A

FIELD TEST RESULTS FOR PASADENA BRIDGE

APPENDIX A. FIELD TEST RESULTS FOR PASADENA BRIDGE

Results and locations of surface temperature and inclinometer measurements observed on the Pasadena entrance ramp structure are presented in this Appendix. Also presented is a tabulation of the wind speed measurements that were observed during the field test. The field test on this structure was performed on 24 August 1974. A summary of the results has been presented in Section 4.3.

Surface temperatures were measured at 40 stations on the bridge's surface. The location of these stations is shown in Fig A.1. Surface temperatures were measured at these stations in approximately one-hour intervals from 0615 (CDT) until 1615 when the test was interrupted by rain. The measured surface temperature variation with time for all 40 stations is shown in Figs A.2 thru A.5. These figures were drawn by plotting the measured temperatures at their time of observation and then connecting the points with straight lines. On a clear day the surface temperature variation with time should be a smooth curve and this method of determining the variation should be a good approximation. However, the day of the test was cloudy and the surface temperatures should have been measured more frequently. The cloudiness has previously been illustrated in Fig 4.5a, the solar radiation measured by the Eppley pyranometer.

Inclinometer measurements were observed at nine stations on the top surface of the slab. These stations were aligned so as to measure the difference in elevation of two ball points parallel to the longitudinal axis of the bridge. The location and alignment of these stations is depicted in Fig A.6. The variation with time of the difference in elevation between the two ball points of the inclinometer is shown in Figs A.7 thru A.9 for all stations. The method of recording the readings and an example have been presented in section 4.2. From Figs A.7 thru A.9, the change in slope between two times is determined by computing the change in the difference in elevation between the two times and then dividing by 24-inches, the distance between the two ball points.

Anemometer measurements of the wind speed were observed on the top and bottom surfaces of the bridge at selected times. These readings were measured by holding the rotating cups of the anemometer near the top or bottom surfaces and recording the wind speed indicated on a mechanical recorder. The measurements observed are presented in Table A.1.

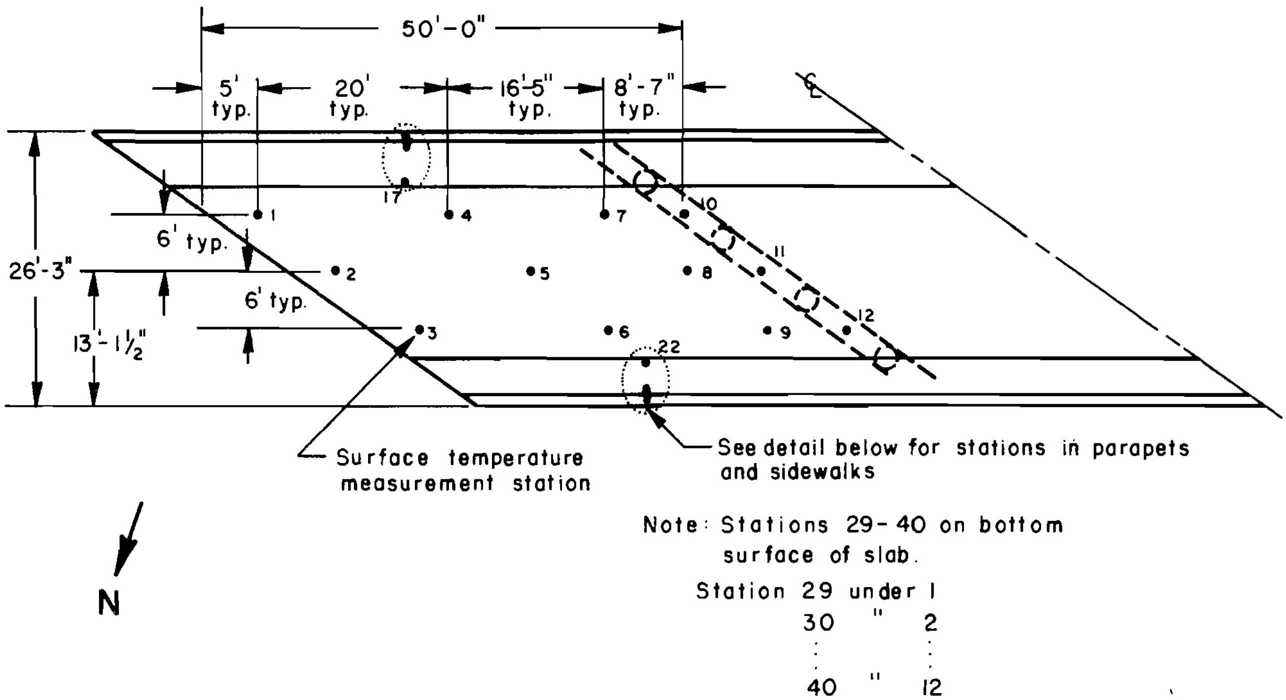

(a) Plan view showing surface temperature stations.

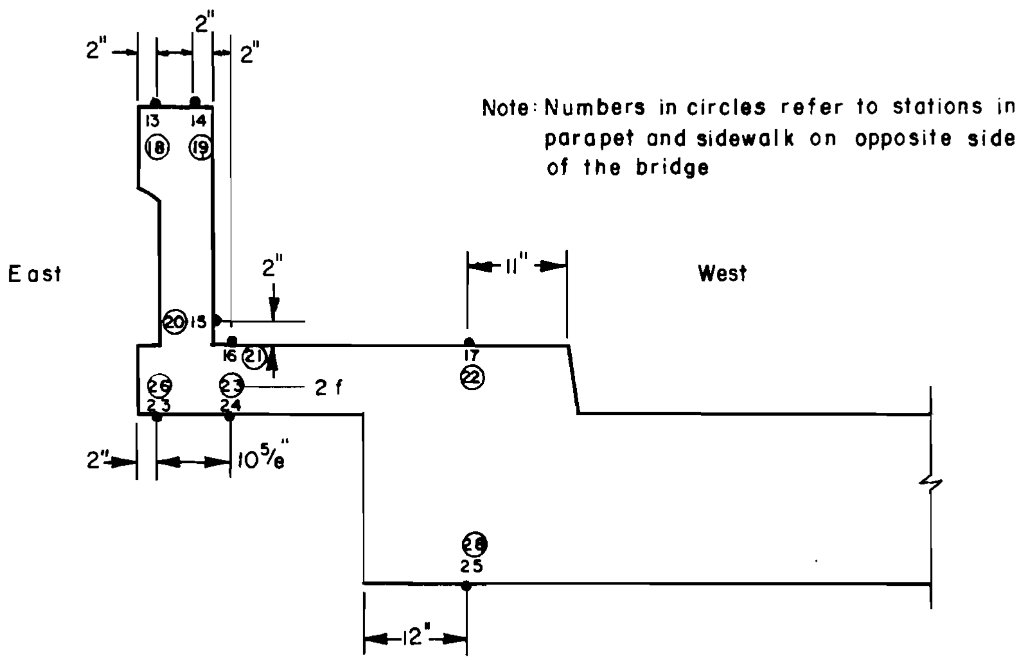

(b) Detail showing stations in parapets and sidewalks.

Fig A.1. Surface temperature measurement stations on Pasadena bridge.

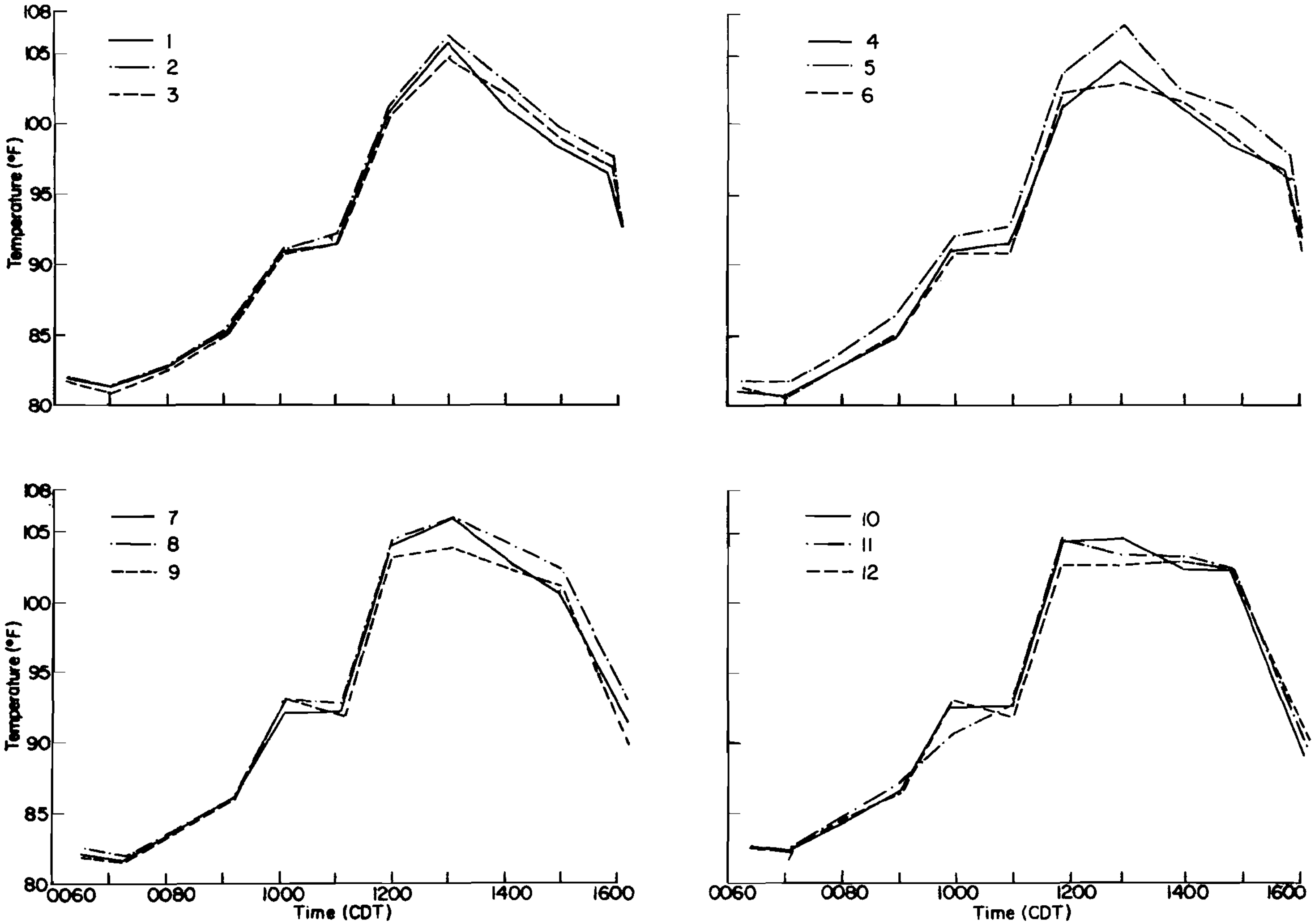

Fig A.2. Measured surface temperature variation for stations 1-12.

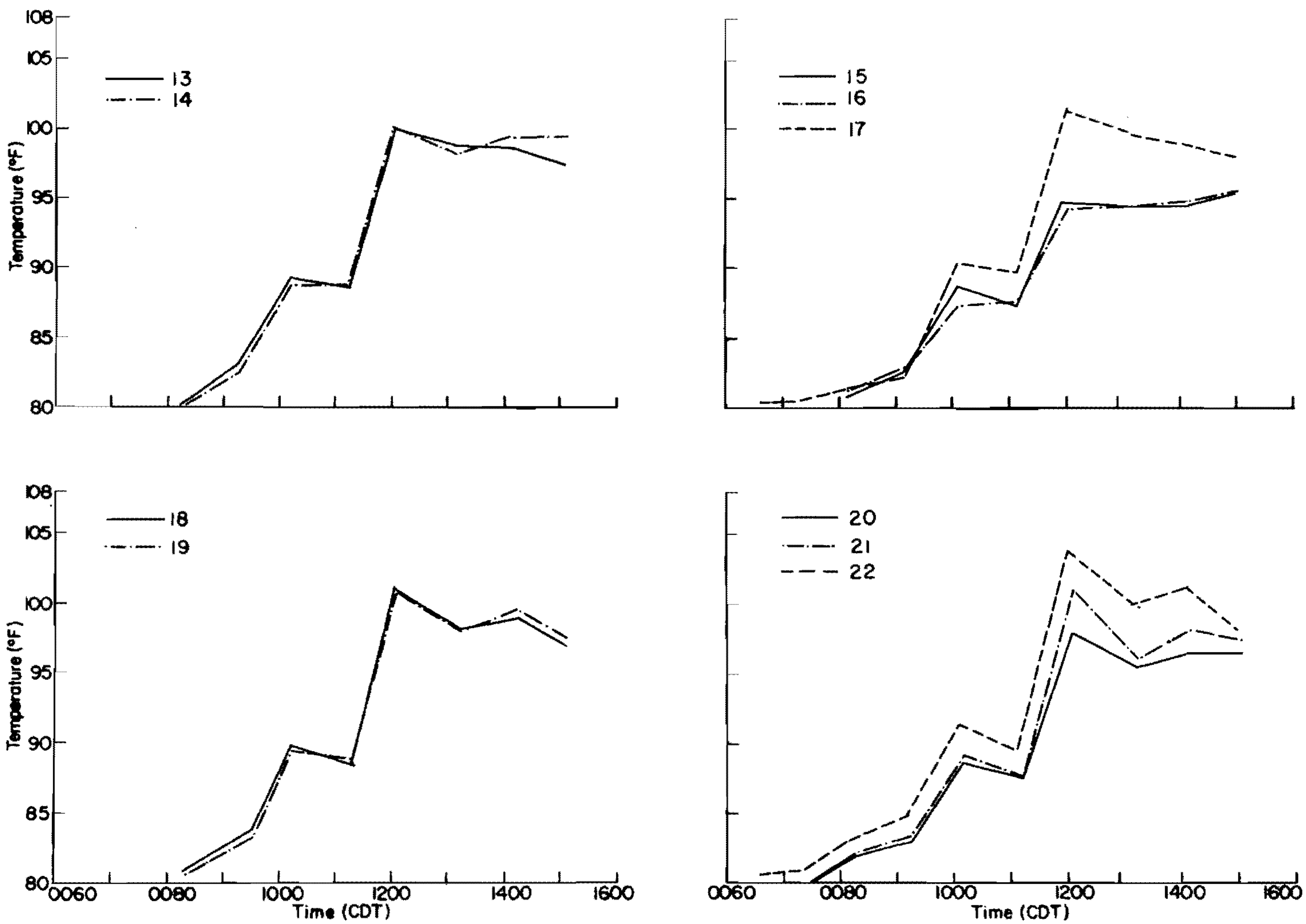

Fig A.3. Measured surface temperature variation for stations 13-22.

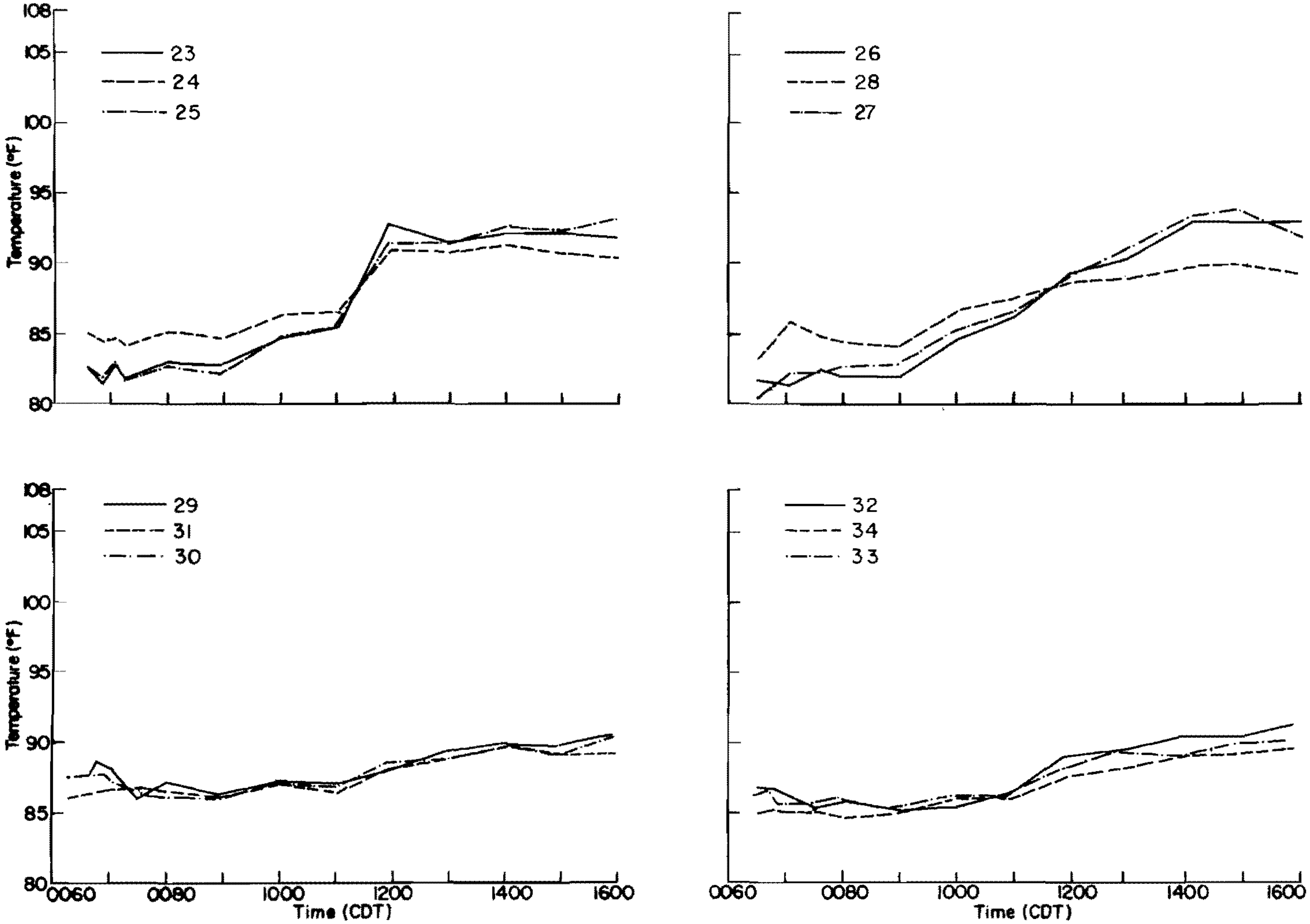

Fig A.4. Measured surface temperature variation for stations 23-34.

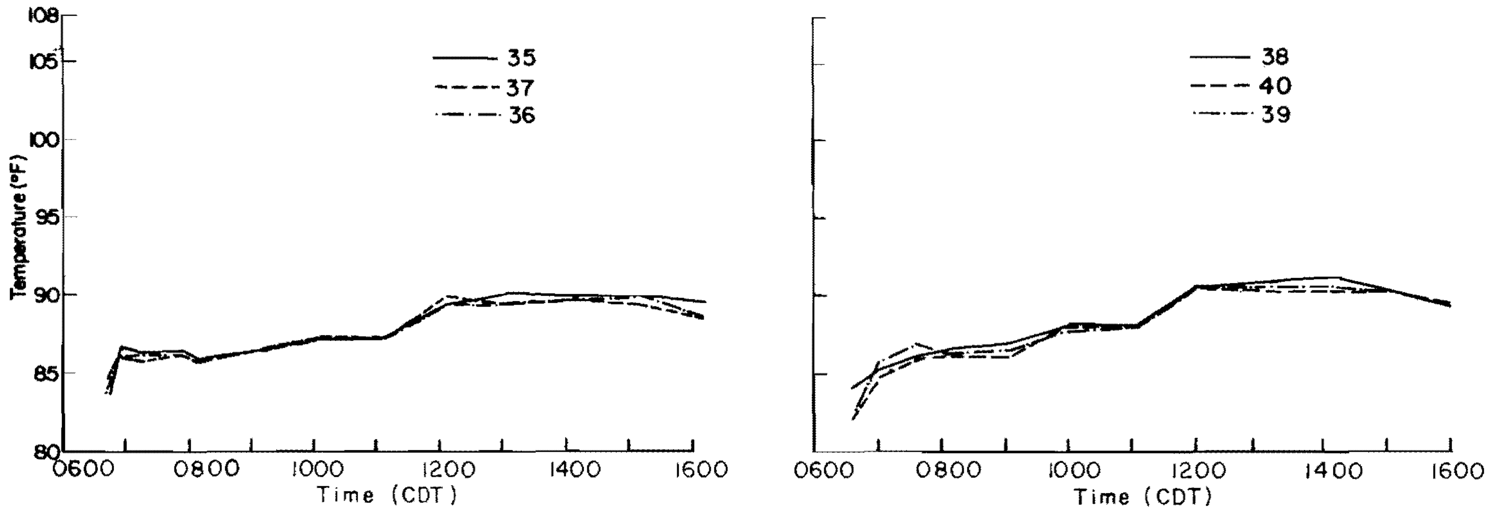

Fig A.5. Measured surface temperature variation for stations 35-40.

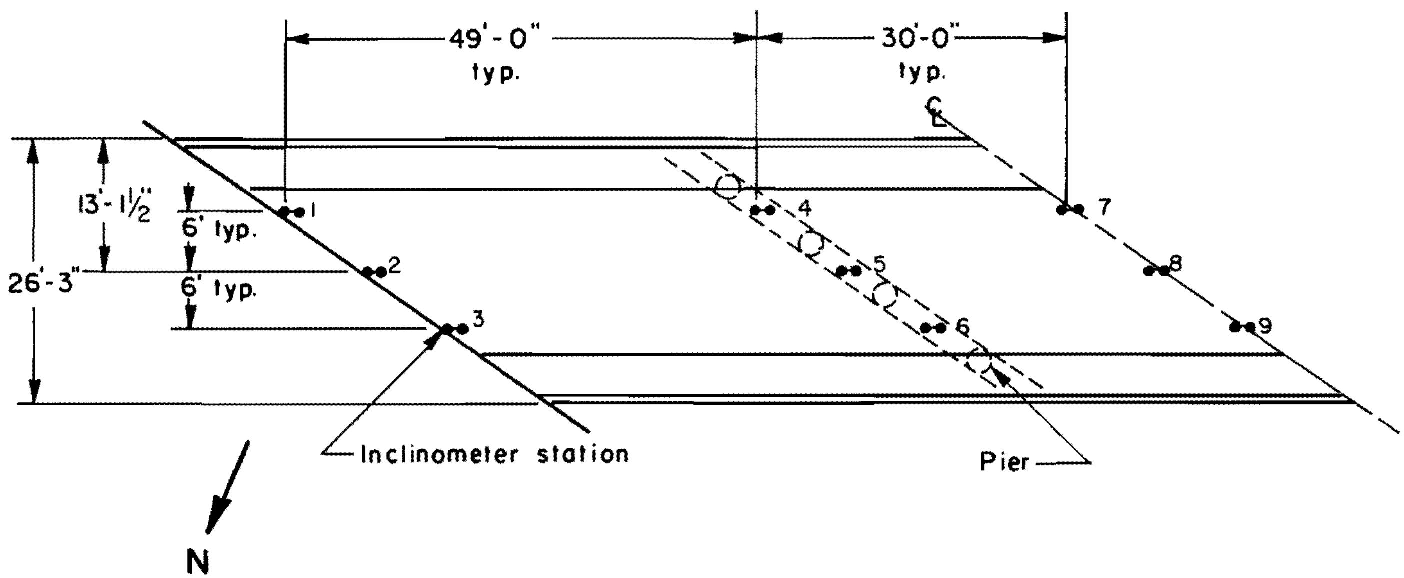

Plan view showing inclinometer locations.

Fig A.6. Inclinometer stations on Pasadena bridge.

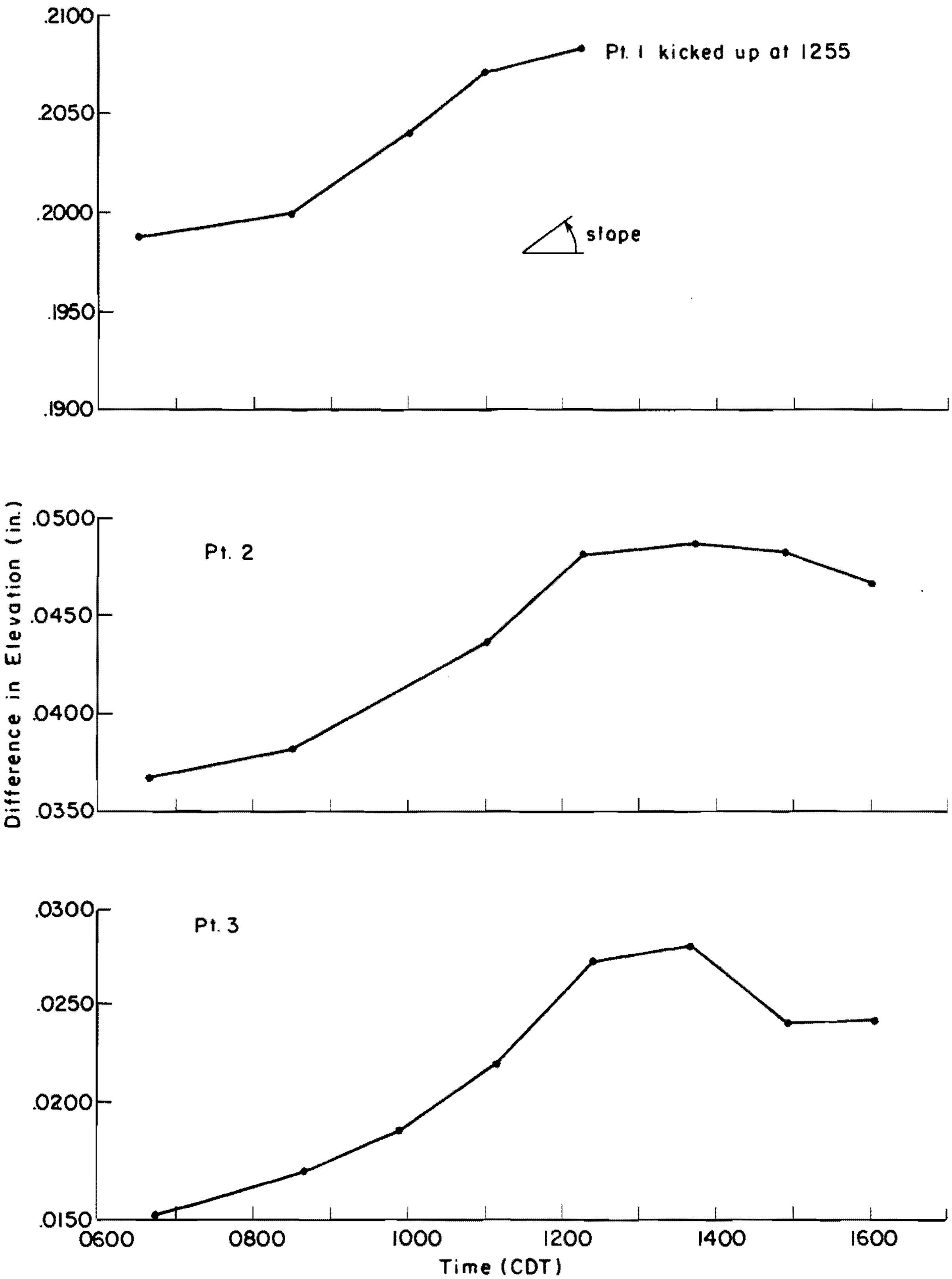

Fig A.7. Inclinometer measurements for points 1, 2, and 3.

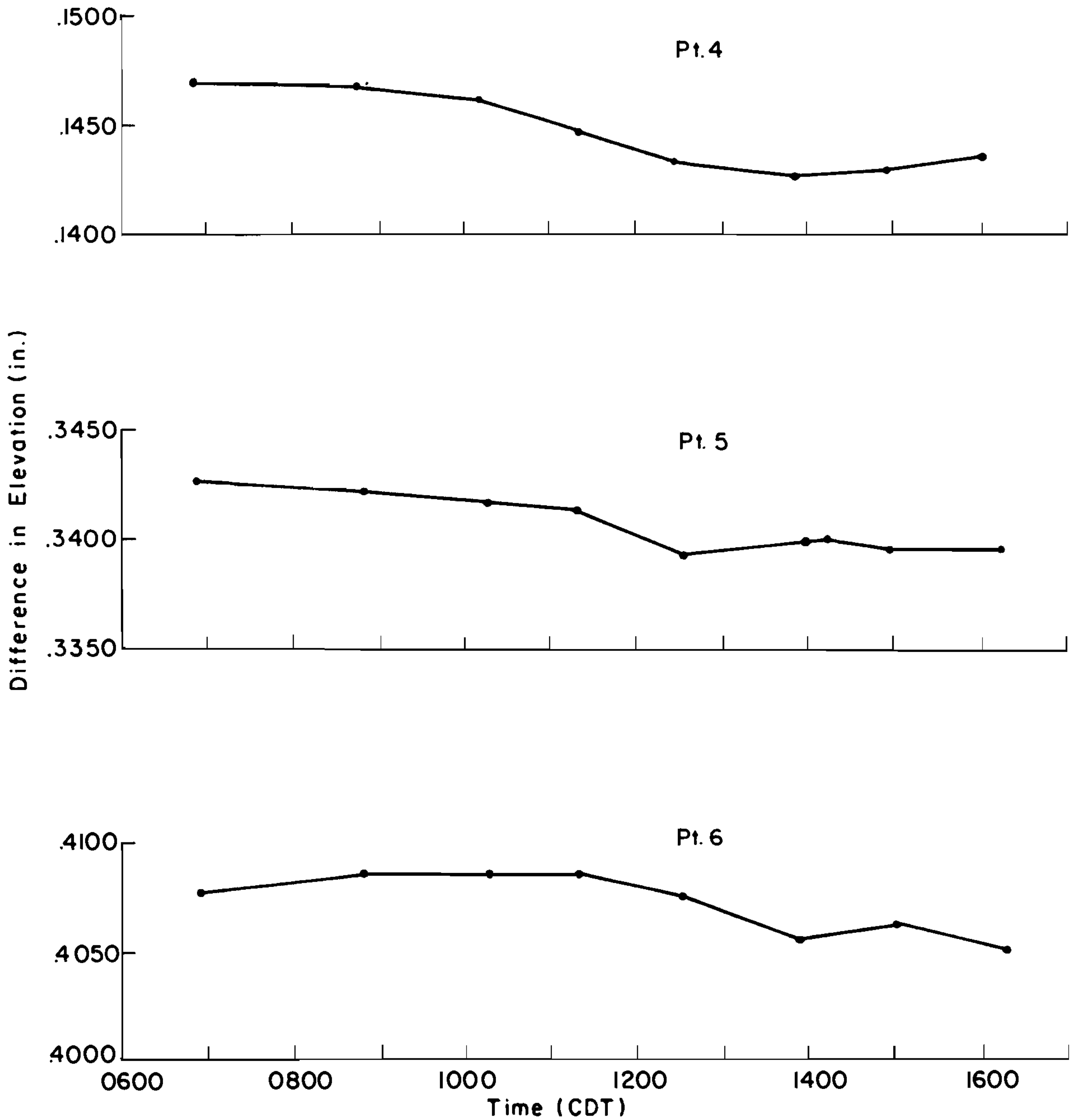

Fig A.8. Inclinometer measurements for points 4, 5, and 6.

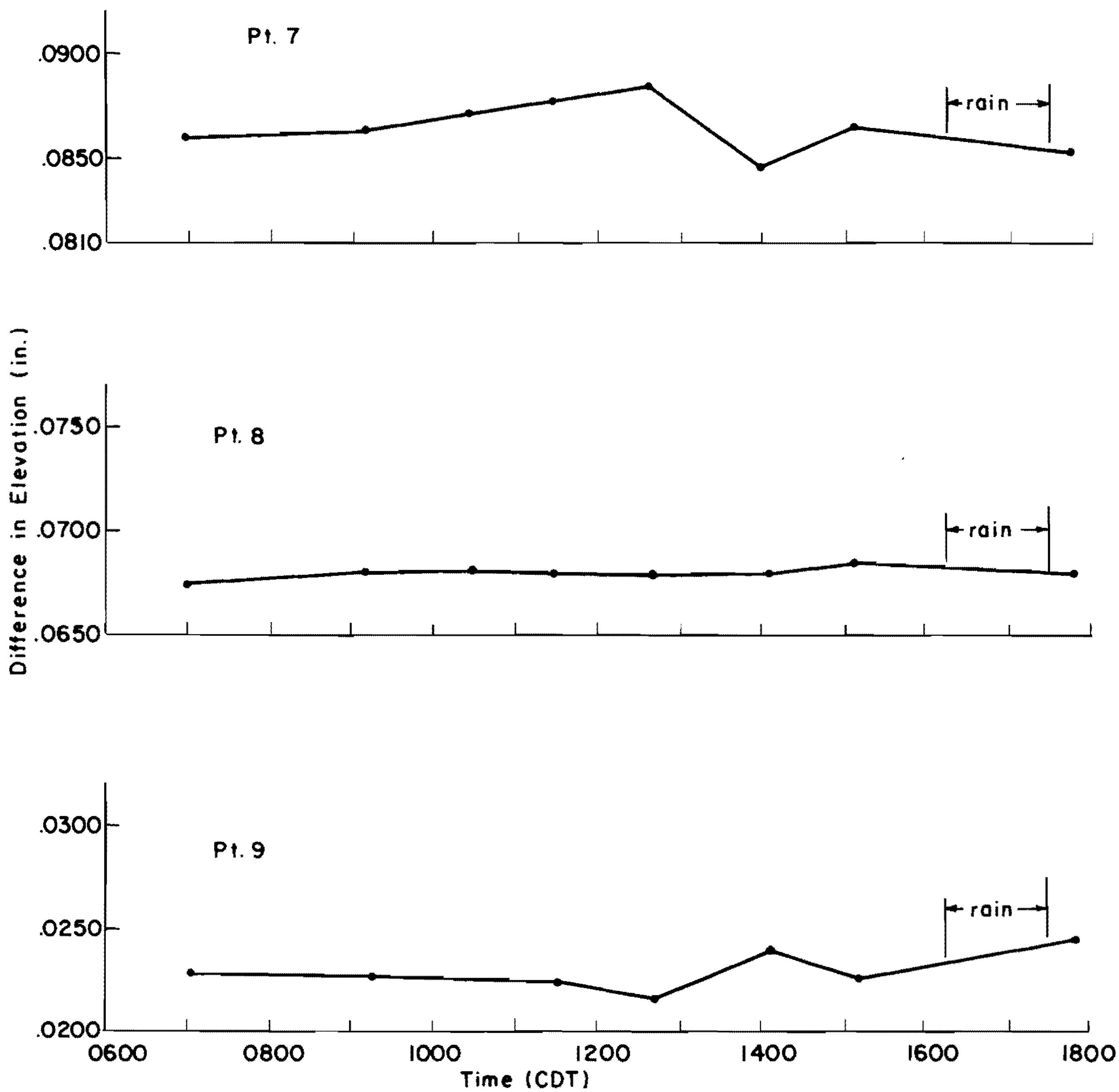

Fig A.9. Inclinometer measurements for points 7, 8, and 9.

TABLE A.1. Wind Speed Measurements during Pasadena Field Test

Time (CDT)	Wind Speed (mph) Top Surface	Wind Speed (mph) Bottom Surface
0640	4 - 5	3
0740	7 - 8	5
0850	6 - 7	0 - 5
1040	8 - 10	8 - 10
1130	6 - 9	4 - 5
1210	8 - 10	6 - 8
1320	4 - 5	4 - 5
1440	1 - 3	1 - 2
1510	13 - 15	8 - 10
1550	5	4
1610	12 - 21	6

APPENDIX B

FIELD TEST RESULTS FOR PEDESTRIAN OVERPASS

APPENDIX B. FIELD TEST RESULTS FOR PEDESTRIAN OVERPASS

Results and locations of surface temperature measurements are described in this Appendix for the 14 March 1975 field test on the pedestrian overpass. A summary of the test has been presented in Section 4.4.

Fifty-six stations were located for surface temperature measurements. These stations were located around the cross section of the bridge twelve feet from the northern abutment. The location of these stations is shown in Fig B.1. As measurements were observed, it became apparent that some of the stations were so close together that the temperatures were almost the same. For this reason, stations 21, 25, and 41 were dropped. Measured temperatures were plotted versus time and the plotted points were joined with straight lines to approximate the surface temperature variation at each station. Figures B.2 thru B.7 illustrate the surface temperature variations obtained using this method. The surface temperature variations for stations 23 and 51 have been presented in Fig 4.7.

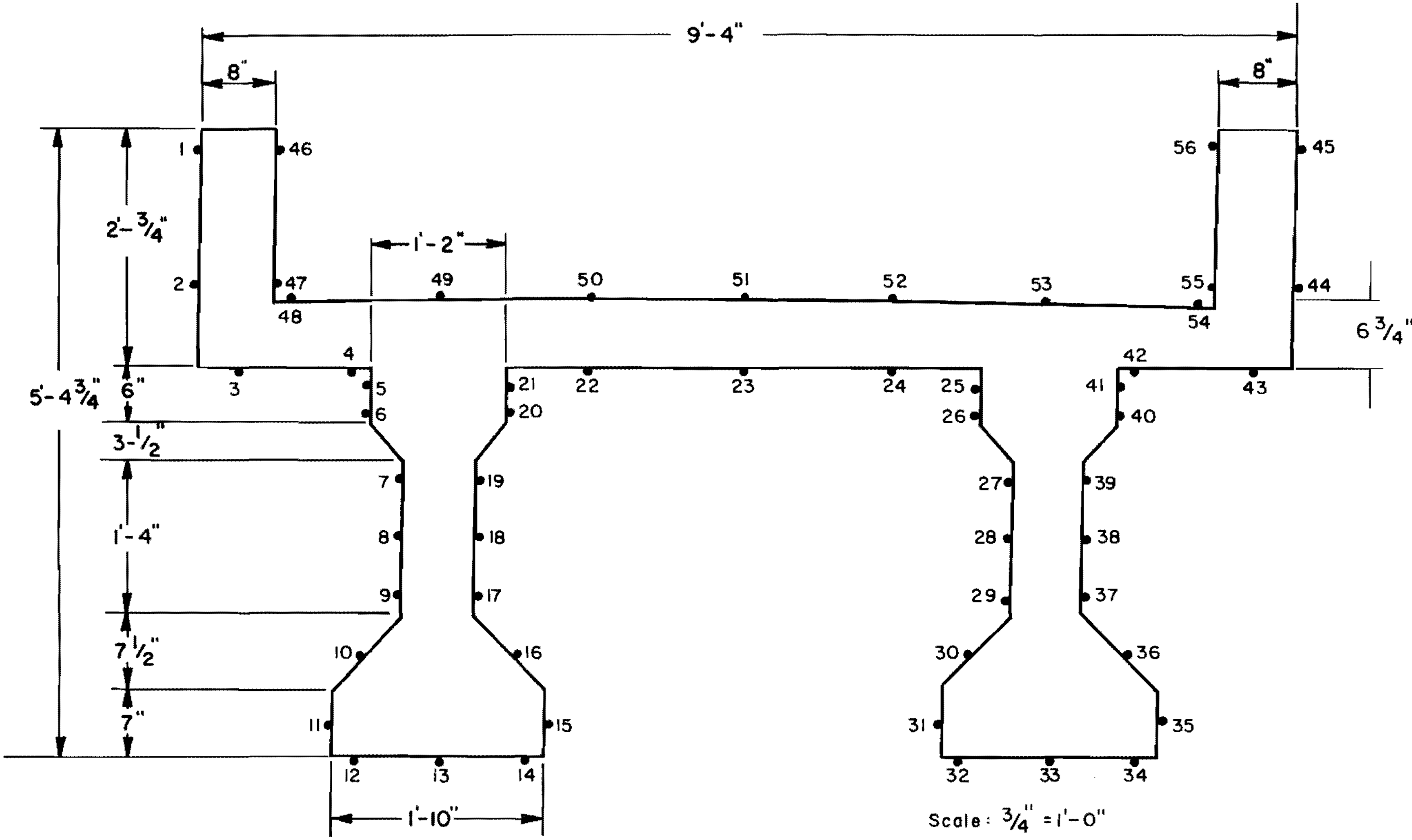

Fig B.1. Location of surface temperature stations for pedestrian overpass.

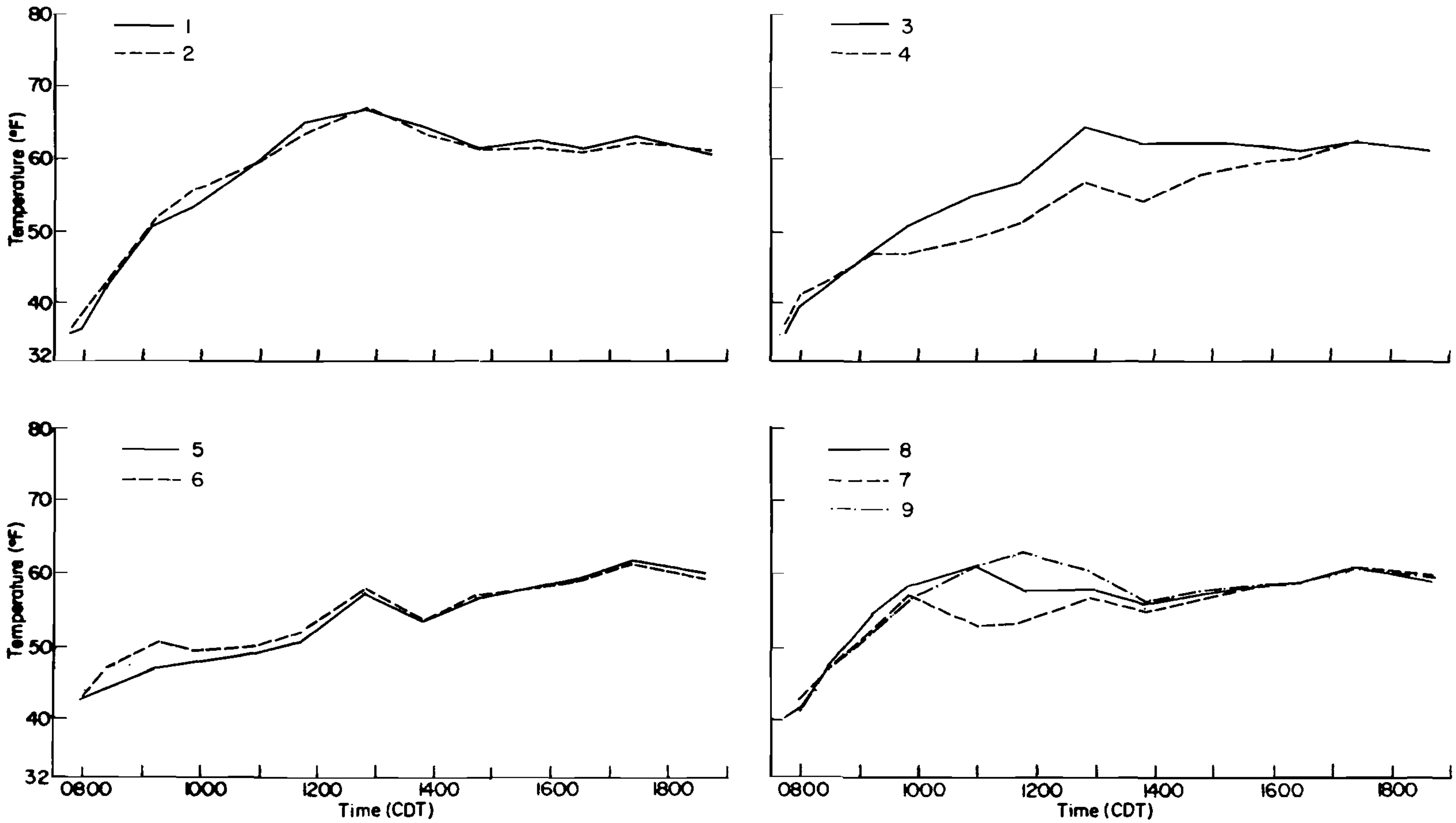

Fig B.2. Measured surface temperature variation for stations 1-9.

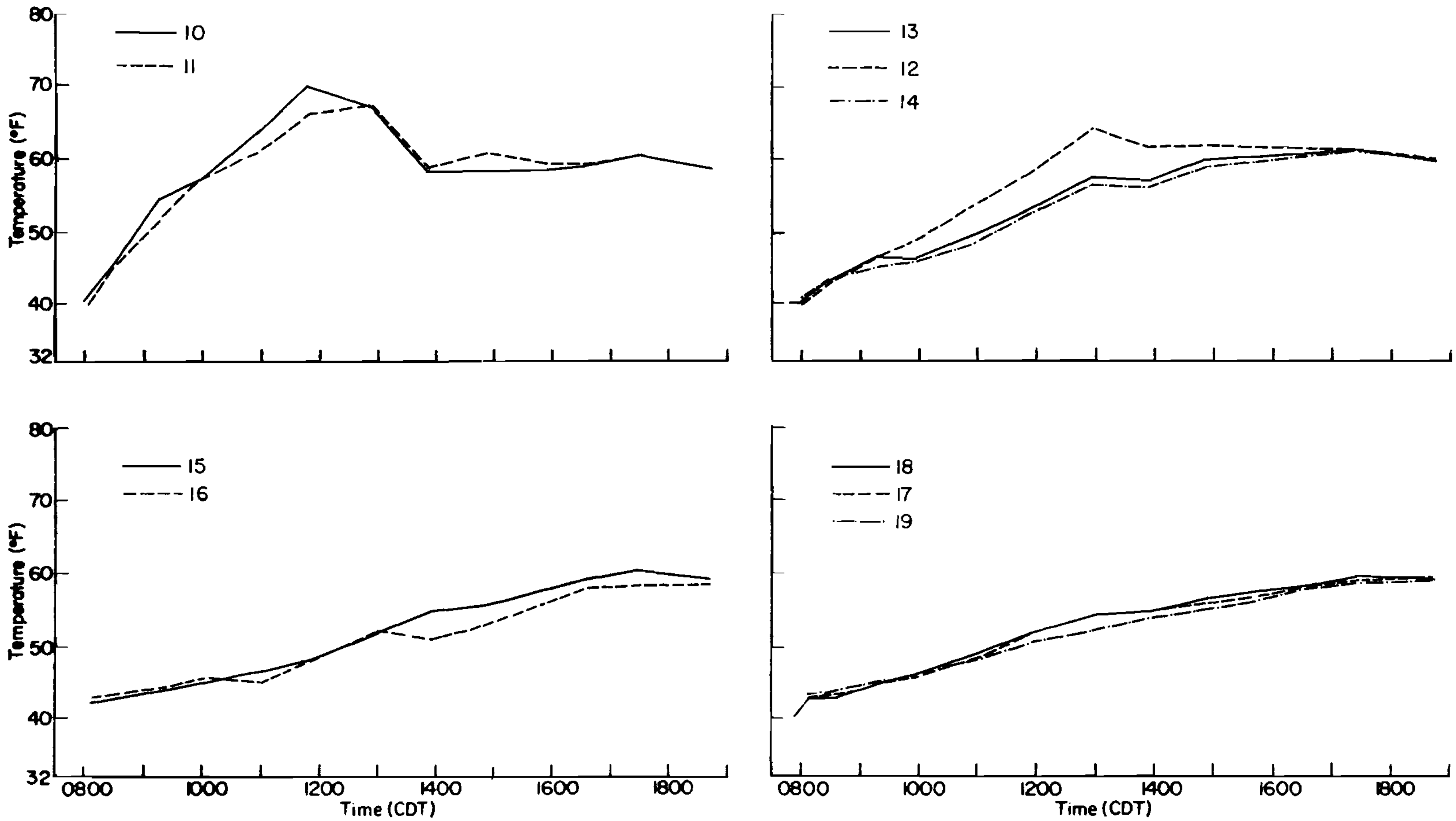

Fig B.3. Measured surface temperature variation for stations 10-19.

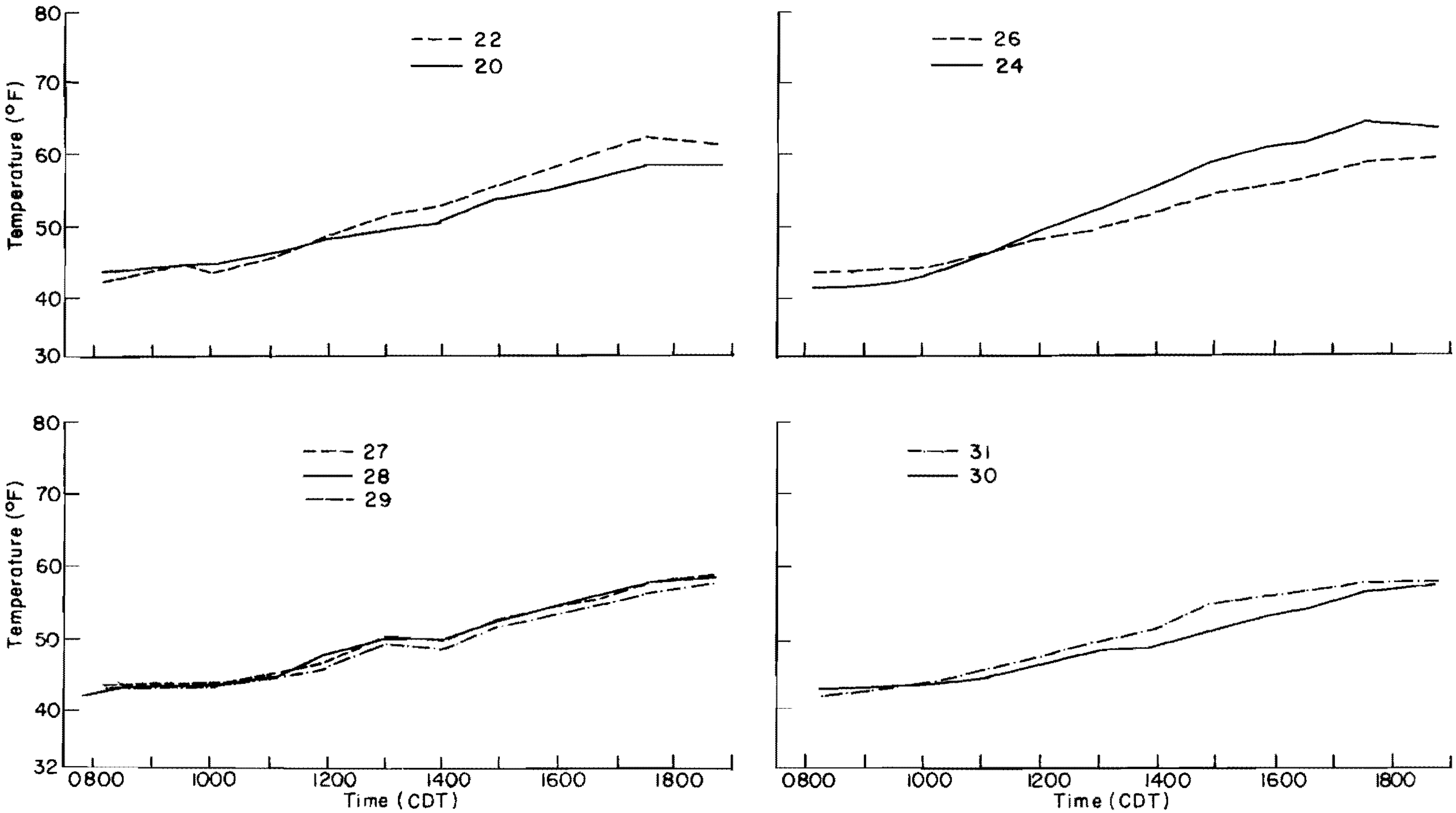

Fig B.4. Measured surface temperature variation for stations 20, 22, 24, 26-31.

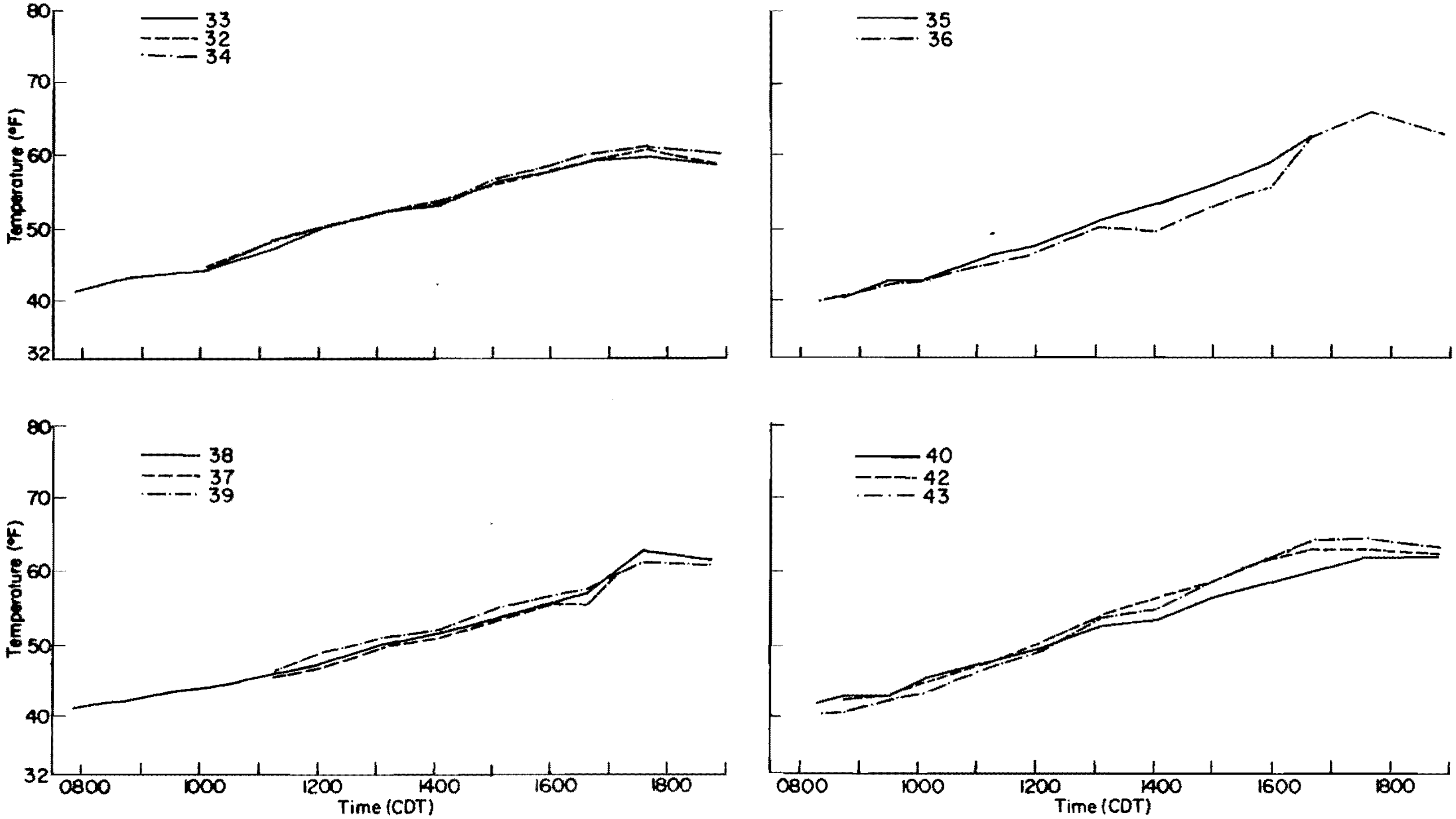

Fig B.5. Measured surface temperature variation for stations 32-40, 42, and 43.

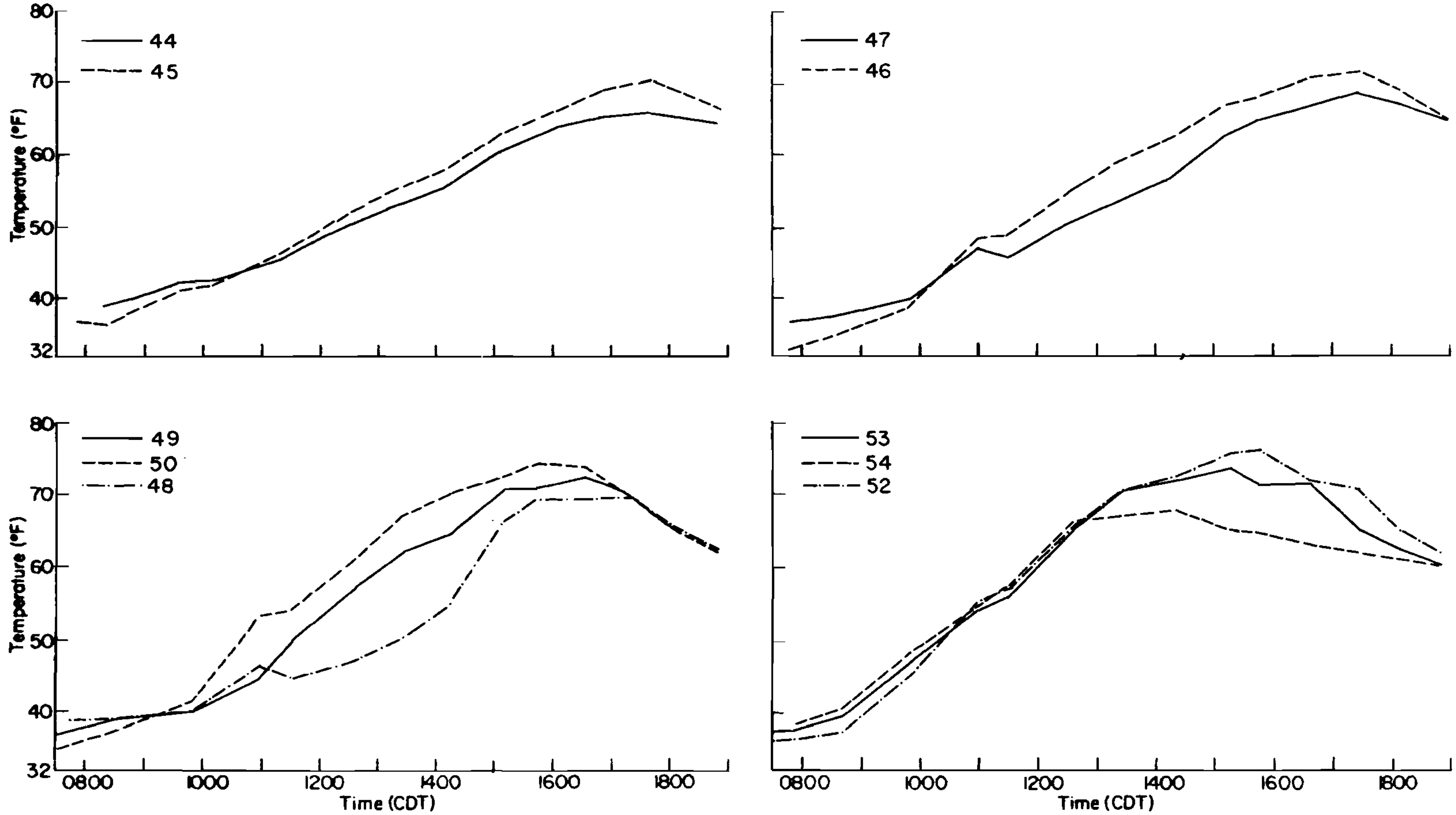

Fig B.6. Measured surface temperature variation for stations 44-50, 52-54.

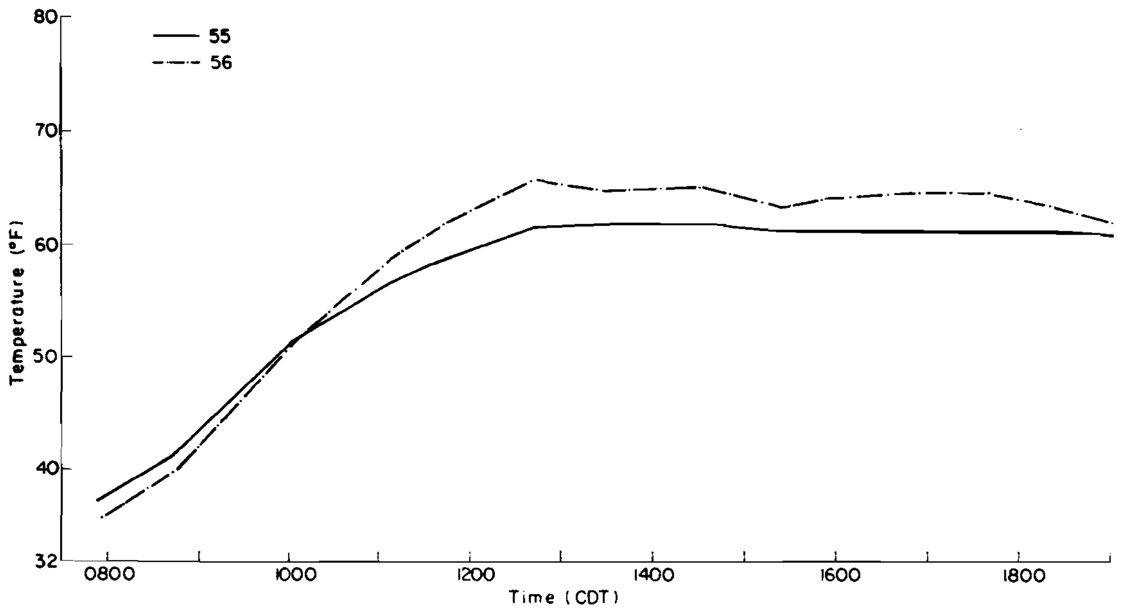

Fig B.7. Measured surface temperature variation for stations 55 and 56.

BIBLIOGRAPHY

1. American Association of State Highway Officials, Standard Specifications for Highway Bridges, AASHO, Washington, D.C., 1973.

2. American Association of State Highway and Transportation Officials, Interim Specifications for Bridges 1974, AASHTO, Washington, D.C., 1974.

3. American Association of State Highway and Transportation Officials, Interim Specifications for Bridges 1975, AASHTO, Washington, D.C., 1975.

4. Barber, E.S., "Calculation of Maximum Pavement Temperatures from Weather Reports," Bulletin 168, Highway Research Board, 1957.

5. Becker, E.B., and Parr, C.H., "Application of the Finite Element Method to Heat Conduction in Solids," Technical Report 5-117, U.S. Army Missile Command, Redstone Arsenal, Alabama, Nov., 1968.

6. Berwanger, C., "Thermal Stresses in Composite Bridges," Proceedings, ASCE Specialty Conference on Steel Structures, Engineering Extension Series, No. 15, University of Missouri - Columbia, Columbia, Mo., June, 1970.

7. Billington, N.S., Thermal Properties of Buildings, Cleaver- Hume Press LTD., 1952.

8. Boley, B., and Weiner, J., Theory of Thermal Stress, John Wiley and Sons Inc., 1960.

9. Brisbane, J., "Heat Conduction and Stress Analysis of Anisotropic Bodies," Vol. 1, Rohm and Haas Company, Redstone Research Laboratories, Huntsville, Alabama, Oct., 1969.

10. Capps, M.W.R., "The Thermal Behavior of Beachley Viaduct/Wye Bridge," RRL Report No. 234, Road Research Laboratory, Ministry of Transport, London, 1968.

11. Clough, R.W., and Tocher, J.L., "Finite Element Stiffness Matrices for the Analysis of Plate Bending," Proceedings, Conference on Matrix Methods in Structural Mechanics, Air Force Institute of Technology, Wright-Patterson Air Force Base, Ohio, 1965.

12. Colville, J., "A General Solution of the Von Karman Plate Equations by the Finite Element Method," Ph.D. Dissertation, The University of Texas, Austin, 1970.

13. Cruz, Carlos, "Elastic Properties of Concrete at High Temperature," Journal of the PCA Research and Development Laboratories, Jan., 1966.

14. Degelman, L.O., "The Mathematical Model for Predicting Solar Heat Gains through Building Walls and Roofs," Better Building Report No. 6, Pennsylvania State University, Institute for Building Research, June, 1966.

15. Desai, C.S., and Abel, J.F., Introduction to the Finite Element Method, Van Nostrand Reinhold Company, 1972.

16. Doherty, W.P., Wilson, E.L., and Taylor, R.L., "Stress Analysis of Axisymmetric Solids Utilizing Higher Order Quadrilateral Finite Elements," SESM Report No. 69-3, University of California, Berkeley, 1966.

17. Emerson, M., "Bridge Temperatures and Movements in the British Isles," RRL Report LR 228, Road Research Laboratory, Ministry of Transport, Crowthorne, 1968.

18. Emerson, M., "The Calculations of the Distribution of Temperatures in Bridges," TRRL Report LR 561, Transport and Road Research Laboratory, Crowthorne, 1973.

19. Gloyne, R.W., "The Diurnal Variation of Global Radiation on a Horizontal Surface - With Special Reference to Aberdeen, Meteorological Magazine 101, 1972.

20. Hilton, M.H., "Factors Affecting Girder Deflections during Bridge Deck Construction," Highway Research Record, No. 400, 1972.

21. Johns, D.J., Thermal Stress Analysis, Pergamon Press, 1965.

22. Johnson, C.P., "The Analysis of Thin Shells by a Finite Element Procedure," SEL Report No. 67-22, University of California, Berkeley, 1967.

23. Johnson, C.P., and Matlock, H., "Temperature Induced Stresses in Highway Bridges by Finite Element Analysis and Field Tests," Research Proposal, Project No. 3-5-73-23, Center for Highway Research, The University of Texas, Austin, 1973.

24. Johnson, C.P., Thepchatri, T., and Will, K., "Static and Buckling Analysis of Highway Bridges by Finite Element Procedures," Research Report No. 155-1F, Center for Highway Research, The University of Texas, Austin, 1973.

25. Jaber, M.M., Fowler, D.W., and Paul, D.R., "Repair of Concrete with Polymers," Research Report 114-3, Center for Highway Research, The University of Texas, Austin, Feb., 1975.

26. Khachaturian, N., and Gurfinkel, G., Prestressed Concrete, McGraw-Hill, 1969.

27. Krishnamurthy, N., "Temperature Effects on Continuous Reinforced Concrete Bridge," HPR Report No. 58, Alabama Highway Research, 1971.

28. Leonhardt, F., and Lippoth, W., "Folgerungen aus Schaden an Spannbetonbrucken," Beton-und Stahlbetonbau, Heft 10, V. 65, October, 1970.

29. Lin, T.Y., Design of Prestressed Concrete Structures, John Wiley & Sons, 1963.

30. Matlock, H., Panak, J.J., Vora, M.R., and Chan, J.H.C., "Field Investigation of a Skewed, Post-Stressed Continuous Slab Structure," Interim Study Report, Center for Highway Research The University of Texas, Austin, 1970.

31. McCullough, B.F., Abou-Ayyash, A., Hudson, R., and Randall, J., "Design of Continuously Reinforced Concrete Pavements for Highways," Final Report, Research Project NCHRP 1-15, Center for Highway Research, University of Texas, Austin, 1974.

32. "Polymer Impregnated Concrete: First Applications," Civil Engineering - ASCE, Jan., 1974.

33. Radolli, M., and Green, R., "Thermal Stresses in Concrete Bridge Superstructures - Summer Conditions," Proceedings, 54th Annual Transportation Research Board Meeting, 1975.

34. Reynolds, J.C., and Emanuel, J.H., "Thermal Stresses and Movements in Bridges," Journal of the Structural Division, ASCE, Jan., 1974.

35. Robinson, N., editor, Solar Radiation, Elsevier Publishing Company, 1966.

36. "Room for Improvement," Engineering News - Record, Vol. 164, No. 5, Feb., 1960.

37. Rushing, H., and Leblanc, E., "Temperature Differential of Swingspan Bridges," Research Report No. 40, Louisiana Department of Highways, June, 1969.

38. Strock, Clifford, editor, Handbook of Air Conditioning, Heating, and Ventilating, New York Industrial Press, 1965.

39. Thepchatri, Thaksin, Johnson, C. Philip, and Matlock, Hudson, "Prediction of Temperature and Stresses in Highway Bridges by a Numerical Procedure Using Daily Weather Reports," Research Report No. 23-1, Center for Highway Research, The University of Texas at Austin, February 1977.

40. Timoshenko, S., and Goodier, J.N., Theory of Elasticity, McGraw-Hill, 1970.

41. Wah, T., and Kirksey, R.E., "Thermal Characteristics of Highway Bridges," Final Report to Highway Research Board, Contract No. HR 12-4, Southwest Research Institute, San Antonio, Texas, July, 1969.

42. Will, K.M., "Elastic Instability Analysis of Thin-Walled Structures by a Refined Finite Element Procedure," CESM Report No. 71-2, The University of Texas, Austin, Dec., 1971.

43. Willems, N., "Experimental Strain Analysis of Continuous Skew Slab Bridge Decks," Report No. HPR-SHC 71-3-F, State Highway Commission of Kansas, Oct., 1973.

44. Wilson, E.L., "The Determination of Temperatures within Mass Concrete Structures," SEL Report No. 68-17, University of California, Berkeley, 1968.

45. Wilson, E.L., and Nickell, R.E., "Application of the Finite Element Method to Heat Conduction Analysis," Nuclear Engineering and Design, Vol. 4, 1966.

46. Zienkiewicz, O.C., The Finite Element Method in Engineering Science, McGraw-Hill, 1971.

47. Zuk, W., "Thermal Behavior of Composite Bridges - Insulated and Uninsulated," Highway Research Record, No. 76, 1965.

48. Zuk, W., "Simplified Design Check of Thermal Stresses in Composite Highway Bridges," Highway Research Record, No. 103, 1965.